DEPARTMENT OF PHYSICS
UNIVERSITY OF JYVÄSKYLÄ
RESEARCH REPORT No. 2/2018

DECAY SPECTROSCOPY OF THE VERY NEUTRON-DEFICIENT LEAD AND THALLIUM ISOTOPES ^{178,179}Pb AND ^{179}Tl

by

Hussam Badran

Academic Dissertation
for the Degree of
Doctor of Philosophy

To be presented, by permission of the
Faculty of Mathematics and Natural Sciences
of the University of Jyväskylä,
for public examination in Auditorium FYS1 of the
University of Jyväskylä on January 12, 2018
at 12 o'clock noon

Jyväskylä, Finland
January 2018

Abstract

Badran, Hussam
Decay spectroscopy of the very neutron-deficient lead and thallium isotopes ^{178,179}Pb and ^{179}Tl.
Jyväskylä: University of Jyväskylä, 2018, 77 P.
Department of Physics Research Report No. 2/2018
ISSN: 0075-465X; 2/2018
ISBN: 978-951-39-7329-2 (paper version)
ISBN: 978-951-39-7330-8 (electronic version)
Diss.

This thesis reports on the production of the very neutron-deficient isotopes ^{178,179}Pb and ^{179}Tl, using heavy-ion fusion-evaporation reactions. The gas-filled separator RITU and the GREAT spectrometer at its focal plane position were used for the decay spectroscopy study. The α decay of ^{178}Pb and its α-decay chain were studied through α-α correlations. The α-particle energy and half-life were measured for ^{178}Pb as, E_α= 7610(30) keV and $t_{1/2} = 0.21^{+0.21}_{-0.08}$ ms, respectively. The half-life is consistent with recent theoretical calculations using the Coulomb and Proximity Potential Model (CPPM). The hindrance factor for ^{178}Pb was deduced and corresponds to an unhindered $\Delta l = 0$ transition. The α-decay reduced width was deduced as well and put into a systematic context advancing the systematics of the even-A Pb isotopes to further neutron deficiency. The decay properties of ^{179}Pb were studied through α-α and α-γ correlations, which has allowed the ground-state of ^{179}Pb to be assigned as $I^\pi = 9/2^-$. In comparison with the literature, a more precise α-particle energy and half-life were measured for the ground state of ^{179}Pb to be, E_α = 7348(5) keV and $t_{1/2}$ = 2.7(2) ms, respectively. A search for a $\nu i_{13/2}$ state in ^{179}Pb was performed, but only a limit of excitation energy and half-life was obtained. In addition, improved α-decay data were also measured for ^{179}Tl. Evidence for an isomeric state at an excitation energy of 904.5(9) keV was identified for the first time in ^{179}Tl, with a half-life of $t_{1/2} = 114^{+18}_{-10}$ ns and is tentatively assigned to be a proton ($9/2^-$) intruder state.

Keywords: nuclear structure, decay spectroscopy, α decay, isomeric states, neutron-deficient nuclei.

Author's address Hussam Badran
Department of Physics
University of Jyväskylä
Finland

Supervisor Dr. Catherine Scholey
Department of Physics
University of Jyväskylä
Finland

Reviewers Prof. David Jenkins
Department of Physics
University of York
U.K.

Dr. Karl Hauschild
CSNSM, CNRS/IN2P3
Université Paris-Saclay
France

Opponent

Prof. John F Smith
School of Engineering
University of the West of Scotland
U.K.

Preface

The work presented here was carried out during the years 2013–2017 at the Department of Physics of the University of Jyväskylä.

I would like to express my deepest thanks to my supervisor Dr. Catherine Scholey for the continuous efforts, guidance and motivation that was given to me during my studies. Thanks for all the valuable help and support. I would like to express my gratitude to Prof. Rauno Julin who introduced me to the world of experimental nuclear physics and giving me the chance to be part of the Nuclear Spectroscopy group in the one of the best facilities in the world. A warm thank you goes to Dr. Juha Uusitalo for his huge help, valuable comments and enormous fruitful discussions regarding my data analysis and my thesis work. I acknowledge the discussions together with Dr. Sakari Juutinen and Prof. Paul Greenlees, the advice they gave me has been of great help.

I would like to thank all of the past and present colleagues in the Nuclear Spectroscopy research group for the relaxed working atmosphere, especially Dr. Pauli Peura and Dr. Ulrika Jakobsson for the help and the guidance in my first year. The time that I have spent working at the lab was spent mostly with Dr. Kalle Auranen, Dr. Joonas Konki, Mr. Jari Partanen and Dr. Sanna Stolze, which made the work most pleasant. Special big thanks goes to my amazing physics friends Antoine, Alex[3], Danny, Fede, Gianluca, Josh, Laetitia, Marjut, Nino, Philippos, Sara, Sarina and Tom, for the nice time that we spent together during lunch, coffee breaks and outside work. I would like also to thank all my international student friends and my basketball teammates for the nice time and the fun that we had during my studies here in Jyväskylä.

I want to thank the pre-examiners, Prof. David Jenkins and Dr. Karl Hauschild, for the careful reading of the manuscript.

Finally, I am really thankful to my close friend Nael and his lovely family, thanks for telling me about the nuclear physics program, helping me in the applying process and for all the nice time that we shared here in Jyväskylä. Above all, I am deeply indebted to my whole family, my mother, Gofran, Abod and Ahmad for their love and unfailing encouragement.
To my father (R.I.P).

Hussam M Badran
Jyväskylä, January 2018

Acknowledgement

The author would like to thank John Greene from Argonne National Laboratory and B. Lommel and the GSI target laboratory staff for producing the Pd targets. The author also thanks the GAMMAPOOL European Spectroscopy Resource for the loan of the clover detectors at the GREAT spectrometer. This work has been supported by the Academy of Finland under the Finnish Centre of Excellence Program (213503 contract number), the Marie Curie Career Integration Grant (Grant No. 304033), the Science and Technology Facilities Council STFC and by the Academy of Finland (Grant No. 257562).

List of publications

The present thesis has been written based on two publications:

I. *Confirmation of the new isotope* ^{178}Pb.
H. Badran, C. Scholey, K. Auranen, T. Grahn, P. T. Greenlees, A. Herzáň, U. Jakobsson, R. Julin, S. Juutinen, J. Konki, M. Leino, M. Mallaburn, J. Pakarinen, P. Papadakis, J. Partanen, P. Peura, P. Rahkila, M. Sandzelius, J. Sarén, J. Sorri, S. Stolze. and J. Uusitalo.
Physical Review C 94, 054301 (2016)

II. *Decay spectroscopy of* $^{179}_{82}\mathrm{Pb}_{97}$ *and evidence for a* $9/2^-$ *intruder state in* $^{179}_{81}\mathrm{Tl}_{98}$.
H. Badran, C. Scholey, J. Uusitalo, K. Auranen, T. Grahn, P. T. Greenlees, A. Herzáň, U. Jakobsson, R. Julin, S. Juutinen, J. Konki, M. Leino, M. J. Mallaburn, J. Pakarinen, P. Papadakis, J. Partanen, P. Peura, P. Rahkila, M. Sandzelius, J. Sarén, J. Sorri and S. Stolze.
Physical Review C 96, 064314 (2017)

In addition, the author[1] has contributed to other publications involving the Department of Physics of the University of Jyväskylä.

[1] Open Researcher and Contributor ID (ORCID iD): 0000-0001-8383-5326

Contents

Chapter 1

Introduction

It all started in $\sim$ 400 BC, when Greek philosopher Démocritus believed that any kind of matter could be subdivided into very small bits until one reached the very limit beyond which no further division was possible, called the atom (atomos = uncuttable). A combined effort for many scientists from the end of the 19^{th} century to mid-1930s defined the start of the atomic and nuclear physics era, trying to understand the atom and structure of the nucleus. A lot of progress has been made during the last 100 years in the nuclear physics studies, where new facilities, instrumentation and experimental methods have been developed. This is not only to have a deeper understanding of nuclear structure, but also to use nuclear physics in various applications from nuclear medicine to studies of ancient art, and from industry to cosmology.

The atomic nucleus is around $\sim 1/10000$ of the size of the atom and consists of positively charged protons and neutral neutrons. The proton number Z is used to identify different elements. For instance, the element lead Pb refers to an atom with $Z = 82$ protons in the nucleus, while the element thallium Tl has $Z = 81$ protons. The term isotope (${}^{A}_{Z}\mathrm{X}_{N}$) refers to an element Z with a varying neutron number N, where the isotope mass number A, is $A = Z + N$. To date 118 elements, and around 3300 isotopes of them have been discovered. The experimental work presented in this thesis is focused on the three different isotopes ${}^{178}_{82}\mathrm{Pb}_{96}$, ${}^{179}_{82}\mathrm{Pb}_{97}$ and ${}^{179}_{81}\mathrm{Tl}_{98}$, marked in Fig. 1.1.

The studied lead isotopes ^{178,179}Pb are located 30 and 29 mass unit away from the stable doubly magic nucleus ${}^{208}_{82}\mathrm{Pb}_{126}$, respectively. The ^{178}Pb isotope is the most neutron-deficient lead isotope known to date [Badran16]. The ^{179}Tl isotope is located 26 mass unit from the closest stable isotope ^{203}Tl, and is three neutrons away from the lightest known thallium isotope ^{176}Tl, which is a proton-emitting isotope [Kettunen04] (see Fig. 1.1). This thesis reports on the production of very

neutron-deficient nuclei ^{178,179}Pb and ^{179}Tl, via fusion-evaporation reactions induced by heavy-ion beams of stable isotopes, and more specifically the study of their α-decay properties. The results are obtained from an experiment performed at the Accelerator Laboratory of the University of Jyväskylä (JYFL), using the combined system of the gas-filled separator RITU [Leino95] and the GREAT spectrometer [Page03].

Alpha-decay fine-structure and hindrance factors HF are powerful tools for identifying low-lying intruder states in the vicinity of $Z = 82$ shell closure of very neutron-deficient nuclei. Direct information on the excitation energy of low-lying states and configurations involved can be obtained. Such information is certainly of great important in this region of shape coexistence [Heyde11, Julin01]. An example of the power of α-decay spectroscopy is the observation of α decays from both the odd- and even-mass polonium isotopes ^{190,191}Po, decaying to different low-lying intruder states which are assumed to have different deformations in ^{186,187}Pb (see Refs. [Andreyev00, Andreyev99b]).

The motivation behind the study of ^{178,179}Pb and ^{179}Tl isotopes, with a brief introduction to previous studies, are summarized as follows:

^{179}Pb ($Z = 82$, $N = 97$)

The very neutron-deficient nucleus ^{179}Pb was observed recently for the first time by Andreyev *et al.* [Andreyev10]. In total, 12 α-decay events of ^{179}Pb were seen over a broad energy range, but no γ rays in coincidence with those events were observed. Furthermore, a spin and parity of $I^{\pi} = 9/2^{-}$ was tentatively assigned to the ground state of ^{179}Pb. This assignment was made based on the broad energy distribution of decay events that were assumed to feed the excited $9/2^{-}$ state in ^{175}Hg [O'Donnell09]. In the heavier odd-mass Pb isotopes $^{183-199}$Pb, the ground state spin and parity of $I^{\pi} = 3/2^{-}$ [Cocolios11, Seliverstov09, ens] are assigned, while the $9/2^{-}$ state is observed only in ^{181}Pb [Andreyev09a] and tentatively assigned for ^{179}Pb as mentioned above, (see Fig. 1.2(b)). Therefore, a detailed decay-spectroscopy study of ^{179}Pb through α-γ and α-α correlation is needed in order to firmly establish the ground state spin and parity of ^{179}Pb. In this thesis the initial findings have been confirmed, but with more accurate α-particle energy and half-life values. In addition, the ground state of ^{179}Pb is firmly assigned to have spin and parity of $I^{\pi} = 9/2^{-}$. This assignment was made based on the coincidences observed between a 80 keV γ-ray transition from a $9/2^{-}$ excited state in ^{175}Hg [O'Donnell09] and the favoured α-decay ($\Delta l = 0$) of ^{179}Pb.

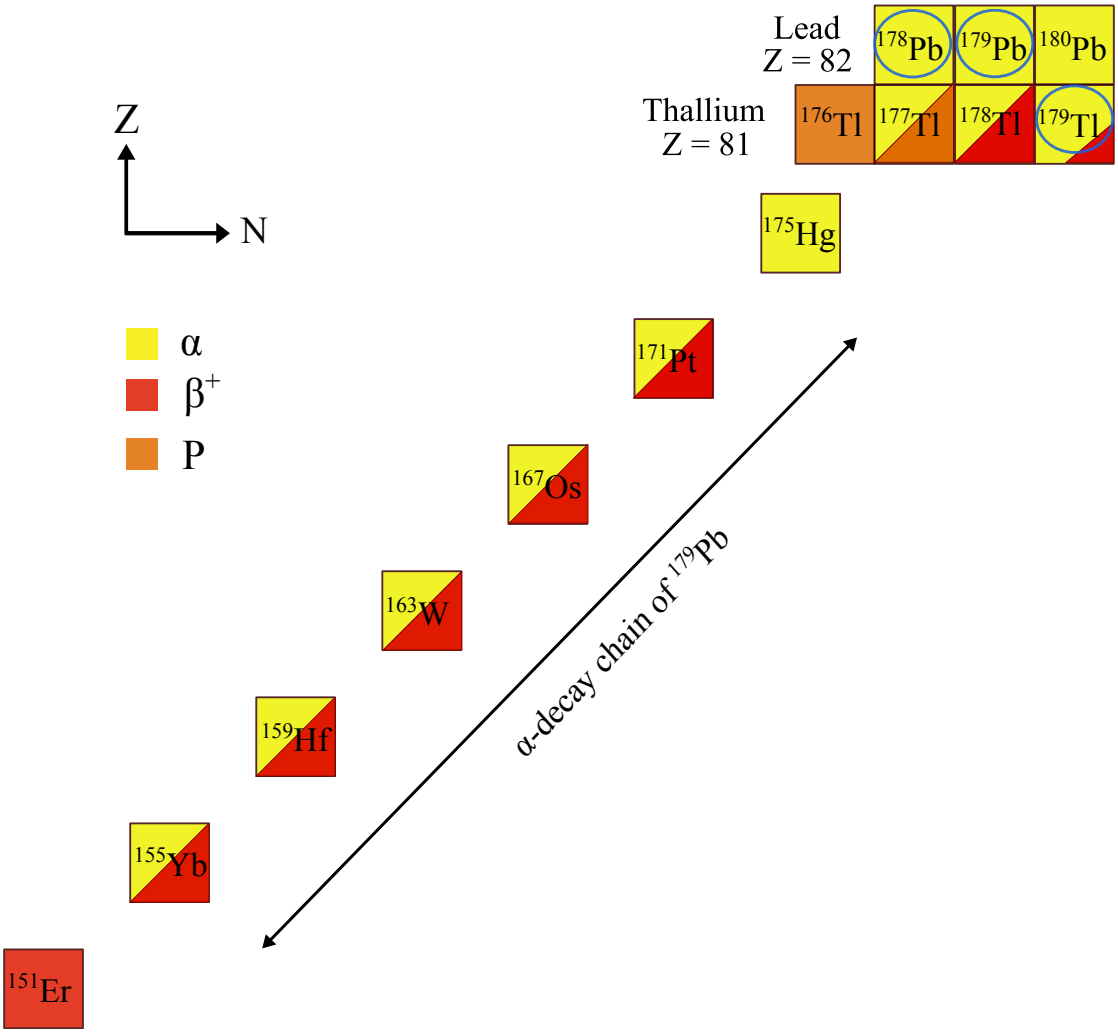

Figure 1.1: A part of the nuclear chart between $82 \leq Z \leq 81$ and $95 \leq N \leq 98$ is shown, where the very neutron-deficient nuclei studied in this thesis are marked. The α-decay chain of ^{179}Pb is also included.

Looking at the nuclear chart, α-decay chains in the neutron-deficient region below Pb give a unique access to study the nuclear structure effects between two closed shells. For instance, the α-decay chain of ^{179}Pb ($Z = 82$) down to ^{151}Er ($N = 83$) presented in Fig. 1.1, shows the most neutron-deficient chain between two closed shells known to date. Part of this chain has been studied before from ^{175}Hg $\rightarrow$ ^{163}W in Refs. [Scholey10, O'Donnell09], and some striking features were noticed across the whole chain. Such as:

- All the ground states from ^{175}Hg $\rightarrow$ ^{151}Er, have the same spin and parity $I^{\pi} = 7/2^{-}$ (See Refs.[O'Donnell09, Scholey10, Fukuchi09]).
- The continuity of $\nu f_{7/2}$ and $\nu h_{9/2}$ orbitals near the Fermi surface, along with the $\nu i_{13/2}$ unique-parity orbital.
- The near constant energy difference between the $13/2^{+}$ and $9/2^{-}$ states along the ^{179}Pb α-decay chain, as can be seen in Fig. 1.2(a).
- The consistency in $B(M2)$ values along the chain for the $\nu i_{13/2} \rightarrow \nu h_{9/2}$ transitions [Scholey10].

An investigation as to where the $\nu i_{13/2}$ intruder state exists in ^{179}Pb is required. This will yield extra verification of the ground state configuration and information on other low-lying states of this very exotic nucleus. In figure 1.2(b), the existence of the $13/2^{+}$ state along the odd-A neutron-deficient lead isotopes is evident at rather low excitation energies $\sim$100 keV for the lighter isotopes. In the present work, no evidence for the $13/2^{+}$ state in ^{179}Pb was observed. Hence, only limits of the excitation energy and half-life were obtained.

^{179}Tl ($Z = 81$, $N = 96$)

Studying odd mass neutron-deficient Tl isotopes has a vital role in understanding of shape coexistence phenomena around $Z = 82$ region, and in identifying orbitals which are responsible for the structure of the neighbouring even-even nuclei. Recently, the ground state spin of ^{179}Tl was determined as $I^{\pi} = 1/2^{+}$ by a laser-spectroscopy study [Barzakh17]. This follows the ground state spin and parity assignment of $I^{\pi} = 1/2^{+}$ for all odd-A Tl isotopes $^{177-201}$Tl [Barzakh13] originating from the $\pi(s_{1/2})^{-1}$ configuration. Furthermore, ^{179}Tl is known to have a $\pi(h_{11/2})^{-1}$ isomeric state that α decays to a $\pi(h_{11/2})^{-1}$ isomeric state in ^{175}Au [Andreyev10]. The proton $9/2^{-}$ and $13/2^{+}$ excited-states are known to exist in odd-mass Tl isotopes $^{183-195}$Tl [Lane95, Muikku01, Reviol92], which originate from one-particle one-hole (1p - 1h) excitation to the $\pi h_{9/2}$ and $\pi i_{13/2}$ orbitals across the $Z = 82$ shell gap. In fact, the $9/2^{-}$ state, which is assigned to have an oblate-deformed shape is known to be present along the majority of the isotopic chain $^{201-181}$Tl [Heyde83, Lane95, Muikku01, Raddon04, Andreyev09b]. Extending the level-energy systematics of odd-A Tl isotopes further beyond the proton drip-line would be interesting. This thesis reports on the first observations of a second isomeric state in ^{179}Tl, which is tentatively assigned a spin and parity of $I^{\pi} = (9/2^{-})$.

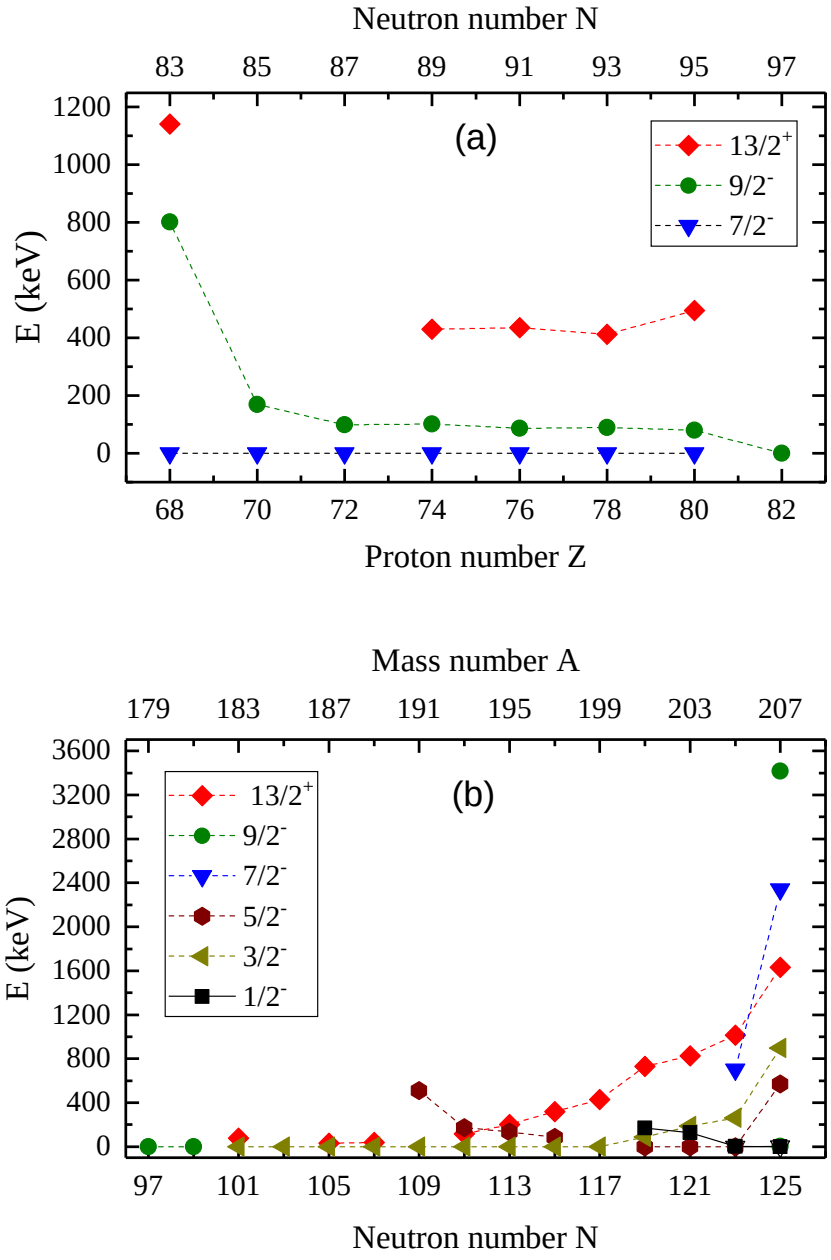

Figure 1.2: (a) A plot of the experimental-excitation energies of $13/2^+$ and $9/2^-$ states relative to $7/2^-$ ground states of even-Z odd-N isotopes in the α-decay chain of ^{179}Pb ($Z = 82 \rightarrow N = 83$). Values are taken from Refs. [Scholey10, O'Donnell09, Fukuchi09]. (b) Excitation energy systematics of single-particle states for the odd-A Pb isotopes $^{179-207}$Pb. Values are taken from Refs. [ens, Cocolios11].

^{178}Pb ($Z = 82$, $N = 96$)

The first identification of ^{178}Pb was reported by Batchelder *et al.* [Batchelder03], where two events were assigned to the α-decay of ^{178}Pb, but only one of these events was correlated to a known daughter α-decay event. In the present thesis confirmation of the new isotope ^{178}Pb is reported. In total, four α-decay events were assigned to ^{178}Pb. The α-particle energy and half-life are reported with improved accuracy. The half-life of ^{178}Pb was compared to recent theoretical calculations [Santhosh15], and put into a systematic context advancing the Pb systematics to further neutron deficiency.

Studying α-decay properties of even-mass Pb isotopes yields information about proton-shell closure over a wide variation of neutron number. In fact, lead nuclei below $N = 113$ have α-decay branches from their ground states [ens] allowing their ground-state properties to be studied despite relatively low production yields. A very powerful quantity revealing most of the nuclear structure information through α decay is the α-decay reduced width δ_α^2 [Rasmussen59], which can be extracted from the α-decay partial half-lives and energies. Systematic studies of reduced widths for ground state to ground state α-decay of even-Pb nuclei and also of known even-even nuclei ranging from platinum $Z = 78$ to thorium $Z = 90$ above and below the closed shell $Z = 82$, have been discussed previously in many articles [Van Duppen00, Toth99, Andreyev97, Venhart12, Wauters94, Andreyev13a]. The general finding for Pb nuclei is that the α-decay reduced widths are smaller than those of its isotonic chain, and that deviations from this trend are brought about by the presence of intruder states and configuration mixing, due to shape coexistence. Also, the α-decay process is strongly accelerated by crossing the $Z = 82$ shell to higher proton numbers. Hence, the existence of the $Z = 82$ closed shell is evident. This disagrees with an earlier study by Toth *et al.* [Toth84], who suggested that there was a disappearance of the $Z = 82$ shell closure midway between $N = 82$ and $N = 126$, where lead nuclei appeared to be less hindered toward α-decay than mercury isotopes in this region.

Recently, the relation between the α-particle preformation probability and the experimental pairing gap energy has been discussed by Andreyev *et al.* [Andreyev13a]. Striking resemblance was noticed, which demonstrated the effect of the shell closures of $N = 126$ and $Z = 82$ on the α-particle preformation probability and pairing gap energy values (see Fig. (2) in Ref. [Andreyev13a]). Extending this study toward more neutron-deficient nuclei to observe the effect of weak proton binding on the α-particle preformation probability, when approaching $N = 82$ would be interesting. Furthermore, the validity of the Geiger-Nuttall rule has also been brought into question by Qi *et al.* [Qi14]. The importance of identifying the

microscopic basis of the Geiger-Nuttall (GN) coefficients and the need for more data points for more accurate α-decay energy and half-life systematics is evident.

Chapter 2

Physics background

In this chapter the theoretical background relevant to the present work is introduced. Firstly, the spherical and deformed nuclei are discussed, with emphasis on topics related to the present thesis. Following that, radioactive decay and its different forms are presented. Lastly, various nuclear decay processes, focusing on both α decay and electromagnetic transitions are discussed.

2.1 Nuclear models

The atomic nucleus is the dense core of an atom consisting of protons and neutrons. The mass of the nucleus is less than the sum of its constituent nucleons (protons and neutrons), due to the nuclear binding energy B, which can be expressed as follows

$$B(Z, A) = [ZM_H + NM_n - M]\, c^2, \tag{2.1}$$

where M is the mass of the atom. The masses of the hydrogen atom and of the neutron are M_H and M_n, respectively. Plotting the binding energy per nucleon (B/A) of the stable nuclei as function of their mass number A gives approximately a constant B/A value except for the very light nuclei (see Ref. [Lilley13, p. 41]). The curve reaches a maximum at $A = 60$, where $B/A \simeq 8.6$ Mev.

The energy required to remove a nucleon either proton or neutron is called the proton separation energy S_p and the neutron separation energy S_n, respectively. Both the neutron and proton separation energies can be defined in terms of the binding energy (i.e. $S_p = B(Z, A) - B(Z-1, A-1)$). In the nuclear chart, as the proton number Z increases with respect to the neutron number N, the proton separation energy decreases until at a certain N/Z ratio, $S_p \lesssim 0$. This leads to proton unbound nuclei, and the point at which $S_p = 0$ defines the proton drip line.

2.1.1 Liquid drop model

Early attempts to understand the behaviour of the B/A curve features, proton and neutron drip line boundaries and some other nuclear properties (e.g. nuclear fission) were made by Weiszäcker [Von Weizsacker35]. He assumed the atomic nucleus behaves like a drop of liquid and formulated the liquid drop model (LDM). The total nuclear binding energy can then be defined using the semi-empirical mass formula (Weiszäcker formula) [Von Weizsacker35] as follows

$$B(Z,A) = a_{vol}A - a_{surf}A^{2/3} - a_{coul}\frac{Z^2}{A^{1/3}} - a_{sym}\frac{(A-2Z)^2}{A} + \delta, \tag{2.2}$$

$$\delta = \begin{cases} 12A^{1/2} & Z \text{ and N are even} \\ 0 & \text{odd A} \\ -12A^{-1/2} & Z \text{ and N are odd} \end{cases}$$

The first two terms describe a spherical liquid drop, which contributes to the total nuclear binding energy B through the volume and surface terms a_{vol} and a_{surf}, respectively. The total nuclear binding energy is also corrected for the electrostatic repulsion between protons, via the Coulomb term a_{coul}. The last two terms deal more with individual nucleons, where the asymmetry term, a_{sym}, corrects for the difference in the number of protons and neutrons in the nucleus. The pairing term δ implies that nucleons prefer to form pairs.

The liquid drop model was successful in explaining and predicting some nuclear properties. However, the LDM failed to describe more specific details. For instance, the deviation of S_p, S_n and Q_α values as a function of nucleon number from a smooth trend at certain numbers of Z and N. These specific nucleon numbers: N, Z = 2, 8, 20, 28, 50, 82, and N = 126, are known as the magic numbers. This limitation of the LDM is caused by the classical approach that considers the nucleus as a macroscopic entity, not taking into account the quantum behaviour.

2.1.2 Spherical nuclei

In order to explain the nuclear magic numbers a shell-like structure for nucleons was considered. Similar to that for the electrons in the atom, the magic numbers represent the shell closures. This shell structure can be expressed using the potential energy $V(r)$ in the equation 2.3, with the assumption that protons and neutrons are moving independently inside the nucleus and the potential is generated by all other surrounding nucleons. Such a potential can be described by a Woods-Saxson (W.S.) potential, defined as

$$V(r) = \frac{-V_0}{1 + exp[\frac{(r-R)}{a}]} \ , \tag{2.3}$$

where R is the mean nucleus radius ($R = 1.25A^{-1/3}$ fm), a is the skin thickness and V_0 is the depth of the potential well.

The resulting energy levels shown in figure 2.1(b), can be obtained by solving the three dimensional Shcrödinger equation using the parametrization in equation 2.3 for the W.S. potential. The type of potential defines the ordering of the levels. For instance, the energy levels in figure 2.1(a) are produced by a nucleon in an infinite spherical well.

In figures 2.1(a) and (b), the orbitals are labelled according to quantum numbers n and l, where n is the number of a given orbital with angular momentum quantum number l. The spectroscopic notation (s, p, d, f, g, h, i, ...) is used for different values of the quantum number l (l = 0, 1, 2, 3, 4, 5, 6, ...). The maximum number of protons or neutrons the orbital l can contain (degeneracy) is $2(2l + 1)$. Both the infinite well and the W.S. potentials fail to reproduce the magic numbers, above N, $Z = 20$ as can be seen in Fig. 2.1. In 1949 a successful attempt was made to reproduce all magic numbers by Mayer and by Haxel, Jensen and Suess by including a spin orbit (SO) potential, resulting in the splitting of l-orbitals as shown in figure 2.1(c). The spin orbit potential has a form of $-V_{so}(r)\boldsymbol{l} \cdot \boldsymbol{s}$, where $\boldsymbol{s}$ is the spin angular momentum. The energy levels in figure.2.1(c) can then be labelled using the quantum numbers n, l and j. The total angular momentum $\boldsymbol{j}$ is defined as follows,

$$\boldsymbol{j} = \boldsymbol{l} + \boldsymbol{s} \ . \tag{2.4}$$

The spin quantum number of the nucleon is, $s = \pm 1/2$. The possible values of the total angular momentum quantum number are $j = l + \frac{1}{2}$ and $j = l - \frac{1}{2}$ (if $l = 0$ only $j = 1/2$ is allowed). The SO term can be calculated from equation 2.4 as

$$< \boldsymbol{l} \cdot \boldsymbol{s} > \ = \frac{1}{2}[j(j+1) - l(l+1) - s(s+1)]\hbar^2 \tag{2.5}$$

$$< \boldsymbol{l} \cdot \boldsymbol{s} > \ = \begin{cases} \frac{1}{2} l \hbar^2 & j = l + \frac{1}{2} \\ \\ -\frac{1}{2}(l+1)\hbar^2 & j = l - \frac{1}{2} \end{cases}$$

The degeneracy for a given j-orbital is $2j + 1$, which comes from the magnetic substates value m_j ($m_j = j, j-1, ... -j+1, -j$), (see Fig. 2.1(c)).

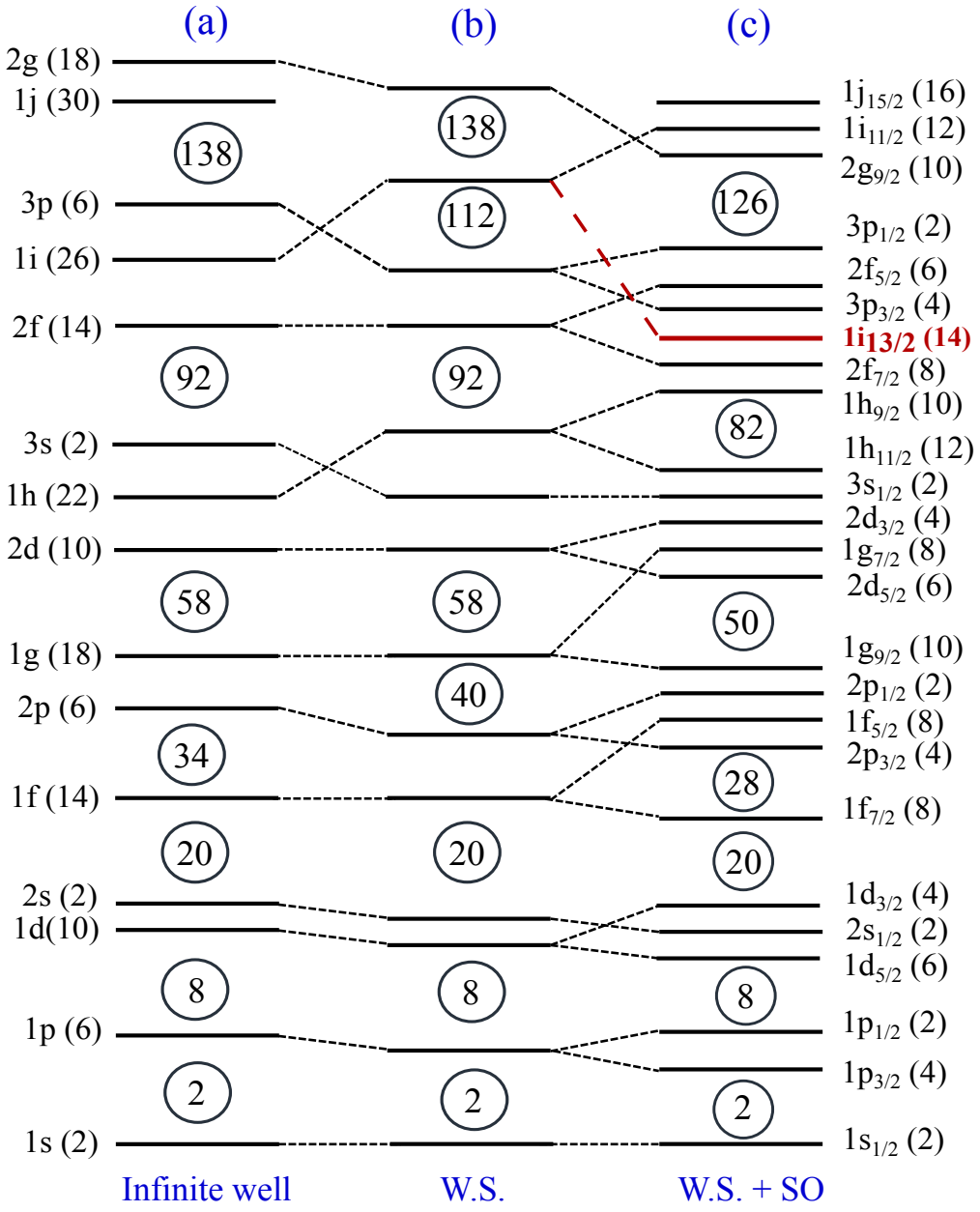

Figure 2.1: A schematic drawing of the energy levels of the single-particle orbitals using different nuclear potentials based on Ref. [Lilley13]: (a) Infinite well, (b) Woods-Saxon potential (W.S.) and (c) Woods-Saxon potential coupled with the spin orbit (SO) interaction. The red line shows an example of the unique parity intruder orbital $1i_{13/2}$.

Nucleons have a strong tendency to be paired, and therefore the neutrons and protons couple to a 0^+ pair, when possible. Hence, the ground state spin[1] and parity I^π of even-Z even-N nuclei is 0^+, while for the odd-A nuclei the ground state spin of a nucleus is determined by the last unpaired nucleon.

Unique-parity orbitals

Parity π is a quantum number which reveals the symmetry properties of the wave function with orbital angular momentum, l. Parity is expressed as $\pi = (-1)^l$. Thus, odd-l orbitals will then have negative parity (π = -) and even-l orbitals have positive (π = +) parity.

In equation 2.5, the effect of the spin-orbit interaction is evident. The splitting of a given l orbital will force the high-j ($j = l + \frac{1}{2}$) down in energy toward the lower orbitals, which have an opposite parity. On the other hand, the lower-j ($j = l - \frac{1}{2}$) orbital is pushed up, gaining more energy. These unique parity orbitals $j = l + \frac{1}{2}$, are called an "intruder" states within the shell-model frame work. Figure 2.1(c) reveals the result of the Woods-Saxson potential and the spin-orbit interaction coupling, previously mentioned. The marked line shows how the $1i_{13/2}$ orbital with positive parity (even-l) pushes down in energy to become a shell-model intruder state, where the neighbouring orbitals have negative parity (odd-l orbitals). The fact that such a state exists, and is surrounded by states with different parities and angular momenta, results in nuclear transitions from these states often being hindered. This phenomenon was noticed in the Pb odd-mass isotopes, where the $\nu i_{13/2}$ unique-parity state in most cases forms an isomeric state [ens]. Also, around the $Z = 82$ closed-shell region both the $h_{11/2}$ and $i_{13/2}$ unique-parity shell-model orbitals are active in determining the structure and shape of nuclei in this region [Scholey10, O'Donnell09, Melerangi03].

2.1.3 Deformed Nuclei

Some experimental features around the nuclear chart could not be explained by the spherical shell model. Assuming that the nucleus can have a deformed shape was a key point in explaining many experimental phenomena, such as the large quadrupole moments [Rainwater50]. The model describing deformed nuclei is called the "deformed shell model" which was introduced for the first time by Nilsson in 1955 [Nilsson55, Mottelson55], by modifying the spherical shell model. The total angular momentum j that was introduced in the spherical shell model is no longer a good quantum number in the case of deformed nuclei. The degeneracy of $2j + 1$,

[1] The word spin is often used for the total angular momentum I of a state.

that was proposed earlier in the spherical case, is broken in the Nilsson model and a new set of quantum numbers is required. The quantum number Ω is presented instead, with only twofold degeneracy (two nucleons $\pm\Omega$), where Ω is defined as the projection of orbital total angular momentum j on the symmetry axis.

The nuclear deformation that was considered in the Nilsson model can be described using the quadrupole-deformation parameter β_2. A negative value of the quadrupole-deformation parameter ($\beta_2 < 0$) stands for oblate (pancake-like) deformation, while a positive value ($\beta_2 > 0$) describes a prolate (cigar-like) deformation. The deformation parameter β_2 can be expressed as follows [Krane88, p.142],

$$\beta_2 = \frac{4}{3}\sqrt{\frac{\pi}{5}}\,\frac{\Delta R}{R_{ave}}\ . \tag{2.6}$$

The average radius R_{ave} is defined as, $R_{ave} \simeq \frac{1}{3}(a + 2b)$ [Bohr75, p.47], where a and b are two axes of the ellipsoid shown in Fig. 2.2. The difference between these axes is $\Delta R = a - b$. The ellipsoid in Fig. 2.2 corresponds to a prolate deformation, where the deformation parameter was chosen to have $\beta_2 \sim 0.2$.

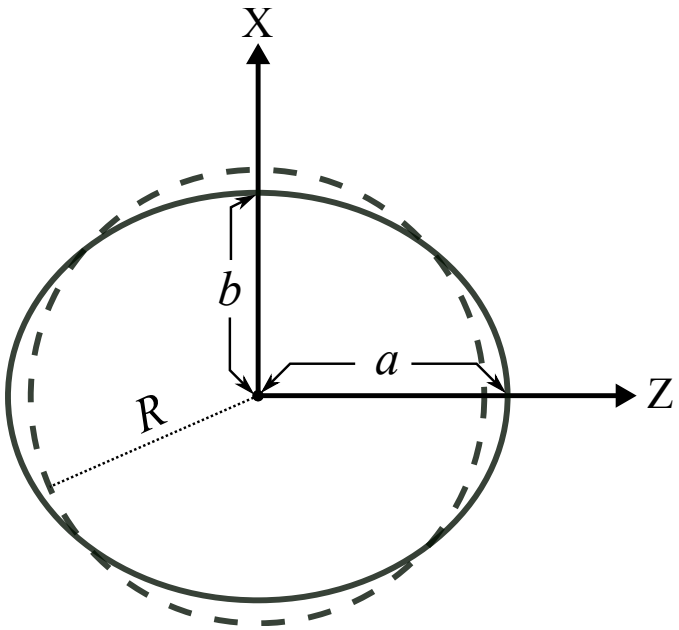

Figure 2.2: The solid line represents an ellipsoid associated with a prolate deformation of $\beta_2 \sim 0.2$. The ellipsoid is compared with a circle ($\beta_2 = 0$) drawn with a dashed line, having a radius R and the same volume as the ellipsoid.

The shape of the nucleus is very sensitive to structural effects. It can change from one nucleus to its neighbour (changing the proton Z or neutron N number), see Ref. [Hilaire07, Fig.1]. Also, the nuclear shape can change at low excitation energy over a very narrow energy range, of two or more states even within the same nucleus. The latter phenomenon, is called "shape coexistence" [Heyde11]. The region of neutron-deficient nuclei around the $Z = 82$ closed shell is particularly rich in shape coexistence, and much experimental information supporting the coexistence of deformed and near-spherical shapes at low excitation energies are deduced in these nuclei, see Ref. [Julin01] and references therein. These low-lying states very near and even at the closed shell are expected to be at a much higher excitation energy, hence the name "intruder states" has been introduced [Heyde94]. The formation of these intruder structures in the shell-model picture is understood as multi-particle multi-hole (mp - mh) excitations across the shell closure. Due to proton excitations across the shell gap a number of valence protons (holes) will be formed. The interaction between the particle-hole configurations and the valence neutrons (proton-neutron residual interaction) results in the low excitation energy of the intruder states [Heyde11, Heyde88]. Another theoretical tool to describe the intruder states, is the Nilsson model [Nilsson55, Mottelson55] discussed above. In this approach, the high-Ω orbitals are lowered in energy when going toward more oblate deformation, while the energy of low-Ω orbitals their energy is decreases with increasing prolate deformation. Hence, the energy needed to excite protons across the shell gap is lowered compared to the spherical situation. For instance, in odd-mass Tl isotopes the well known low-lying $9/2^-$ intruder states are understood within the deformed shell-model as an odd-proton occupying the oblate-driving $9/2^-[505]$ Nilsson orbital. In the spherical shell-model approach, these intruder low-lying states are one-particle two-hole ($1p - 2h$) states, resulting from proton excitation across the $Z = 82$ shell gap to the $\pi h_{9/2}$ orbital.

2.2 Radioactive decay

Radioactive decay is the process by which an unstable nucleus 'mother' is transformed to a more stable nucleus 'daughter' by emitting a particle ($\alpha, \beta, p, ..$). This process will continue in a decay chain until a stable nucleus is reached. Electromagnetic transitions will be able to compete with particle emission, when the particle emission is hindered. In the present work we will discuss both α decay and electromagnetic transitions.

The decay rate of a radioactive sample having N nuclei can be described by the radioactive-decay law using the following equation

$$\frac{dN}{dt} = -\lambda \cdot N, \tag{2.7}$$

where λ is the decay constant and the minus sign indicates that the number of nuclei decreases as the time t increases. The solution of the previous equation can then be defined as

$$N(t) = N_0 \cdot e^{-\lambda t}, \tag{2.8}$$

where N_0 is the number of decaying nuclei at t = 0. The decay constant is related to the half-life $t_{1/2}$ of the decaying nuclei, which is the time when half of the nuclei in a given sample have decayed, defined as

$$t_{1/2} = \frac{ln(2)}{\lambda}. \tag{2.9}$$

Furthermore, the nuclear state may have decay branches to several final states. In this case the total decay constant for the all branches is the sum of individual partial decay constants. The partial half-life $t^a_{1/2}$ for a branch a, can be determined from the total half-life as follows,

$$t^a_{1/2} = \frac{t_{1/2}}{b_a}, \tag{2.10}$$

where b_a is the branching ratio.

2.2.1 Alpha decay

α decay is a type of radioactive decay, which occurs naturally in many of the heavy nuclei. α particles were first identified by Rutherford [Rutherford99] in 1899 and then correctly described as a system consisting of two protons and two neutrons, forming the nucleus of the helium atom ${}^4_2\mathrm{He}_2$ in 1907. The α-decay process is illustrated in equation 2.11, where the mother nucleus X loses both mass and charge by emitting an α particle resulting in the daughter nucleus Y.

$${}^{A}_{Z}\mathrm{X}_{\mathrm{N}} \longrightarrow {}^{\mathrm{A-4}}_{\mathrm{Z-2}}\mathrm{Y}_{\mathrm{N-2}} + \alpha \tag{2.11}$$

In α decay the angular momentum carried by the α-particle l_α must obey angular momentum conversation such that,

$$|I_i - I_f| \leq l_\alpha \leq |I_i + I_f|, \tag{2.12}$$

where I_i and I_f are the total angular momentum of the initial and final state, respectively. The parity selection rule can be expressed from $\pi_f = \pi_i(-1)^{l_\alpha}$. Hence, if the parities of the initial and the final state are the same $\pi_f = \pi_i$ then l_α must be even and if $\pi_f \neq \pi_i$ then l_α must be odd.

Alpha-decay Q-value

The energy release in the α-decay process known as the Q-value can be calculated from the mass difference of the α-decaying mother nucleus and the final products as follows:

$$Q_\alpha = (M_m - M_d - M_\alpha)\, c^2, \tag{2.13}$$

where M_m, M_d and M_α are the atomic masses of the mother, the daughter nuclei and the α particle, respectively. By measuring the α-particle energy E_α, the experimental α-decay Q_α-value can be derived from energy and momentum conservation as

$$Q_\alpha = E_\alpha \left(1 + \frac{M_\alpha}{M_d}\right) \simeq E_\alpha \left(1 + \frac{4}{A_d}\right), \tag{2.14}$$

where A_d is the daughter mass number.

In the case of electron bare nuclei the α-decay Q_α^{bare}-value should be corrected for the screening effect E_{Sc} of the atomic electrons on the α particle. The equation 2.14 will then be defined as

$$Q_\alpha^{bare} \simeq E_\alpha \left(1 + \frac{4}{A_d}\right) + E_{Sc}, \tag{2.15}$$

for the bare nuclei.

The electron-screening correction term E_{Sc} for the α decay was discussed earlier by Perlman *et al.* [Perlman57], and is given as

$$E_{Sc} = 65.3 \cdot Z_m^{7/5} + 80 \cdot Z_m^{2/5}. \tag{2.16}$$

On the other hand, Huang *et al.* [Huang76] derived the screening term coefficients for different atomic numbers of the mother Z_m and daughter Z_d nuclei using the following equations

$$\begin{aligned} E_{Sc} &= k(Z_m^\epsilon - Z_d^\epsilon) \\ k &= 8.7\ eV, \epsilon = 2.517 \quad \text{for Z} \geq 60 \\ k &= 13.6\ eV, \epsilon = 2.408 \quad \text{for Z} < 60 \end{aligned} \tag{2.17}$$

where E_{Sc} in both equations is in eV. For instance, the electron-screening correction for lead nuclei ($Z = 82$) using the equation 2.16, is $E_{Sc} \sim 30$ keV.

Theory of alpha decay

The relation between the α-particle energy and the α-decay partial half-life was investigated earlier by Geiger and Nuttall (GN) in 1911 [Geiger11]. This relation can be expressed using the following equation:

$$log_{10}(t_{1/2}) = A(Z) \cdot Q_{\alpha}^{-1/2} + B(Z), \tag{2.18}$$

where $t_{1/2}$ is the α-decay partial half-life in s and Q_α is in MeV. As can be seen from this equation, the higher the total energy of the α-decay process (Q-value) the shorter the half-life is. The correction coefficients $A(Z)$ and $B(Z)$ are obtained by fitting the experimental data of different α-decays from the same isotopic chains. Recently, Qi *et al.* [Qi14] discussed the physical meaning of the $A(Z)$ and $B(Z)$ coefficients and the relation between the α preformation probability and the GN law.

The first attempt to explain the α particle emission process was developed in 1929 by Gurney and Condon [Gurney29] and separately by Gamow [Gamow29]. The theory assumes that the α particle is preformed inside the mother nucleus and tries to escape through the potential barrier $V(r)$ of the daughter nucleus. In the quantum mechanical frame work the α particle can escape through the Coulomb barrier by the tunnelling effect. The penetration probability p, can then be expressed as

$$p = exp\left\{-2\int_{R_i}^{R_0} \frac{2\mu^{1/2}}{\hbar}\left[V(r) - Q_{\alpha}^{bare}\right]^{1/2} \cdot dr\right\}, \tag{2.19}$$

where μ is the reduced mass which is expressed as

$$\mu \simeq \frac{4 \cdot A_d}{(4 + A_d)} \cdot m_u, \tag{2.20}$$

where m_u is the atomic mass unit.
The penetration probability p in equation 2.19 can be calculated by applying the WKB-integral over the radius r in the classically forbidden region between the inner R_i and outer R_0 turning points [Rasmussen59].

The calculated decay time constant λ_{calc} in the α decay, can then be defined as

$$\lambda_{calc} = \frac{ln(2)}{t_{1/2}^{calc}} = f \cdot p, \tag{2.21}$$

where f is the knocking frequency of the α particle toward the potential wall of the daughter nucleus and λ_{calc} is in unit of s^{-1}.

Hindrance factor and reduced alpha-decay width

Comparisons between theoretical and measured half-life values are a very powerful means for revealing the structural changes between the mother and daughter nuclei of the α decay. One such spectroscopic tool is the α-decay reduced width δ_α^2 [Perlman57] which can be expressed as

$$\delta_\alpha^2 = \lambda_{exp} \cdot \frac{h}{p}, \tag{2.22}$$

where p is the penetration probability discussed above, λ_{exp} is the experimental α decay rate in units of s^{-1}, h is Planck's constant and δ_α^2 is in units of eV.

The potential barrier $V(r)$ in equation 2.19 was calculated by Rasmussen [Rasmussen59] using three different terms as follows

$$V(r) = -1100 \cdot exp\left[-\left(\frac{r - 1.17 \cdot A^{1/3}}{0.574}\right)\right] + \frac{2Ze^2}{4\pi\epsilon_0 r} + \frac{\hbar^2}{2\mu r^2} l(l+1)\ . \tag{2.23}$$

The first term is the nuclear potential presented by Igo [Igo58], where r is the distance in femtometres and A is the mass number of the daughter nucleus. The second term is the Coulomb potential and the third one is the centrifugal potential, where Ze is the charge on the daughter nucleus and l is the orbital angular momentum carried by the alpha particle.

The ratio between the experimental partial half-life $t_{1/2}^{exp}$ and calculated half-life $t_{1/2}^{calc}$ defines another spectroscopic tool, the hindrance factor HF as follows

$$HF = \frac{t_{1/2}^{exp}}{t_{1/2}^{calc}}\ . \tag{2.24}$$

The half-life $t_{1/2}^{calc}$ can be calculated using the Rasmussen method [Rasmussen59] in the equation 2.21. The knocking frequency f needed for the $t_{1/2}^{calc}$ estimation is normalised to the unhindered ground-state to ground-state α decay of ^{212}Po to the doubly magic ^{208}Pb nucleus. For a favoured α decay the hindrance factor HF value is less than four. This is an indication that the configuration of the initial and the final state is the same. Hindrance factor values larger than four are associated with hindered (unfavoured) α decays.

In addition to the Rasmussen method [Rasmussen59] that was discussed in this section, many other models has also been developed to predict the half-lives of the α decay of heavy and super heavy nuclei (see Ref. [Santhosh15] and references therein).

2.2.2 Gamma-ray Transitions

In radioactive decays and nuclear reactions the residual nucleus likely ends up in an excited state. This nucleus can de-excite via electromagnetic transitions, by emitting γ rays. When a nucleus de-excites from an initial state with energy E_i, an angular momentum I_i and parity π_i to a final state E_i, I_f and π_f, the γ-ray transition energy can be defined as

$$E_\gamma \simeq E_i - E_f \ . \tag{2.25}$$

The emitted γ-ray photon will carry non zero angular momentum L, which is called "multipolarity" and parity denoted as π_γ. The type σ of the electromagnetic radiation can be either an electric E or magnetic M for each L value. The parity of each radiation type can then be expressed as

$$\begin{aligned} \pi_\gamma(ML) &= (-1)^{L+1} \\ \pi_\gamma(EL) &= (-1)^{L} \ . \end{aligned} \tag{2.26}$$

Conservation of angular momentum demands that the initial angular momentum must be equal to the total final angular momentum, $\overrightarrow{I_i} = \overrightarrow{L} + \overrightarrow{I_f}$. The angular momentum selection rules can then be defined as

$$|I_i - I_f| \leq L \leq |I_i + I_f| \ . \tag{2.27}$$

The identification of the type of the electromagnetic radiation as either magnetic, M, or electric, E, is determined by the parity of the initial and final states. As shown in the equation 2.26, electric and magnetic electromagnetic radiation are different in their parity. Thus, the parity selection rules can be summarized as follows [Krane88]

$$\begin{aligned} \Delta\pi = &\text{No} \quad L = \text{even for electric, } L = \text{odd for magnetic,} \\ \Delta\pi = &\text{Yes} \quad L = \text{odd for electric, } L = \text{even for magnetic,} \end{aligned} \tag{2.28}$$

where $\Delta\pi$ is the parity change between the initial and final state.

A comparison between the experimental partial γ-ray half-life $t_{1/2}^{exp}$ and theoretical calculations $t_{1/2}^{w}$, can be made using the ratio $t_{1/2}^{w}/t_{1/2}^{exp}$, where the theoretical γ-ray half-life $t_{1/2}^{w}$ is determined using single-particle estimates as proposed by Weisskopf [Weisskopf51]. Weisskopf estimated the transition probability λ of the electromagnetic radiation (see equation 2.29), by assuming that the emitted radiation is due to a transition of a single proton in the nucleus.

$$\lambda = \frac{ln(2)}{t^{w}_{1/2}} \ . \tag{2.29}$$

Table 2.1 shows the resulting transition probabilities evaluated by Weisskopf [Weisskopf51] for several multipolarities.

Table 2.1: Weisskopf estimates of transition probabilities for the first four electric and magnetic multipoles. The transition energies are given in units of MeV. The equations are taken from Ref. [Krane88, p.332].

EL	$\lambda(EL)$ [s^{-1}]	ML	$\lambda(ML)$ [s^{-1}]
$E1$	$1.0 \times 10^{14} A^{2/3} E^3$	$M1$	$5.6 \times 10^{13} E^3$
$E2$	$7.3 \times 10^{7} A^{4/3} E^5$	$M2$	$3.5 \times 10^{7} A^{2/3} E^5$
$E3$	$34 \times A^2 E^7$	$M3$	$16 \times A^{4/3} E^7$
$E4$	$1.1 \times 10^{-5} A^{8/3} E^9$	$M4$	$4.5 \times 10^{-6} A^2 E^9$

2.2.3 Internal conversion

Internal conversion is a competing process to γ-ray emission whereby the nucleus de-excites by transferring its energy to an inner orbital atomic electron. Hence, the ejected electron in the internal conversion process will have an energy as follows

$$E_e = E_\gamma - B_e, \tag{2.30}$$

where B_e is the binding energy of the atomic electron listed in Ref. [Firestone97] and E_γ is the transition energy obtained from relation 2.25. In addition, emitting a conversion electron leaves a vacancy in the inner electronic shell. This vacancy will be rapidly filled by a less-bound electron from a higher orbital and the released energy is carried away by characteristic X-rays. Identification of the produced isotopes is possible by observing such characteristic X-rays experimentally. As an alternative to X-ray emission the released energy could be carried away by another atomic electron, called an Auger electron.

The competition between γ-ray emission and internal conversion can be expressed using the total conversion coefficient α_{tot} as follows

$$\alpha_{tot} = \frac{\lambda_e}{\lambda_\gamma}, \tag{2.31}$$

where λ_e and λ_γ are the partial decay time constant of internal conversion and γ-ray emission, respectively. The total decay time constant can then be defined in terms of the total conversion coefficient as follows

$$\lambda_{tot} = \lambda_e + \lambda_\gamma = \lambda_\gamma(1 + \alpha_{tot}) = \lambda_e(1 + \frac{1}{\alpha_{tot}}) \ . \tag{2.32}$$

Furthermore, the total conversion coefficient α_{tot} is expressed as the sum of all partial conversion coefficients of the electrons in atomic orbitals $(K, L, M, ...)$

$$\alpha_{tot} = \alpha_K + \alpha_L + \alpha_M + ... \ . \tag{2.33}$$

A comparison between the experimental internal-conversion coefficient and the theoretical calculation gives an indication to the multipolarity of the transition. The experimental internal-conversion coefficient can be deduced by measuring the intensity ratio of γ rays and conversion electrons, while the calculated one can be obtained using the equations in Ref. [Kibedi08] or with software codes such as BRICC.

Chapter 3

Experimental techniques

A brief introduction to the fusion-evaporation reaction that was used to produce the studied neutron-deficient nuclei will be presented at the beginning of this chapter. That is followed by a brief description of the main experimental instrumentation that was used in the present work. Lastly, the data processing and analysis technique will be presented at the end of the chapter.

3.1 Fusion evaporation reactions

A common method of producing very neutron-deficient nuclei is via fusion-evaporation reactions. Looking at the nuclear chart it can be seen that as both the neutron and the proton number increases the valley of stability moves away from the $N = Z$ line toward more neutron rich nuclei. This opens up the possibility to produce exotic nuclei on the neutron-deficient side of the valley of stability by fusing two stable nuclei. Figure 3.1 reveals an example of forming exotic nuclei beyond the proton drip-line. In a fusion-evaporation reaction two nuclei are brought together at a certain energy above the Coulomb barrier V_c resulting in a highly-excited compound nucleus. The Coulomb barrier between the projectile and target nucleus can be expressed by the following formula:

$$V_c \simeq \frac{Z_p \cdot Z_t}{A_p^{1/3} + A_t^{1/3}} \text{ MeV} , \tag{3.1}$$

where the (Z_p, A_p) and (Z_t, A_t) represent the atomic and mass number of the projectile and target nuclei, respectively. The highly-excited compound nuclei subsequently undergo particle (neutron, proton, alpha etc) evaporation before decaying via γ-ray emission. The excitation energy E^* of the compound system can be defined by the reaction Q-value as follows

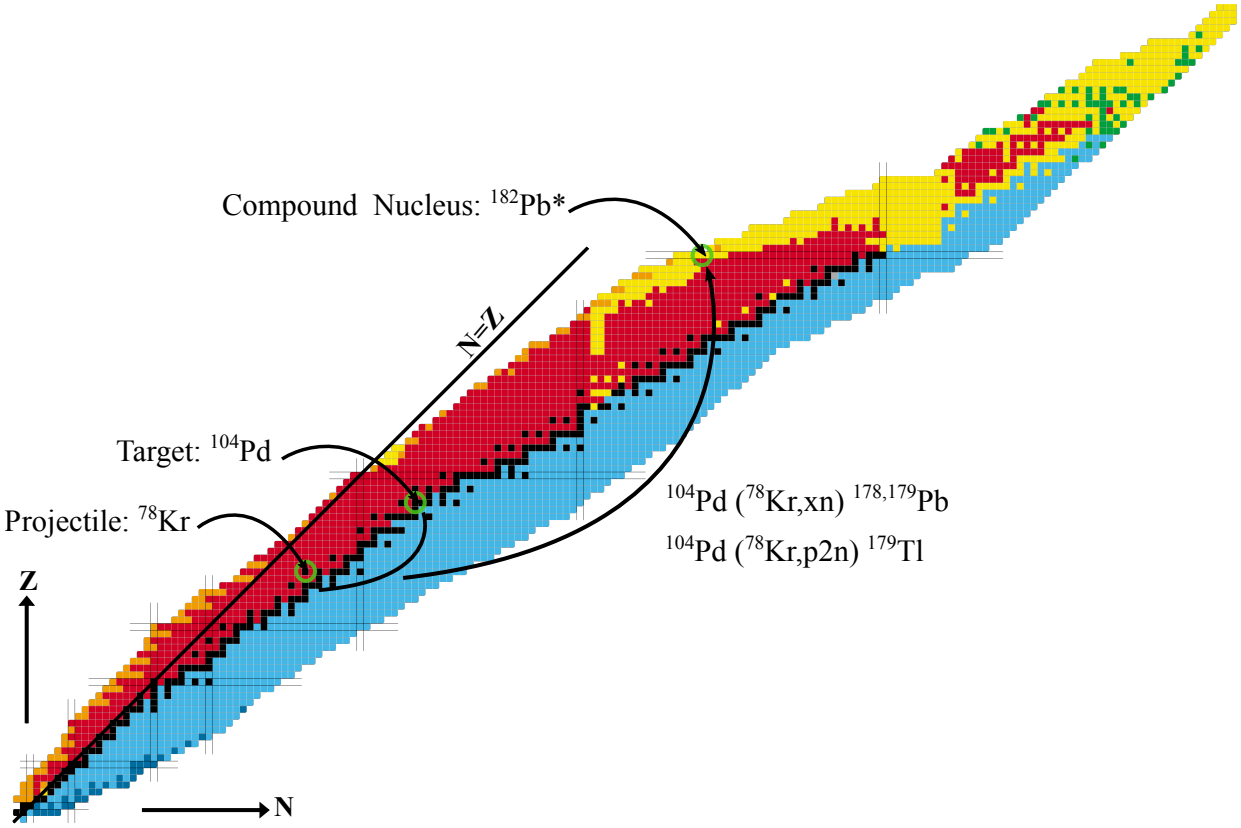

Figure 3.1: An illustration of the nuclear chart with the $N = Z$ line labelled. The figure shows the possibility of producing exotic nuclei beyond the proton drip-line by fusing two stable nuclei in a fusion-evaporation reaction. The reaction used in the present work is shown.

$$E^* = E_{cm} + Q \ , \tag{3.2}$$

where E_{cm} is the kinetic energy of the nuclei at the centre of mass, which can be written in terms of the kinetic energy in laboratory frame E_{lab} as

$$E_{cm} = \frac{A_t}{A_t + A_p} E_{lab}. \tag{3.3}$$

Figure 3.2 shows a schematic illustration of the fusion-evaporation process, where the different reaction phases and emission times are shown.

In the present work, the very neutron-deficient isotopes of interest ^{179,178}Pb and ^{179}Tl were produced using the fusion-evaporation reaction of ^{104}Pd(^{78}Kr,xn) and ^{104}Pd(^{78}Kr,$p2n$), respectively, at the Accelerator Laboratory of the University of

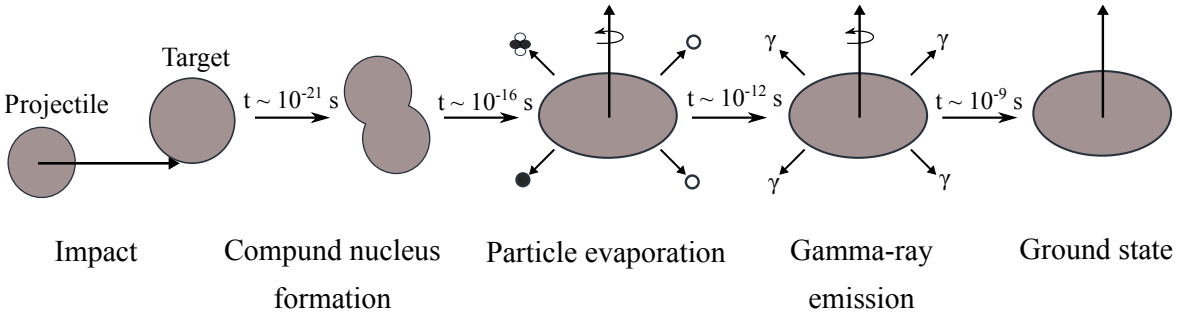

Figure 3.2: A schematic of the fusion-evaporation reaction process. The time scale of each phase for the case of heavy compound-nucleus is taken from Ref. [Bass80].

Jyväskylä, Finland. A heavy-ion beam of krypton $^{78}Kr^{15+}$ was produced using an electron cyclotron resonance ion source [Koivisto01] and accelerated by the K-130 cyclotron to an energy of 358 MeV. The beam impinged on a self-supporting ^{104}Pd target with a thickness and enrichment of 745 μg cm^{-2} and 95.25 %, respectively, which was rotated throughout the experiment. A 34 μg cm^{-2} thick carbon charge reset foil was positioned behind the target. The beam intensity during 224 hours of irradiation was, on average 140 pnA. The total production cross section σ of the evaporation residue of interest can be deduced from its reaction rate R as follows,

$$\sigma = \frac{R}{N \cdot I} , \tag{3.4}$$

where N is the number of target nuclei per unit area and I is the beam intensity. In the region of neutron-deficient nuclei in the vicinity of $Z = 82$ and above, the compound nucleus is likely to fission. In the present thesis work, it was estimated that more than $\sim$ 95 % of the total production cross-section fissioned. Table. 3.1 lists the production cross section estimates for $^{179,178}Pb$ and ^{179}Tl, taking into account the calculated RITU transmission efficiency [Sarén11], DSSD coverage and full energy α-particle detection efficiency of 50 %, 70 % and 55 %, respectively.

3.2 Instrumentation

3.2.1 The gas-filled separator RITU

Recoil separators have become a primary tool for nuclear structure studies, especially for the isotopes along proton drip-line produced in weak fusion-evaporation channels. In a gas-filled mode the separation of the recoiling nuclei of interest (recoils) from the beam and unwanted reaction products occurs based on the difference in the magnetic rigidity. The magnetic rigidity Bρ can be expressed as follows:

Table 3.1: Estimates of production cross-sections (σ) for ^{179,178}Pb and ^{179}Tl that were produced in the present work during 224 h of irradiation time. The E_b^{lab}, I_b^{ave} and d_t represent the beam energy, the average beam intensity and the target thickness, respectively.

Reaction	E_b^{lab} (MeV)	I_b^{ave} (pnA)	d_t (μg/cm^2)	σ (nb)
Pd(^{78}Kr, 3n)^{179}Pb	358	140	745	~ 0.2
Pd(^{78}Kr, 4n)^{178}Pb	”	”	”	~ 0.004
Pd(^{78}Kr, p2n)^{179}Tl	”	”	”	~ 30

$$B\rho = \frac{m\nu}{q_{ave}} , \tag{3.5}$$

where mν and q$_{ave}$ are the momentum of the reaction products and the average charge state of the ions, respectively.
The Recoil Ion Transport Unit (RITU) is a gas-filled recoil separator at the accelerator laboratory of the University of Jyväskylä [Leino95]. RITU is based on a standard DQQ magnetic configuration, where the magnetic quadrupoles (Q) are the focusing components and the dipole magnet (D) represents the separating component. An extra vertically focusing quadrupole magnet in front of the dispersion element was added, thus giving RITU a QDQQ configuration (see Fig. 3.3). The inner volume of the RITU separator is filled with a dilute He gas at a pressure of $\sim$ 1 mbar (0.9 mbar in the present work). The fusion-evaporation products (recoils) trajectory is determined by the average ionic charge state in the gas q$_{ave}$ and is independent of the original charge state at the exit of the thin target [Leino95]. This gives the gas-filled separator significantly higher transmission efficiency compared to the vacuum-mode separators, but at the expense of the mass resolution. Recoils are transported to the focal plane of RITU, while the beam-like particles will end up in the beam dump, as can be seen in Fig. 3.3.

3.2.2 The GREAT focal plane spectrometer

The Gamma Recoil Electron Alpha Tagging (GREAT) spectrometer [Page03] is positioned at the focal plane of the gas-filled separator RITU. GREAT comprises a combination of a gas detector (multi-wire proportional counter), silicon detectors used for charged-particle implantation, an array of silicon diodes for escaping

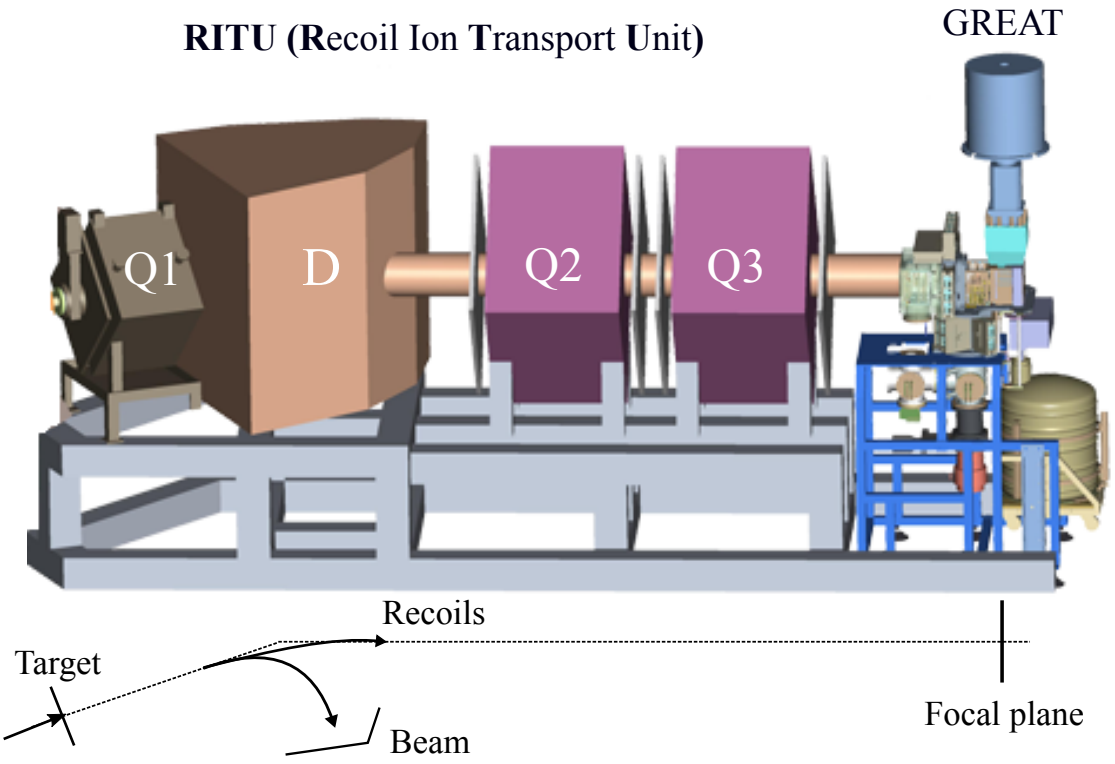

Figure 3.3: The gas-filled recoil separator RITU. The focusing quadrupole magnets and separating dipole magnet is denoted by letters (D) and (Q), respectively. RITU is typically filled with ~ 1 mbar of helium. Recoils are separated from the beam-like particle products in the dipole magnet and transported to the focal plane, where the GREAT spectrometer is placed.

particle detection and conversion electrons and a set of germanium detectors (planar and clovers) for γ-ray and X-ray detection. Figure. 3.4 shows a schematic view of the GREAT spectrometer set-up, comprising different detector types. GREAT was designed for isomer and decay spectroscopy studies of exotic nuclei that are produced with very low cross-sections, down to the pico barn level [Page03]; see table 3.1.

A multi-wire proportional counter (MWPC) is set at the entrance of GREAT filled with ~ 3.5 mbar of isobutane. Two 0.5 μm Mylar windows are at the entrance and the exit of the MWPC in order to contain the isobutane within the detector volume. Recoils that are transmitted through the RITU separator will then pass through the MWPC before being implanted in the double-sided silicon strip detectors (DSSDs). Information about energy loss (dE), time and position is obtained from the MWPC. The Time Of Flight (TOF) between the MWPC and DSSDs is also recorded.

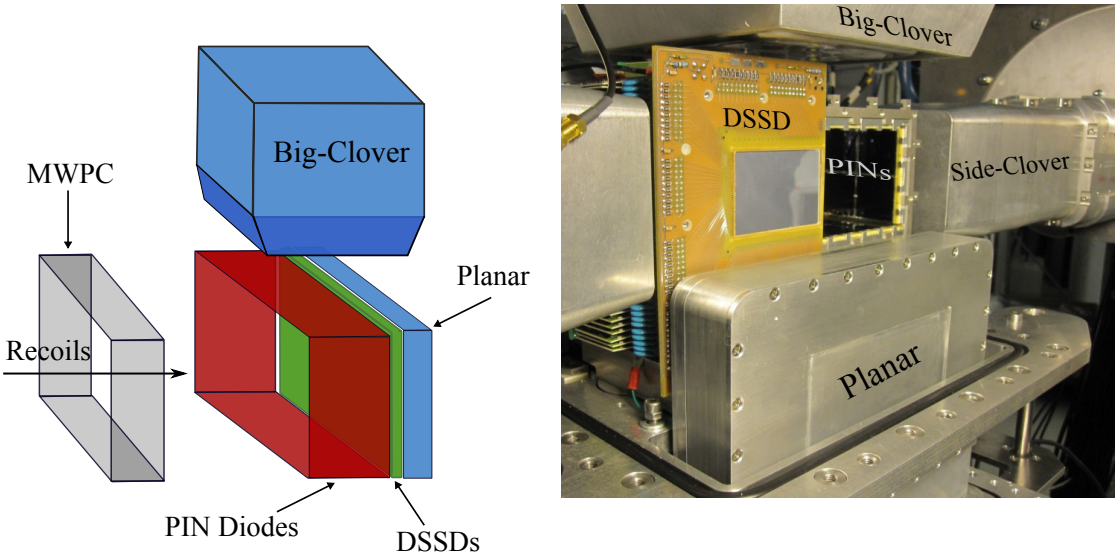

Figure 3.4: The GREAT spectrometer at the RITU focal plane, where the different elements of the spectrometer is shown.

Downstream from the MWPC, inside the vacuum chamber ($\sim 10^{-6}$ mbar) a set of two adjacent, 300 μm thick Double-Sided Silicon Strip Detectors (DSSD) are placed. Both DSSDs have an active area of 60×40 mm^2 and a strip pitch of 1 mm on both faces yielding 4800 pixels. The amplifier gain of both horizontal and vertical strips of the DSSDs were set to measure α-particle energies. The DSSD strips were first gain matched using a mixed ^{239}Pu, ^{241}Am and ^{244}Cm α-decay source. An internal calibration was then performed using the known α-particle energies of ^{176,179}Hg and ^{176}Pt, the values were taken from Refs. [Andreyev13b, Baglin09, Singh95]. Figure 3.5(a) shows an example of an α-particle energy spectrum detected in the GREAT DSSDs and vetoed by the gas counter (MWPC). The α-decaying nuclei used for an internal calibration are marked as well. The GREAT spectrometer has an adjustable degrader-foil system of aluminized mylar. In the present work a 700 μg/cm^2 degrader was positioned between the DSSDs and MWPC to reduce low-energy reaction products in the implantation detectors. Recoils are typically implanted into the DSSDs at depths of $\sim$ 1–10 μm [Page03], with the addition of a degrader foil the probability for α particles to escape from the detector without depositing its full energy will increase. Due to the shallow implantation depth of the fusion products in the DSSDs the full energy α-particle detection efficiency is $\sim$ 55 %.

An array of 14 PIN diodes, each with an active area of 28 x 56 mm^2 and 1 mm thickness, surrounds the DSSDs in the upstream position with respect to the beam

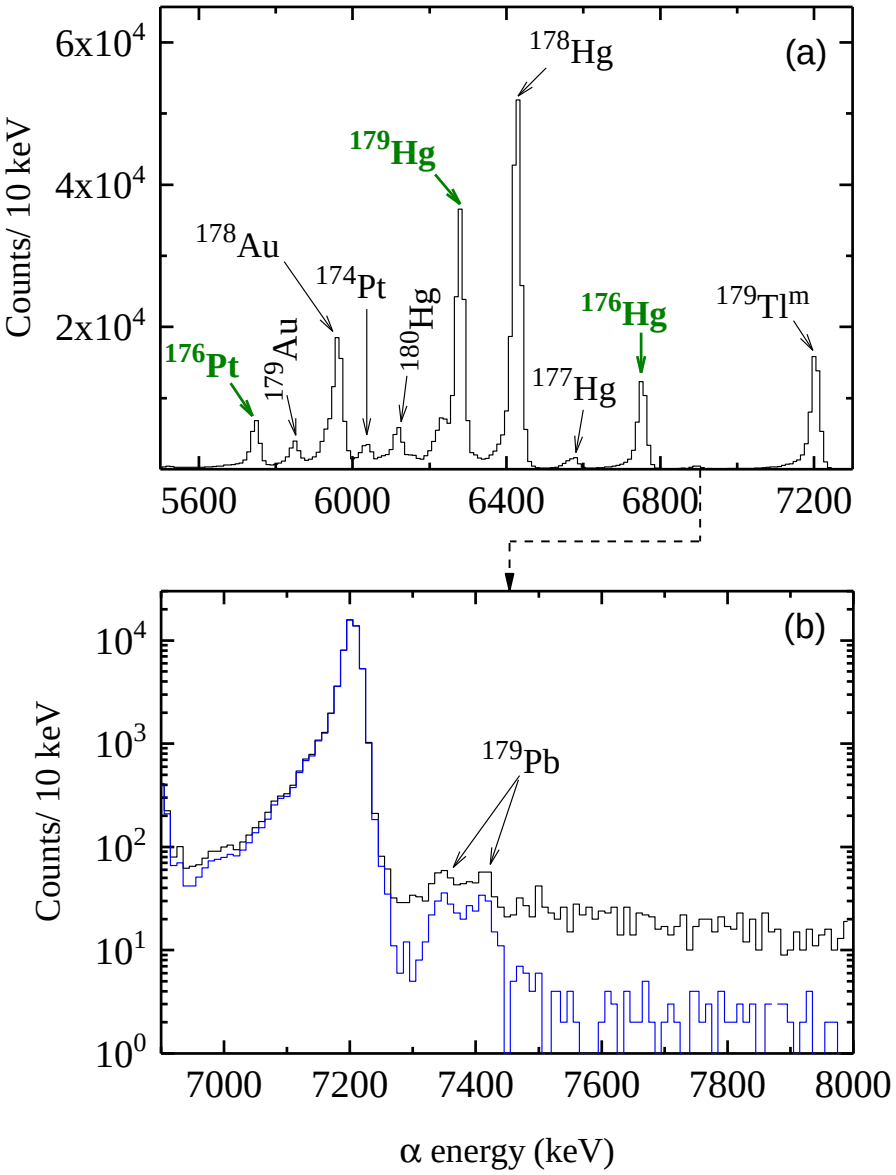

Figure 3.5: Energy spectra of α-particles correlated to a recoil implant within the same pixel in the DSSDs at the focal plane of RITU. A maximum search time of 20 ms was used for recoil-α correlation. (a) and (b) (black line) are correlated spectra vetoed by the gas counter (MWPC). The α-decays used for the internal calibration are marked (green colour). The blue line spectrum in (b) shows the effect of the planar Ge detector veto.

axis inside the vacuum chamber. The PIN diodes are used to detect escaping α-particles and conversion-electron events. To improve the detector resolution,

both the DSSDs and the PIN-diodes are mounted on an aluminium cooling block, which was cooled using circulating ethanol at a temperature of -25 °C.

A 15 mm thick planar double-sided germanium strip detector, with a 120×60 mm^2 active area and strip pitch of 5 mm, is positioned downstream directly behind the DSSDs inside the vacuum chamber. The planar Ge detector is used to detect low-energy γ rays and X-rays. In addition, it can be used to veto energetic light-particles that pass through the DSSDs depositing an amount of energy that overlaps with the α-particle energies from the nuclei of interest. Figure 3.5(b) (blue line) represents an example of using the planar Ge detector as a beam-like particle veto.

Surrounding the vacuum chamber of the GREAT spectrometer are one large volume and two EUROGAM type clover [Duchêne99] germanium detectors. The clover detectors are used for high-energy γ-ray and X-ray detection. Both the planar Ge detector and the clover detectors were calibrated using known γ-ray energies from ^{152}Eu and ^{133}Ba sources.

The efficiencies of the PIN diodes, planar Ge detector and the clovers that have been used in the present work are based on the result of GEANT4 simulations taken from Refs. [Hauschild13, Taimi15].

3.3 Data analysis

The data acquisition in the present work was performed using the triggerless Total Data Readout (TDR) system [Lazarus01]. All detectors channels are treated independently, meaning all events are read out individually and time-stamped with a precision of 10 ns. This precision is achieved by using a 100 MHz metronome.

An "OR" logic signal of any vertical DSSD strip of GREAT spectrometer was used as a software trigger in the present work. The trigger width was set depending on the decay properties of the nuclei of interest. The half-lives of states which decay via gamma-ray emission or conversion electrons is a dominating factor. Only events that occur within the trigger width are chosen for further analysis (see Fig. 3.6(a)). Furthermore, the identification of the fusion-evaporation products (recoils) was performed using a two-dimensional plot of the TOF versus the energy loss signal in the MWPC as can be seen in Fig. 3.6 (b). Hence, an appropriate 2D-gate was set to select the recoiling nuclei from beam/target-like particle events. Recoils are usually followed by multiple α-decay events. Only α-decay events that were observed subsequent to a recoil implanted within the same pixel in the DSSDs and within a predetermined time window were chosen for further processing.

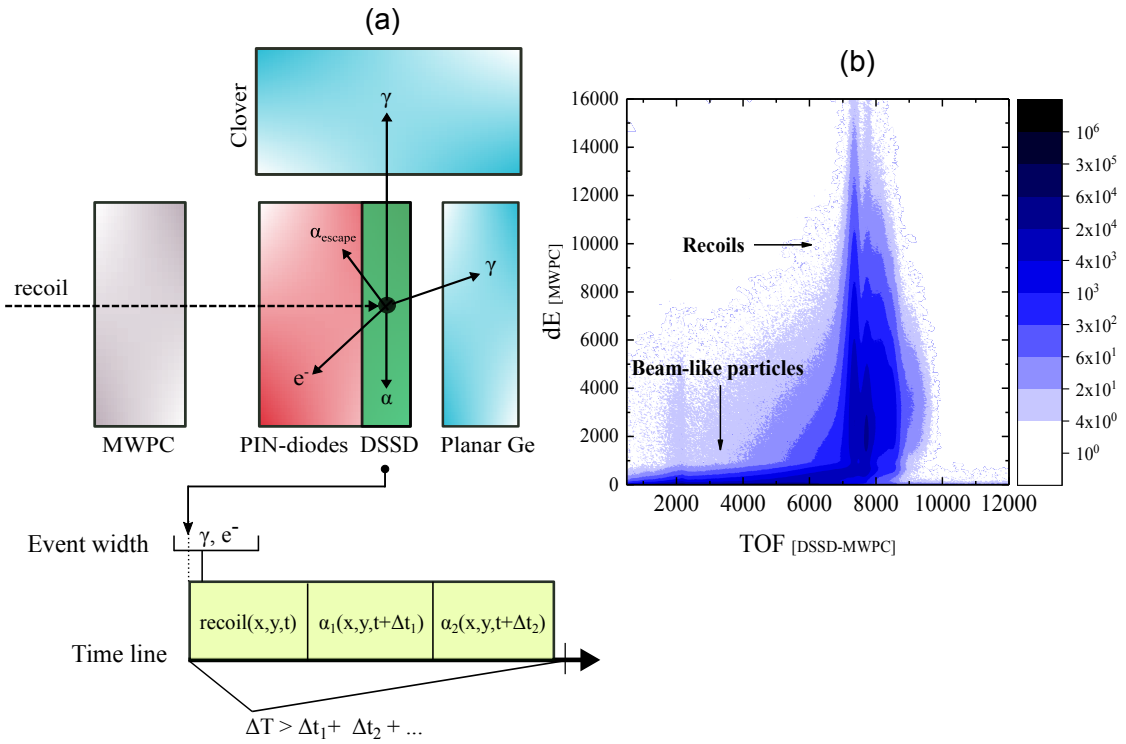

Figure 3.6: (a) A schematic representation of the decay spectroscopy technique using the GREAT spectrometer; (b) A matrix of energy loss (dE) in the MWPC versus TOF, where both the fusion-evaporation products (recoils) and beam-like particle contribution are marked. The data are taken from, the ^{78}Kr + ^{104}Pd $\rightarrow$ ^{182}Pb* fusion-evaporation reaction used in the present work.

The data analysis was performed using the GRAIN software package [Rahkila08].

3.3.1 Decay spectroscopy with the GREAT spectrometer

The combined system of RITU+GREAT was used in the present work in order to identify and study the nuclei of interest. The α-decay study was performed using the technique of recoil-α_1-α_2- ....-α_n correlations, where n is the generation of the correlated α-decaying nuclei. Thus, α_1 and α_2 represent the mother and daughter α decays after a recoil implant within the same pixel in the DSSDs. A search time of $\sim 3 \times t_{1/2}$ was applied for each generation in the α-decay chain. The total correlation search time (ΔT) within the same pixel in the DSSDs is chosen to be longer than the sum of all individual time-differences of the α-decay events ($\Delta T > \Delta t_1 + \Delta t_2 + ...$); see Fig. 3.6(a). For instance, in the case of ^{178}Pb the correlation along the whole α-decay chain down to ^{150}Er (n=7) was performed

and the total correlation search time was set to be $\Delta T = 30$ s, see section 4.3.

The time of flight for a recoil through RITU of ~ 400 ns was calculated for the reaction used in the present work. Transitions from isomeric states can be detected in the GREAT spectrometer using the clovers and planar Ge detector in the case of γ-ray transitions and the PIN diodes for the conversion-electrons as can be seen in Fig. 3.6(a). The flight time through RITU is one of the major limitations of the system when searching for short lived ($\sim$ few hundreds of nano second) isomers. The isomeric decay study was performed using the technique of [recoil-γ/e^-] -α_1-α_2-....-α_n correlations. As mentioned previously the trigger width is set according to the half-life of the isomeric state. For instance, in ^{179}Tl the γ-ray transitions were detected in the planar Ge and clover detectors within ~ 10 half-lives of a recoil implantation in the DSSDs. On the other hand, a correlation time of $3 \times t_{1/2}$ was applied to the α-decay chain that followed the isomeric decays. Moreover, γ-ray transitions following an α-decay event can be detected using the technique of recoil-[α_1-γ]-α_2....-α_n correlations, as an example, see the 80 keV transition that followed 7348 keV α decay of ^{179}Pb in section 4.1.

Half-life determination

The half-lives of the α-decaying nuclei were extracted by studying the time difference between the α particle and its recoil implanted in the DSSDs. The time difference between an isomeric transition and the proceeding event (recoil implanted in the DSSDs), were recorded to extract the half-life of the isomeric state. In the present work two methods used to measure the half-life for the nuclei of interest are explained below:

(I). The maximum-likelihood method: this method is used in the case of low statistics and low background, for instance the α-decay of ^{178}Pb and the isomeric state in ^{179}Tl (see sections 4.2 and 4.3). The lifetime τ is obtained from the number of detected decay events n and their time differences Δt_i as follows

$$\tau = \frac{1}{n} \sum_{i=1}^{n} \Delta t_i \ . \tag{3.6}$$

A correction term to the mean life-time should be added due to finite search time T [Enge81], as

$$\tau = \frac{1}{n} \sum_{i=1}^{n} \Delta t_i + \frac{T}{e^{T/\tau} - 1} \ . \tag{3.7}$$

The error analysis procedure for the measured life-time is described in Ref. [Schmidt84]. An upper and lower limit τ_u and τ_l are calculated as

follows, respectively.

$$\begin{aligned} \tau_u &\simeq \frac{\tau}{1+\frac{1}{\sqrt{n}}} \\ \tau_l &\simeq \frac{\tau}{1-\frac{1}{\sqrt{n}}} \end{aligned} \tag{3.8}$$

(II). The logarithmic method: this method has been proposed and discussed by Karl-Heinz Schmidt *et al.* [Schmidt84, Schmidt00]. Plotting the decay times on a logarithmic scale has a huge advantage to distinguish between the different components in the time distribution originating from different event groups. The density distribution (number of decay events per unit of time) of radioactive decays of one species of nuclei, can be expressed from equations 2.7 and 2.8 as follows:

$$\frac{dN}{dt} = N \cdot \lambda e^{-\lambda \Delta t} \ , \tag{3.9}$$

where N is the total number of decay events, λ is the decay constant and t is the measured decay time. Thus, for logarithmic decay times $\Theta = ln(\Delta t)$ the equation 3.9 can be written as

$$\frac{dN}{d\Theta} = N \cdot \lambda e^{\Theta} \cdot e^{-\lambda e^{\Theta}} \ . \tag{3.10}$$

The shape of this universal distribution is independent of the decay time constant, while the height and the peak position are determined by the total number of counts N and $\Theta_{max} = ln(1/\lambda)$, respectively. Figure 3.7 shows an example of using the logarithmic method to extract the half-life of ^{175}Hg. The logarithmic time difference spectrum $ln(\Delta t)$ between the α decay of ^{179}Pb and its daughter ^{175}Hg α decay is plotted. The red line represents a one-component fit procedure, described above using the equation 3.10, thus the half-life is extracted as $t_{1/2} = 9.6(4)$ ms. In the present work, this method was also used to measure the half-lives of the α-decaying nuclei ^{179}Pb, ^{179}Tl^{g,m} and ^{175}Au^{g,m} (see sections 4.1 and 4.2). Furthermore, the logarithmic-method was used as a test procedure to verify that all events assigned to the α decay of ^{178}Pb originated from the same radioactive nucleus (see section 4.3.2 for details).

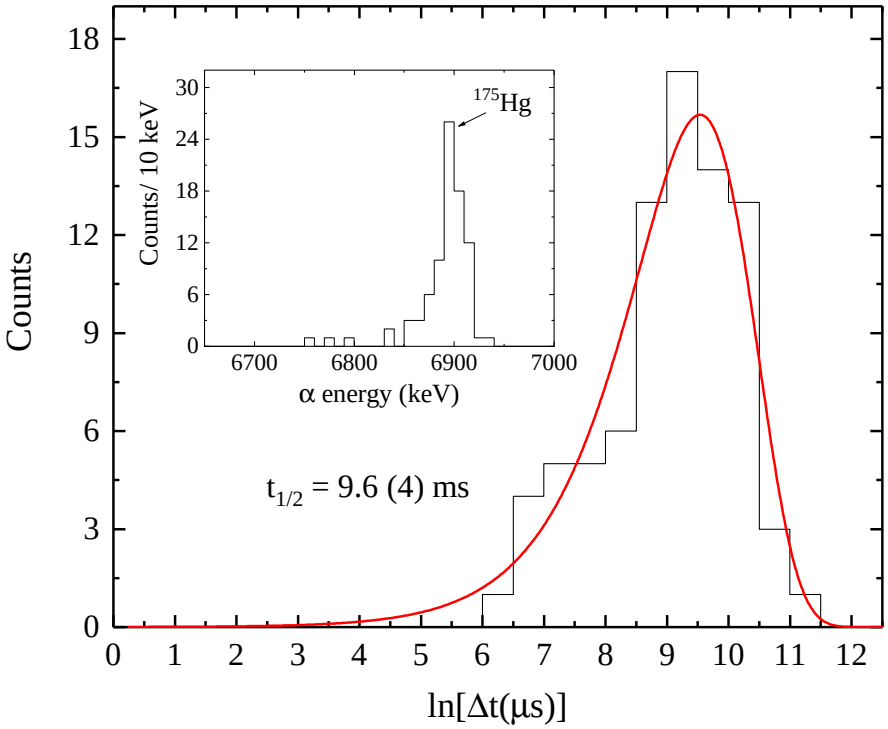

Figure 3.7: The logarithmic-time difference for the $\alpha_1(^{179}\mathrm{Pb})$- $\alpha_2(^{175}\mathrm{Hg})$ correlation, where the red-line is from a fitting procedure described in the text and yields a half-life of ^{175}Hg as $t_{1/2} = 9.6(4)$ ms. The inset is an α-particle energy spectrum of ^{175}Hg correlated with the α-decay of ^{179}Pb. Maximum search times of 20 ms and 12 s were used for recoil-α_1 and α_1-α_2 correlations, respectively.

Chapter 4

Experimental results

The experimental results regarding the decay spectroscopy of the very neutron-deficient isotopes ^{178,179}Pb and ^{179}Tl that were obtained from the present work, will be discussed in this chapter.

4.1 Decay spectroscopy of ^{179}Pb

4.1.1 Identification of ^{179}Pb

The identification of ^{179}Pb was performed using the technique of recoil-α_1(mother)-α_2(daughter)-α_3(granddaughter) correlations. The α decay of ^{179}Pb has been observed previously by Andreyev *et al.* [Andreyev10], where a total of 12 events over a broad energy range were observed. Figure 4.1 shows a two-dimensional plot of mother and daughter α-particle energies for all chains of the type recoil-α_1-α_2 correlations. The plot is vetoed by the gas counter (MWPC) and the planar Ge detector. Maximum correlation search times of 20 ms and 45 ms were used for the recoil-α_1 and α_1-α_2 correlation events, respectively. The group of α-particle events between 7320 - 7450 keV in Fig. 4.1 corresponds to the α decay of ^{179}Pb produced in the 3n-exit fusion-evaporation channel of the ^{78}Kr + ^{104}Pd reaction. In total, 105 ^{179}Pb α-decay events were observed correlated with its daughter ^{175}Hg, having an α-particle energy and half-life of E_{α_2} = 6898(4) keV and $t_{1/2}$ = 9.6(4) ms, respectively, (see Fig. 3.7). The α-particle energy for ^{175}Hg reported in this thesis is consistent within errors with values reported in Refs. [Page96, Uusitalo97]. Figure 4.2 (a) shows the projection of Fig. 4.1 for recoil-α_1 events, correlated with α_2-decay of ^{175}Hg. A few events corresponding to ^{179}Pb α decay were observed to be correlated with its granddaughter ^{171}Pt α_3-decay [Scholey10], [E_{α_3} = 6453(3) keV, $t_{1/2}$ = 48(1) ms], as can be seen in Fig. 4.1.

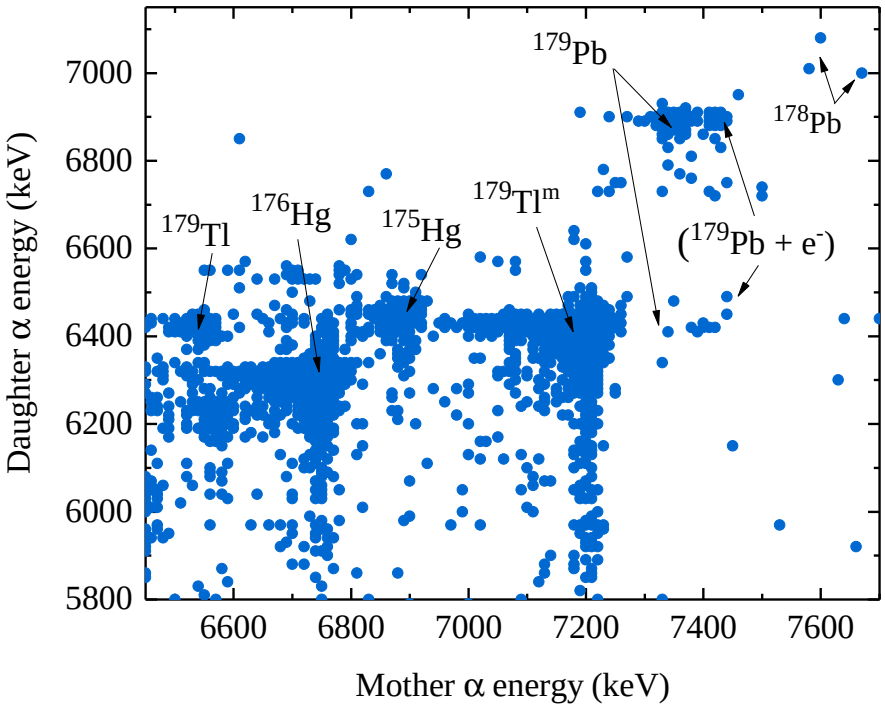

Figure 4.1: A matrix of mother and daughter α-particle energies. Maximum search times of 20 ms and 45 ms were used for recoil-α_1 and α_1-α_2 correlations, respectively.

Furthermore, other isotopes can be recognized in the plot. Such as the mercury isotopes ^{175}Hg [ens] and ^{176}Hg [Andreyev13b], produced in the $\alpha 3n$ and $\alpha 2n$ fusion-evaporation exit-channels, respectively. In the $p2n$ fusion-evaporation channel ^{179}Tl^{m} and ^{179}Tl [Andreyev13b, Andreyev10] were produced (see section 4.2), while ^{178}Pb [Badran16] was observed from the $4n$ exit-channel (see section 4.3).

In order to explain the broad distribution in the α-particle energy spectrum of ^{179}Pb in Figs. 4.1 and 4.2 (a), an $\alpha - \gamma$ coincidence analysis was performed. In figure 4.2(b), a two-dimensional plot of mother α_1-particle energies versus γ-ray energy is shown. The α_1-particle energy spectrum is correlated within a maximum search time of 20 ms to a recoil implant within the same pixel in the DSSDs at the focal plane of RITU, vetoed by the gas counter (MWPC) and the planar Ge detector. An additional requirement for the γ rays is that they arrived within a 750 ns time window following an α_1 decay. γ-ray events were detected in both clovers and the planar Ge detectors. In figure 4.2(b) the group of α-particle events at an energy of E$_\alpha$= 7348(5) keV is coincident with a γ-ray energy of 80.0(5) keV. Hence, the 7348(5) keV α-particle energy of ^{179}Pb is assigned to feed an excited

state in the daughter nucleus ^{175}Hg [O'Donnell09]. Based on this coincidence between the γ-rays and α-decay events, it can be concluded that the structure in the α-decay energy spectrum of ^{179}Pb, shown in Figs. 4.1 and 4.2 (a), is due to the known effect of the conversion electron energies summing with the α-decay energies ($E_\alpha + E_e$) in the same pixel of the DSSDs. The α-particle energy of E$_\alpha$= 7348(5) keV was determined for ^{179}Pb from the coincidence discussed above to avoid the conversion-electron summing. The error in the α-particle energy was calculated as the sum of the mean error and the systematic error (deviations between calibrated and reference energies). This energy is consistent within errors with the α-particle energy value reported in Ref. [Andreyev10]. Figure 4.2(c) reveals 13 γ-ray events of E$_\gamma$ = 80.0(5) keV that were detected in prompt coincidence with the ^{179}Pb α_1 decay having an energy of 7348(5) keV. An 80 keV transition was observed previously in ^{175}Hg by D. O'Donnell *et al.* [O'Donnell09]. This transition was assigned to have an $M1$ multipolarity, and depopulates the $I^\pi = 9/2^-$ state and feeds the $7/2^-$ ground state of ^{175}Hg. Moreover, Ref .[O'Donnell09] reports that the $9/2^-$ excited state is populated by the decay of a 0.34(3) μs $13/2^+$ isomeric state via an $M2$ transition. The observation of this strong coincidence between the α decay of ^{179}Pb and the 80.0(5) keV γ ray transition in ^{175}Hg along with $\Delta l = 0$ favoured transition (will be discussed later in section 5.1.1), allows the ground state spin and parity of $I^\pi = 9/2^-$ to be firmly assigned for ^{179}Pb.

The theoretical total internal-conversion coefficient (see section 2.2.3) for an 80 keV $M1$ transition in ^{175}Hg can be obtained from Ref. [Kibedi08], as $\alpha_{tot} = \lambda_e/\lambda_\gamma$ = 2.74(2). The K- binding energy for Hg is B_k = 88.1 keV [Firestone97], which is larger than the transition energy of 80 keV. Hence, mainly L and M -electron conversion will contribute. In fact, the L-electronic shell will dominate over M, where the ratio of L/M is 4.29(9) [Kibedi08]. An electron energy of $E_e^L \simeq$ 65.17 keV and $E_e^M \simeq$ 76.44 keV is calculated using equation 2.30, for the L and weaker M internal-conversion electrons lines, respectively. In Fig. 4.2 (a), the peak around 7356 keV represents the α-decay of ^{179}Pb to the same 80.0(5) keV exited state in ^{175}Hg that was reported earlier. Therefore, there is an energy shift of approximately $\sim$ 10 keV compared to the 7348(5) keV, which was determined from the $\alpha - \gamma$ coincidences in Fig. 4.2 (b). This can be explained by the summing of the α-particle energy with the energy deposited by the escaped conversion-electrons and the subsequent low-energy Hg X-rays [Firestone97] ($\lesssim$ 15 keV) and Auger electrons. The group of events around $\sim$ 7440 keV are due to the same additional summing. The L and M conversion-electrons will contribute in the spectrum (with an additional energy from Auger electrons as well), as can be seen in Fig. 4.2 (a). A full energy of $E_\alpha(7348) + E_e^L(65.17) \simeq$ 7413(5) keV or $E_\alpha(7348) + E_e^M(76.44) \simeq$ 7424(5) keV will be deposited in the DSSDs. Alternatively,

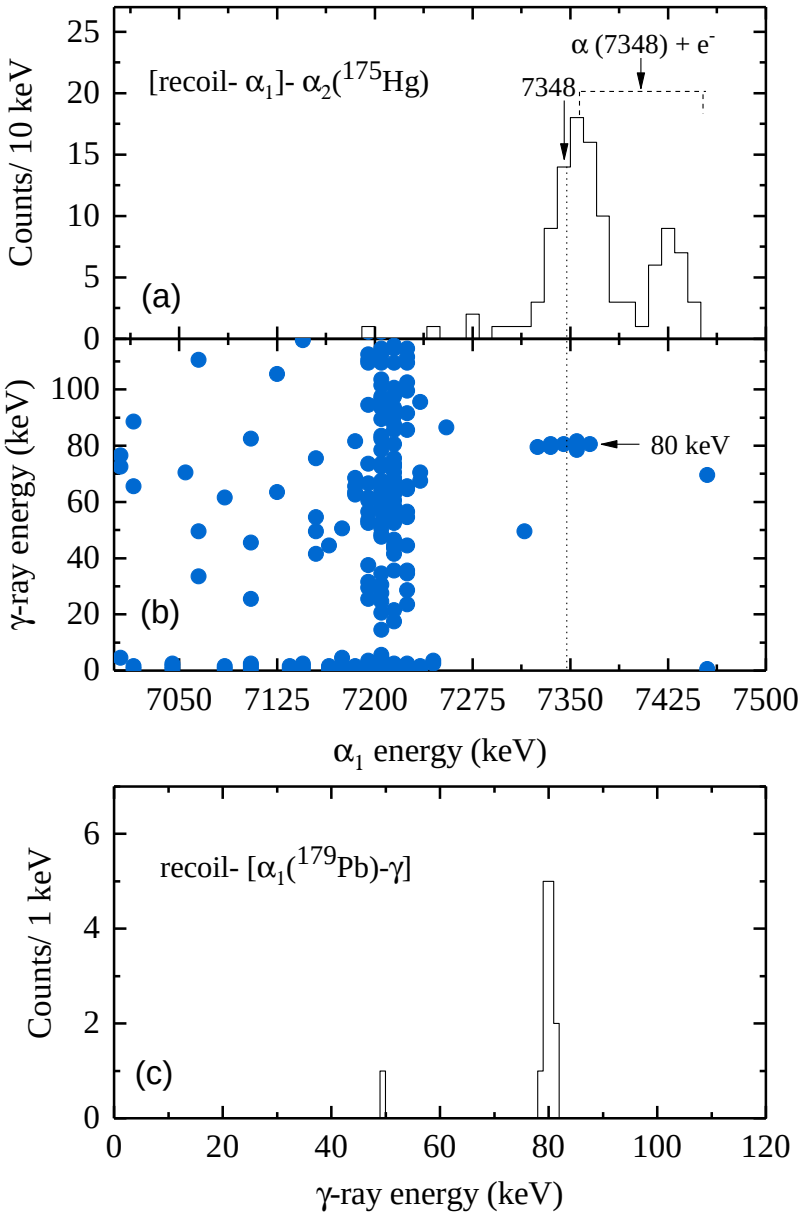

Figure 4.2: (a) recoil-α_1 particle energy spectrum correlated with the α_2-decay of ^{175}Hg. Maximum correlation times of 20 ms and 45 ms were set for recoil-α_1 and α_1-α_2 correlation, respectively. (b) α-γ energy matrix vetoed by MWPC and planar Ge detector within 20 ms correlation time for recoil-mother pairs. The dashed line from (a) to (b) represents the α decay of the ^{179}Pb ground state (c) A γ-ray energy spectrum following the 7348(5) keV α decay of ^{179}Pb within 750 ns time window.

an escaping α particle can also sum with the electron or vice versa. The fact that α particles and electrons can escape from the DSSDs depositing little or no energy, can be understood due to the shallow implantation depth of the recoil in the Si detector, especially after the degrader of aluminized mylar was installed between the DSSDs and MWPC. In figure 4.2(a) it can be noticed that the energy difference between the peak at $\sim$ 7427 keV and the α-particle energy of ^{179}Pb at 7348(5) keV is $\sim$ 80 keV which is due to the summing with the low-energy Hg X-rays and Auger electrons as mentioned above. This energy difference matches well with the 80 keV excitation energy of the $9/2^-$ state in ^{175}Hg. As stated previously the total internal-conversion coefficient is $\alpha_{tot} = 2.74(2)$ [Kibedi08]. The experimental total internal-conversion coefficient was calculated to be $\alpha_{tot}^{exp} \simeq 3(1)$. This was obtained by comparing the number of the α-decay events of ^{179}Pb in Fig. 4.2 (a) with the number of these decays in coincidence with the 80.0(5) keV γ ray in Fig. 4.2 (b) (13 γ-ray events), taking into account both the γ-ray and full-energy α detection efficiencies. This value is consistent within errors with the theoretical calculation and confirms an $M1$ multipolarity assignment for this transition in ^{175}Hg as reported in Ref. [O'Donnell09]. The total internal-conversion coefficient for other multipolarities is much higher: $\alpha_{tot}(E2) = 14.12(20)$ and $\alpha_{tot}(M2) = 60.3(9)$.

The half-life of the ground state of ^{179}Pb was determined to be $t_{1/2} = 2.44^{+0.25}_{-0.20}$ ms using the maximum-likelihood method (see section 3.3.1). In Fig. 4.3 the logarithmic-time difference (Δt) spectrum between the implanted recoils in the DSSDs and the α decay of ^{179}Pb is plotted. The inset reveals an α-particle energy of ^{179}Pb correlated with a recoil within 20 ms followed by α_2-decay of ^{175}Hg within 45 ms. The red line curve is a one-component fit made to ln(Δt). Thus, the half-life of ^{179}Pb could be extracted from the fit as $t_{1/2} = 2.7(2)$ ms, which is consistent with the maximum-likelihood method value of $t_{1/2} = 2.44^{+0.25}_{-0.20}$ ms. This value is also consistent within errors with the half-life value of $t_{1/2} = 3.5^{+1.4}_{-0.8}$ ms, reported in Ref. [Andreyev10].

4.1.2 Searching for the $\nu i_{13/2}$ state

In order to identify the excitation energy and decay of the $13/2^+$ state in ^{179}Pb, a search for [recoil-γ] events in both the clover and planar Ge detectors correlated with an α_1-(^{179}Pb) decay was undertaken. The maximum search time for [recoil-α_1] events was 20 ms. In addition, a [recoil-α_1(^{179}Pb)] versus conversion electron (e^-) coincidences in the PIN diodes was also carried out. No evidence for an isomeric state de-excited by an electromagnetic transition was found in the present data set for ^{179}Pb. Furthermore, a search for α decays populating the $13/2^+$ isomeric state in ^{175}Hg [O'Donnell09] was also carried out, and again no evidence was found for such a decay.

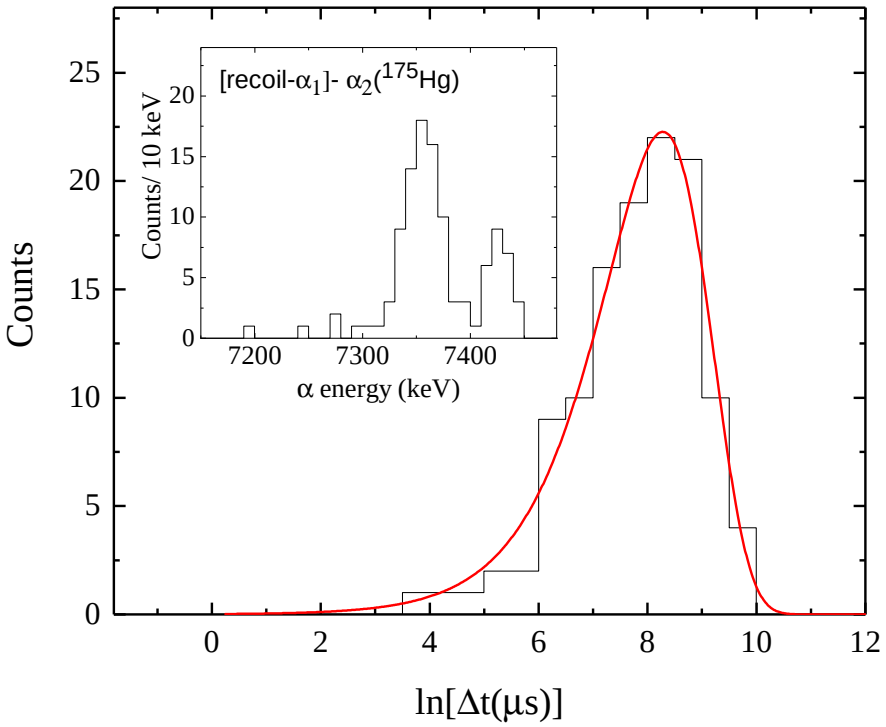

Figure 4.3: Time spectrum of the ^{179}Pb α decay, which shows the logarithm of the time difference (Δt) between the implanted recoil and α decay of ^{179}Pb followed by ^{175}Hg α decay. The maximum correlation search time of 20 ms and 45 ms for recoil-α_1(^{179}Pb) and α_1(^{179}Pb) - α_2(^{175}Hg) were used, respectively. The red line is a one-component fit and yields a half-life of $t_{1/2}$ = 2.7(2) ms for ^{179}Pb. The inset shows α-particle energy of ^{179}Pb correlated with the ^{175}Hg α decay. The figure is adapted from Ref. [Badran17].

4.2 Decay spectroscopy of ^{179}Tl

4.2.1 Alpha decay of ^{179}Tl

The study of ^{179}Tl α-decay was produced through the recoil-α_1-α_2 correlation technique. Figure 4.4 (a) shows an α-particle energy spectrum of recoil-α_1 correlation collected in the DSSDs and vetoed by both the MWPC and the planar Ge detector. A maximum search time of 1400 ms was employed for this recoil-α_1 correlation. In Fig. 4.4 (b) a two-dimensional α-particle energy plot of α_1(mother)-α_2(daughter) correlations is shown where the marked isotopes correspond to α_2 decays. Maximum search times of 1400 ms and 620 ms were set for recoil-α_1 and α_1-α_2 correlations.

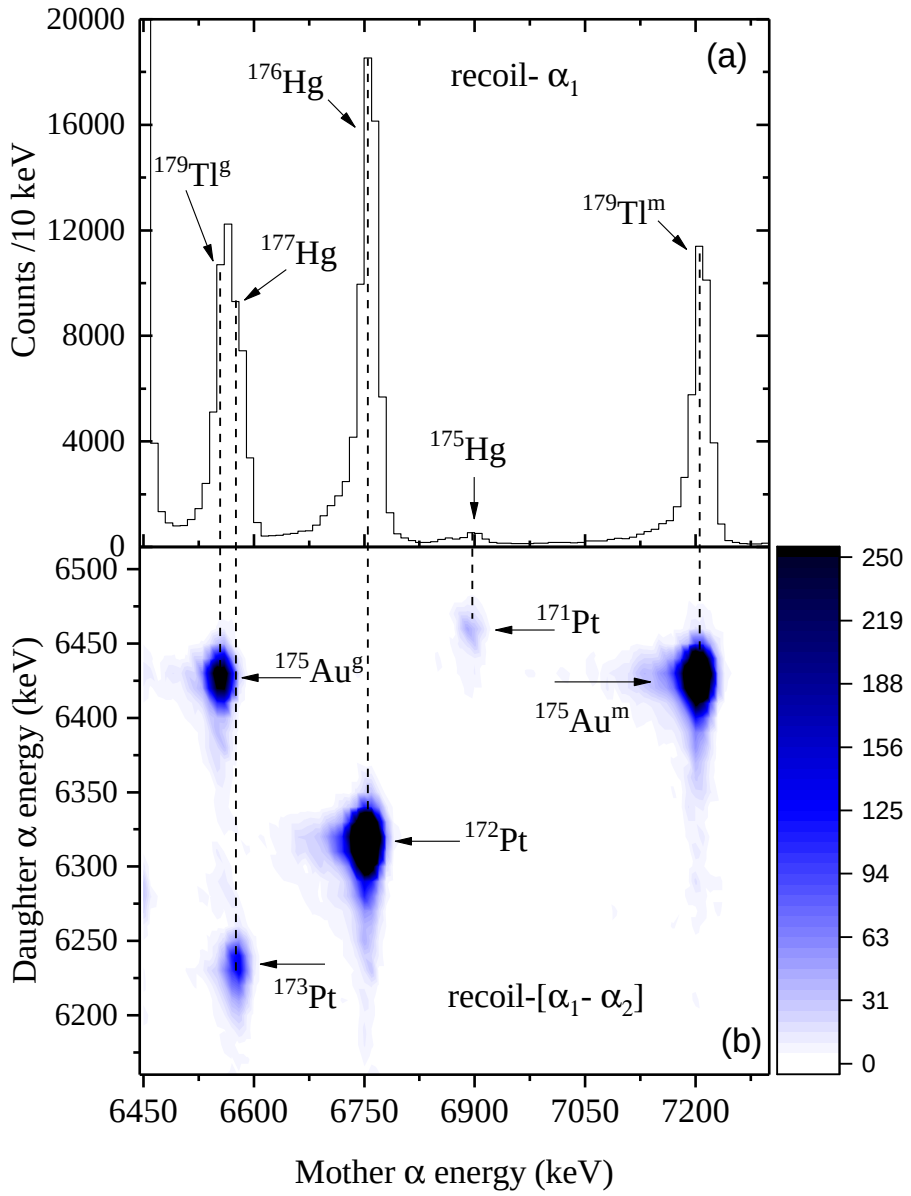

Figure 4.4: α-particle energy spectra vetoed by MWPC and planar Ge detector. (a) α-particle energy spectrum of recoil-α_1 correlation within 1400 ms search time; (b) A matrix of mother and daughter α-particle energies, where recoil-α_1 and α_1-α_2 correlation times are 1400 ms and 620 ms, respectively.

The confirmation of the α-decay correlation between the ground state of $^{179}Tl^{g} \rightarrow {}^{175}Au^{g}$ is obtained from Fig. 4.4 (see Ref. [Andreyev13b]). Thus, the α-particle energies of the α-decaying ground states $^{179}Tl^{g}$ and $^{175}Au^{g}$ can be deduced from the present work as $E_{\alpha_1} = 6557(4)$ keV and $E_{\alpha_2} = 6432(4)$ keV, respectively. Also, there is a known isomeric state with a spin and parity of $I^{\pi}=(11/2^{-})$ in ^{179}Tl [Andreyev10] which α-decays to an isomeric state in $^{175}Au^{m}$. This correlation is also visible in Fig. 4.4, from which α-particle energies of $E_{\alpha_1}(^{179}Tl^{m}) = 7206(4)$ keV and $E_{\alpha_2}(^{175}Au^{m}) = 6432(4)$ keV were measured. In addition, α_1-α_2 correlations of ^{177}Hg- ^{173}Pt, ^{176}Hg- ^{172}Pt and ^{175}Hg- ^{171}Pt can be noticed. In order to deduce accurate half-life values for $^{179}Tl^{g} \rightarrow {}^{175}Au^{g}$ and $^{179}Tl^{m} \rightarrow {}^{175}Au^{m}$ α decays a longer search time for recoil-α_1 and α_1-α_2 was required. These half-life values were deduced using the logarithmic method described by Schmidt *et al.* [Schmidt00] (see section 3.3.1). Table 4.1 summarizes α-particle energies and half-lives of $^{179}Tl^{g,m}$ and $^{175}Au^{g,m}$ measured in the present work and are compared with earlier studies.

- $^{179}Tl^{g} \xrightarrow{\alpha\text{-decay}} {}^{175}Au^{g}$:

  The logarithmic-time difference (Δt) spectrum between the implanted recoils in the DSSDs and the α decay of $^{179}Tl^{g}$ followed by the α decay of $^{175}Au^{g}$ is plotted in Fig. 4.5 (a). Maximum search times of 12 s and 620 ms were used for recoil-α_1 and α_1-α_2 correlations, respectively. The red line is a two-component fit, which yields the half-life of $^{179}Tl^{g}$ as $t_{1/2} = 426(10)$ ms. The second component is the contribution from the random correlation (background) and has $t_{1/2}$(random) = 2.7(5) s. Figure 4.5(b) shows an α_2-particle energy spectrum correlated with recoil-$\alpha_1(^{179}Tl^{g})$ and voted by the MWPC and planar Ge detector. Maximum search times of 1400 ms and 3 s were used for recoil-α_1 and α_1-α_2 correlations, respectively. α_2 decays of $^{175}Au^{g}$ and ^{173}Pt [Page96] can be seen. The inset is a ln(Δt) spectrum of $\alpha_1(^{179}Tl^{g})$-$\alpha_2(^{175}Au^{g})$ correlations obtained using the same search parameters, where the half-life of $^{175}Au^{g}$ can be extracted using a one-component fit (red line), and is $t_{1/2} = 200(3)$ ms.

- $^{179}Tl^{m} \xrightarrow{\alpha\text{-decay}} {}^{175}Au^{m}$:

  Figure 4.6 (a) shows an α_1-particle energy spectrum correlated with $^{175}Au^{m}$ α decays and vetoed by the MWPC and planar Ge detector. Maximum search times of 13 ms and 410 ms were set for recoil-α_1 and α_1-α_2 correlations, respectively. The α decay from an $^{179}Tl^{m}$ isomeric state in ^{179}Tl was identified and the half-life was extracted from the inset in Fig. 4.6 (a) to be $t_{1/2} = 1.40(3)$ ms. Figure 4.6 (b) reveals a α_2-particle energy spectrum correlated with recoil-$\alpha_1(^{179}Tl^{m})$, where search times of 5 ms and 3 s were required for

recoil-α_1 and α_1-α_2 correlations, respectively. In the inset figure the half-life of $^{175}Au^m$ isomeric state is shown to be $t_{1/2} = 136(1)$ ms.

Table 4.1: Comparison between α-particle energies E_α and half-life values $t_{1/2}$ of $^{179}Tl^{g,m}$ and $^{175}Au^{g,m}$ isotopes obtained in the present work and earlier studies.

Isotope	E_α (keV)	$t_{1/2}$ (ms)	Reference
$^{179}Tl^g$	6557(4)	426(10)	Present work
	6560(4)	265(10)	[Andreyev13b]
	6568	415(55)	[Rowe02]
	6568(18)	430(350)	[Page96]
$^{179}Tl^m$	7206(4)	1.40(3)	Present work
	7207(5)	1.46(4)	[Andreyev10]
$^{175}Au^g$	6433(4)	200(3)	Present work
	6433(4)	207(7)	[Andreyev13b]
$^{175}Au^m$	6433(4)	136(1)	Present work
	6432(5)	138(5)	[Andreyev10]

4.2.2 Excited states in ^{179}Tl

Excited states decaying to the ground state of $^{179}Tl^g$ via γ-ray transitions were identified using [recoil-γ]-α_1-α_2 correlations, where α_1 and α_2 in this case are the mother $^{179}Tl^g$ and daughter $^{175}Au^g$ α decays after a recoil implant within the same pixel in the DSSDs, respectively.

In Fig. 4.7, the summed γ-ray energy spectrum collected in both clover and planar Ge detector within a 1 μs time-window of a recoil implant is shown. The spectrum is produced by gating on the ground state α decay ($E_\alpha = 6557(4)$ keV) of ^{179}Tl within a 1400 ms recoil-α_1 correlation time. Figure 4.7 is dominated by the known 77 keV and 246 keV γ-ray transitions in ^{177}Hg (see Ref. [Melerangi03]). In addition, K_α and K_β Hg X-rays are also present. On the other hand, γ-ray peaks marked with an asterisk are newly observed transitions now known to feed the ground state of ^{179}Tl. The inset shows an α_1-particle energy spectrum in coincidence with γ-ray transitions vetoed by the MWPC and the planar Ge detector, where a search time of 1400 ms was set for recoil-α_1 correlations.

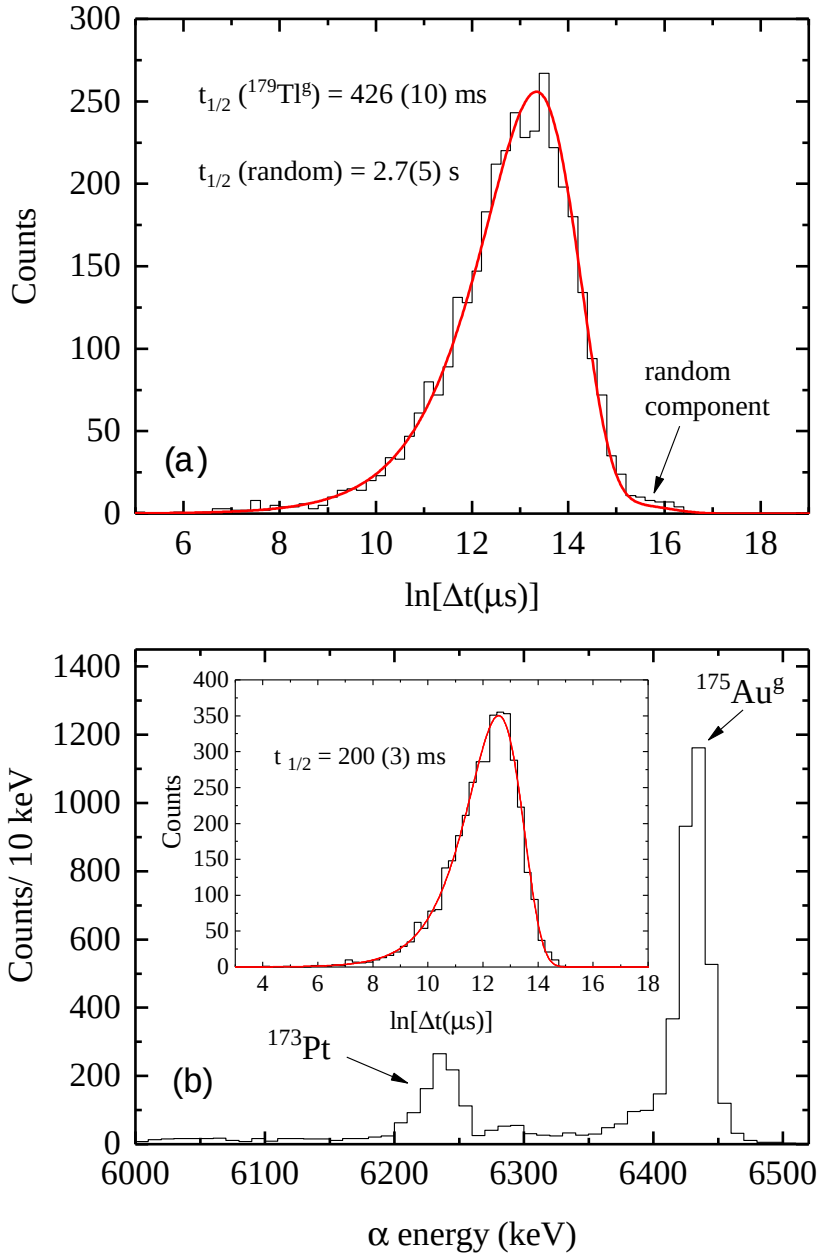

Figure 4.5: (see text for details) (a) ln(Δt) spectrum of recoil-α_1(^{179}Tl^g) correlations within 12 s. An α-particle energy condition of recoil-α_1(^{179}Tl^g)-α_2(^{175}Au^g) correlation was set within a 620 ms search time of α_1-α_2 correlations; (b) α_2-particle energy spectrum of recoil-α_1(^{179}Tl^9)-α_2 correlations within a 3 s search time for α_1-α_2 correlations. The inset ln(Δt) spectrum was produced by gating on α-decays of ^{175}Au^g.

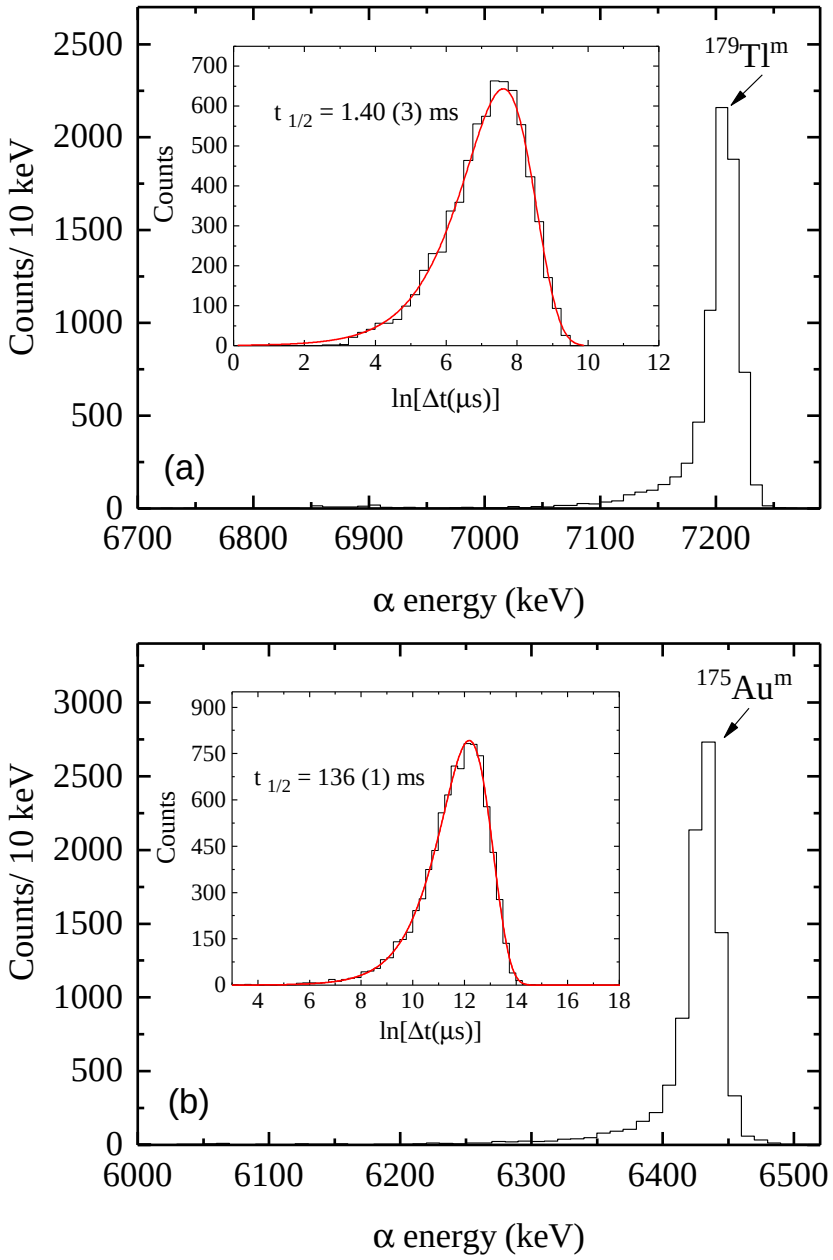

Figure 4.6: (see text for details) α-particle energy spectrum of recoil-α_1 correlations within a 13 ms search time. An α_1-α_2(^{175}Au^m) correlation was required within a 410 ms search time. The inset is a ln(Δt) spectrum produced by gating on the ^{179}Tl^m α-particle energies. (b) α_2-particle energy spectrum of recoil-α_1(^{179}Tl^m)-α_2 correlations within a 3 s search time for α_1-α_2 correlation. The inset ln(Δt) spectrum was produced by gating on the α-decay of ^{175}Au^m.

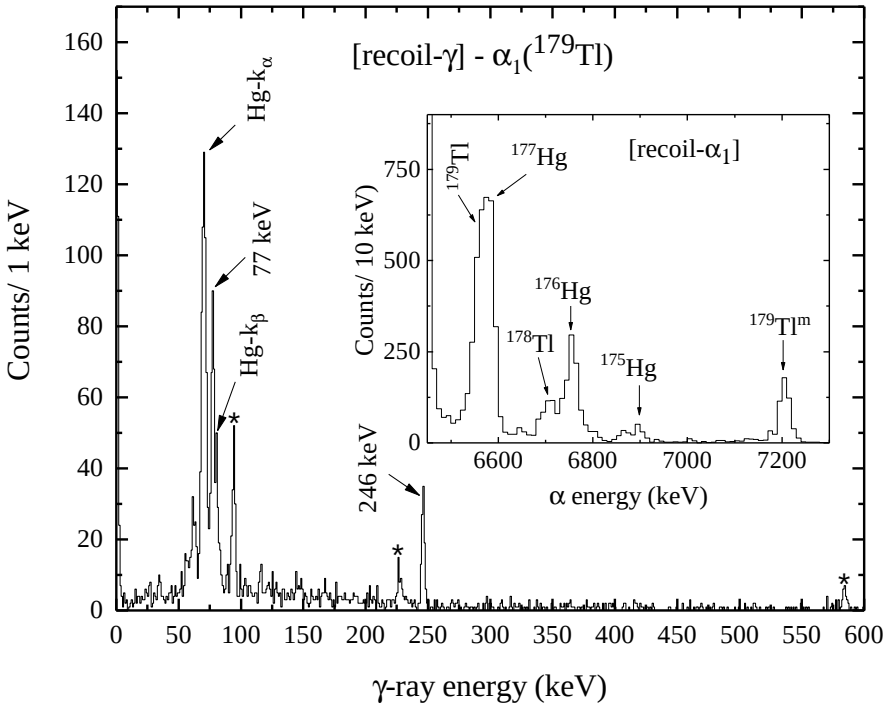

Figure 4.7: Energy spectrum of γ-ray singles of [recoil-γ]-$\alpha_1(^{179}\mathrm{Tl})$ events with time conditions of 1 μs and 1.4 s for recoil-γ and recoil-α_1, respectively. The inset is correlated α_1-particle energy spectrum within 1.4 s of a recoil implant in a DSSD pixel and in coincidence with recoil-γ events. The figure is adapted from Ref. [Badran17].

The overlap of the α-decay characteristics of ^{179}Tl and ^{177}Hg is clear, having α-particle energies and half-lives of [$E_\alpha(^{179}\mathrm{Tl}) = 6557(4)$ keV, $E_\alpha(^{177}\mathrm{Hg}) = 6577(9)$ keV] and [$t_{1/2}(^{179}\mathrm{Tl}) = 426(10)$ ms, $t_{1/2}(^{177}\mathrm{Hg}) = 114(15)$ ms], respectively.

In order to exclude the contribution of ^{177}Hg only recoils that were correlated with $\alpha_1(^{179}\mathrm{Tl})$ and $\alpha_2(^{175}\mathrm{Au})$ decays were accepted. Figure 4.8 (a) shows an α_1-particle energy spectrum correlated with $\alpha_2(^{175}\mathrm{Au})$ and in coincidence with recoil-γ events that were detected at the focal plane within 1 μs of a recoil implant. The disappearing of ^{177}Hg is evident. Maximum search times of 1400 ms and 620 ms were used for recoil-α_1 and α_1-α_2 correlation, respectively. Furthermore, the α-decay of $^{179}\mathrm{Tl}^m$ [Andreyev10] observed in Fig. 4.8 (a) can be explained by the overlapping of $^{175}\mathrm{Au}^g$ and $^{175}\mathrm{Au}^m$ α-decay properties, as discussed earlier (see table 4.1).
Figure 4.8 (b) represents the summed γ-ray energy spectrum (clover and planar Ge detector) within 1 μs of a recoil implant and correlated with $\alpha_1(^{179}\mathrm{Tl}^g)$-$\alpha_2(^{175}\mathrm{Au}^g)$, where γ-ray peaks of 94.0(5) keV, 226.0(6) keV and 584.5(5) keV are evident.

The aforementioned γ-ray transitions follow the decay of an isomeric state, which finally feeds the ground state of ^{179}Tl. Thallium K-shell X-rays are also evident in Fig. 4.8 (b) as a composite peak due to the resolution of the Ge detectors, having energies of $K_{\alpha 1}$= 72.87 keV and $K_{\alpha 2}$= 70.83 keV with intensities of 46.3% and 27.6%, respectively, obtained from Ref. [Firestone97].
In the present work, the low statistics related to γ-ray transitions feeding the ground state of ^{179}Tl did not allow a recoil-$(\gamma-\gamma)$ coincidence analysis. From Fig 4.8 (b) it can be seen that the intensity ratio between the 94 keV transition and K_α X-rays is $(I_{K_\alpha}/I_{94}) < 1$. The possible transitions multipolarities which have an $\alpha_k < 1$ are $E1$, $E2$ and $E3$ with calculated $\alpha_k = 0.396$, 0.562 and 0.398, respectively, [Kibedi08]. By comparing the number of observed 94 keV transitions with the number of α particles from ^{179}Tl ground state, we concluded that around $\sim 40\%$ of the flux that populates the ^{179}Tl^g will go through the 94 keV transition with an $E1$ character. This calculation was performed taking into account both the γ-ray and α particle detection efficiencies. Assuming all the flux that populates the ^{179}Tl^g goes through the 94 keV transition, a factor of 2 and 50 higher α-decay yield for the ^{179}Tl^g is needed compared to what was observed if the 94 keV transition has an $E2$ or $E3$ character, respectively. Hence, the 94 keV transition is assigned to have an $E1$ character based on the intensity ratio and both $\alpha_{tot}(E1) = 0.500(7)$ and $\alpha_k(E1) = 0.396(6)$ values. Any other multipolarity for this energy has an α_{tot} more than an order of magnitude greater than $\alpha_{tot}(E1) = 0.500(7)$ value. In addition, the 226 keV and 584.5 keV transitions are assigned to have $M1$ and $E2$ multipolarites with total internal-conversion coefficients of $\alpha_{tot}(M1) = 0.856(12)$ and $\alpha_{tot}(E2) = 0.0193(3)$, respectively. This assignment is based on the fact that 94 keV, 226 keV and 584.5 keV transitions form a cascade, where their intensities are balanced within errors (see table 4.2). For no other combination of multipolarities do the intensities balance. The yield of K_α X-rays $I_{\mathrm{X}}^{\mathrm{det}}(K_\alpha)$ observed in Fig. 4.8 (b) supports the multipolarity assignments of the three transitions (see table 4.2). Table 4.2 shows the different properties of the γ-ray transitions that are stated above. The total γ-ray intensities I_{tot} were corrected for internal-conversion using equation 2.32 and normalized to the strongest γ-ray transition (94 keV). An efficiency correction for both the clover and planar Ge detector was taken into account as well, obtained from Refs.[Hauschild13, Taimi15].

Due to the low statistics of the observed γ-ray transitions, the half-life of the isomeric state was measured using the maximum-likelihood method within a 1 μs search time ($\sim 10\times$ $\mathrm{t}_{1/2}$). Half-lives of $\mathrm{t}_{1/2} = 112^{+20}_{-15}$ ns, $\mathrm{t}_{1/2} = 130^{+50}_{-30}$ ns and $\mathrm{t}_{1/2} = 100^{+50}_{-30}$ ns were deduced for the 94 keV, 226 keV and 584 keV transitions, respectively. These values are consistent within errors proving that these transitions arise from the depopulation of the same isomeric state.

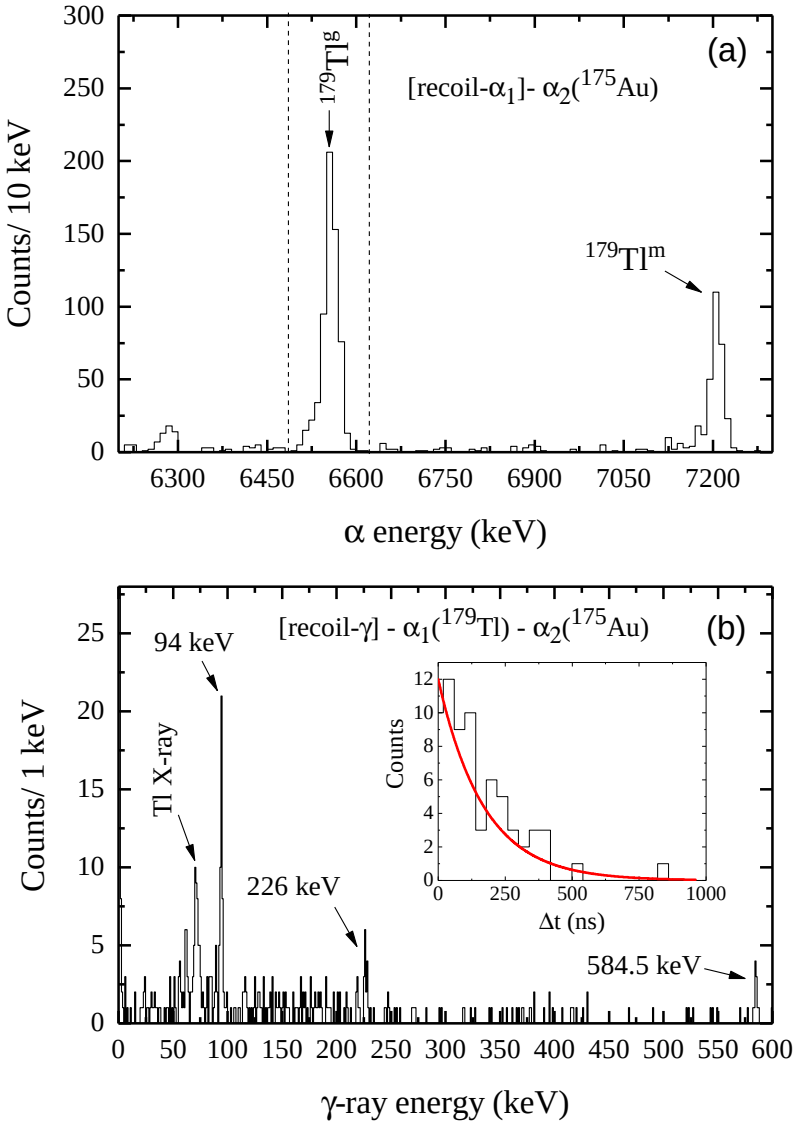

Figure 4.8: (a) α_1-particle energy spectrum correlated with $\alpha_2(^{175}\mathrm{Au})$ within time conditions of 1400 ms and 620 ms for recoil-α_1 and α_1-α_2, respectively, and in coincidence with recoil-γ events within 1 μs of a recoil implant. (b) A summed γ-ray energy spectrum of [recoil-γ]-$\alpha_1(^{179}\mathrm{Tl})$-$\alpha_2(^{175}\mathrm{Au})$ events within 1 μs of a recoil implantation in the DSSDs. The dashed lines in (a) represent the energy limits to produce spectrum (b). The inset is the summed decay curve of the 94.0(5) keV, 226.0(6) keV and 584.5(5) keV transitions. The red line is an exponential distribution plotted using the weighted-average half-life value of $t_{1/2} = 114^{+18}_{-10}$ ns (see the text for details). The figure is adapted from Ref. [Badran17].

Table 4.2: The transition energies E_γ, multipolarities and total internal-conversion coefficients α_{tot} for γ-rays that were observed in both the clover and planar Ge detectors of the GREAT spectrometer which are cascading to the ground state of ^{179}Tl. Intensities I_γ and I_{tot} are normalized such that $I_\gamma(94\text{ keV})$ and $I_{tot}(94\text{ keV})$ are 100. $I_X(K_\alpha)$ and $I_X^{det}(K_\alpha)$ represent the expected K_α X-rays yield from each transition and the observed K_α X-rays, respectively, taking into account the focal plane efficiency. The measured half-lives $t_{1/2}$ were calculated using the maximum-likelihood method. α_{tot} values and their errors are taken from Ref. [Kibedi08].

E_γ (keV)	$I_\gamma(\%)$	α_{tot}	$I_{tot}(\%)$	$t_{1/2}$ (ns)	Multipolarity	$I_X(K_\alpha)$
94.0(5)	100(25)	0.500(7)	100(25)	112^{+20}_{-15}	E1	67(15)
226.0(6)	63(22)	0.856(12)	78(28)	130^{+50}_{-30}	M1	74(20)
584.5(5)	120(50)	0.0193(3)	80(30)	100^{+50}_{-30}	E2	3(2)
K_α X-rays	92(36)					
					$I_X^{sum}(K_\alpha)$	144(25)
					$I_X^{det}(K_\alpha)$	155(40)

The weighted-average half-life value for the isomeric state can then be expressed as $t_{1/2} = 114^{+18}_{-10}$ ns. Thus far, in total three transitions of 94.0(5) keV, 584.5(5) keV and 226.0(6) keV were observed for the first time to depopulate the newly observed $t_{1/2} = 114^{+18}_{-10}$ ns isomeric state in ^{179}Tl.

Transitions between ^{179}Tl^m and the $t_{1/2} = 114^{+18}_{-10}$ ns isomeric state

The existence of an α-decaying isomeric state ^{179}Tl^m was discussed in section 4.2.1, where recoil-α_1(^{179}Tl^m)-α_2(^{175}Au^m) correlations were presented. Whilst the excitation energy of this state is still unknown, a search for transitions between the newly observed $t_{1/2} = 114^{+18}_{-10}$ ns isomeric state and the $11/2^-$ state ($t_{1/2} = 1.40(3)$ ms) was performed to ascertain the order of their excitation energies. This search was performed for (a) transitions feeding ^{179}Tl^m and (b) long-lived transitions feeding ^{179}Tl^g, in the following manner:

(a) For such a transition [recoil-γ]- α_1(^{179}Tl^m) and [recoil- e^-]- α_1(^{179}Tl^m) correlation analyses were performed, where e^- are conversion-electron events correlated with recoils in the same pixel in the DSSDs. A time window of 1 μs was set for the [recoil-γ] coincidences, while a 5 ms search time was applied to both [recoil-α_1] and [recoil- e^--α_1] correlations.

(b) In this case, a [recoil-e^-]- α_1 (^{179}Tl^g) correlation analysis is required, where the maximum search times of 5 ms and 1.4 s were applied, respectively. In addition, a [recoil-γ]- e^- coincidence analysis was also performed.
No [recoil-γ]- e^- coincidences were found.

The above searches found no evidence for transitions between the two isomeric states, within the sensitivity limits of the detector set-up used for these measurements. Hence, the 94 keV, 226 keV and 584.5 keV γ-ray transitions appear to only feed the ^{179}Tl^g not the ^{179}Tl^m.

4.3 Alpha decay spectroscopy of ^{178}Pb

4.3.1 Identification of ^{178}Pb

Figure. 4.9(a) shows a two-dimensional plot of α-particle energy α_1 (mother)- α_2 (daughter) correlations. The maximum search times of 5 ms and 50 ms were used for recoil-α_1 and α_1-α_2 correlation, respectively. Three events of ^{178}Pb can be identified correlated with its daughter ^{174}Hg [Seweryniak99], having an α-particle energy and half-life of E_{α_2} = 7066(8) keV and $t_{1/2} = 1.9^{+0.4}_{-0.3}$ ms, respectively. Furthermore, another event of recoil- α_1(^{178}Pb)- α_3(^{170}Pt) correlation can also be seen in Fig. 4.9(a), where the α-particle energy and half-life of the grand-daughter ^{170}Pt [Kettunen04] are E_{α_3} = 6549(2) keV and $t_{1/2}$ = 14(2) ms, respectively. α_1-α_2 correlations of ^{179}Tl^m [Andreyev13b], ^{176}Hg [Andreyev13b], ^{175}Hg [O'Donnell09] and ^{179}Pb are also clearly visible.

Figure. 4.9(b) reveals an α-particle energy spectrum of recoil-correlated decay events detected in the DSSDs within a 5 ms search time vetoed by the MWPC and the planar Ge detector. The α decay of ^{179}Pb, ^{178}Pb [Badran16] and ^{177}Tl [Kettunen04] can be seen in Fig. 4.9(b). In the software analysis the random correlations can be produced by shifting the DSSD's pixel with which to correlate the α-decay with the recoil by a certain number. In figure. 4.9(b), the red colour spectrum represents random correlations which were produced by shifting the horizontal and vertical strip number of the recoil implant by two. Hence, when shifting the DSSDs pixel number by two and only random correlations are observed. Only very few random events were observed, as can be seen in Fig. 4.9(b), and the disappearing of ^{178}Pb α-particle events attributed to the α decay of ^{178}Pb is clear.

As a further identification of the four counts that have been assigned to ^{178}Pb in Figure. 4.9(a), an event by event analysis was performed along the α-decay chain of ^{178}Pb as follows:

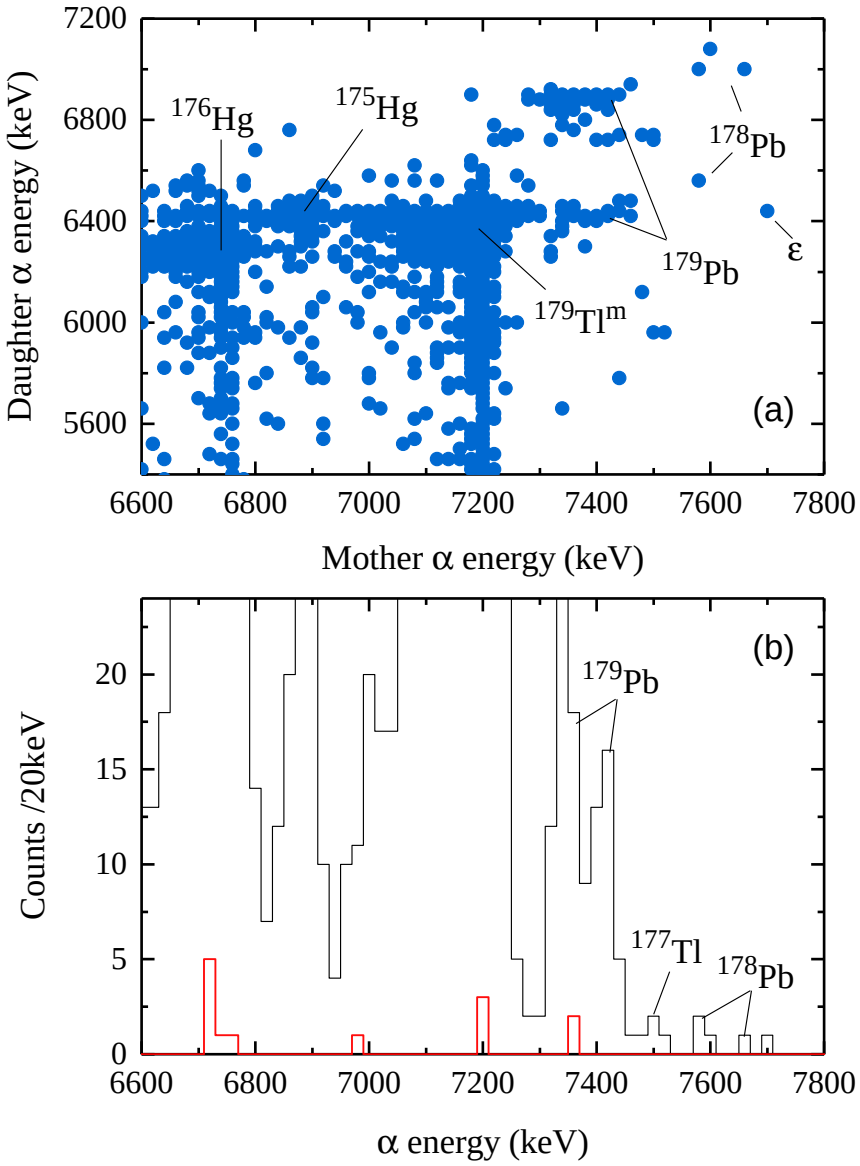

Figure 4.9: (a) A matrix of mother and daughter α-particle energies vetoed by MWPC and planar Ge detector. Maximum search times of 5 ms and 50 ms were used for recoil-α_1 and α_1-α_2 correlations, respectively. The letter ϵ represents an unidentified α-particle with an energy and half-life of E_α= 7700 keV and $t_{1/2} \simeq$ 4 ms; (b) overlay of the α-decay spectra MWPC and planar Ge detector vetoed within 5 ms correlation time. The black line shows the real correlations, while the red coloured spectrum presents the random correlations produced in the analysis (see text for details). The figure is adapted from Ref. [Badran16].

^{178}Pb $\xrightarrow[\text{chain}]{\alpha-\text{decay}}$ ^{174}Hg [Seweryniak99] $\xrightarrow[1.9^{+0.4}_{-0.3}\ \text{ms}]{7066(8)\ \text{keV}}$ ^{170}Pt [Kettunen04] $\xrightarrow[14(2)\ \text{ms}]{6549(2)\ \text{keV}}$

^{166}Os [Appelbe02] $\xrightarrow[220(7)\ \text{ms}]{6000(6)\ \text{keV}}$ ^{162}W [Li15] $\xrightarrow[0.99(3)\ \text{s}]{5541(5)\ \text{keV}}$ ^{158}Hf [Page96] $\xrightarrow[2.85(7)\ \text{s}]{5269(4)\ \text{keV}}$

^{154}Yb [Page96] $\xrightarrow[409(2)\ \text{ms}]{5331(4)\ \text{keV}}$ ^{150}Er.

Maximum search times of 5 ms and 50 ms were used for recoil- $\alpha_1(^{178}\text{Pb})$ and $\alpha_1(^{178}\text{Pb})$- $\alpha_2(^{174}\text{Hg})$ correlations, respectively, while a 30 s maximum search time was applied to the rest of the decay chain.

Figure 4.10 shows the four observed α-decay chains of ^{178}Pb. These chains will now be discussed:

- Chain number (1): consists of three generations of full-energy α decays. In addition, an α particle of ^{178}Pb correlated beyond the α decay of ^{166}Os was not observed.
- Chain number (2) and (4): consists of three generations of full-energy α decays down to ^{166}Os and one escape event of $^{166}\text{Os} \rightarrow {}^{162}\text{W}$ correlated with a full ^{178}Pb α decay. These chains stopped at ^{162}W.
- Chain number (3): two escaping α particles of $^{174}\text{Hg} \rightarrow {}^{170}\text{Pt}$ and $^{162}\text{W} \rightarrow {}^{158}\text{Hf}$ were correlated with a full energy ^{178}Pb α decay. This chain terminated at ^{158}Hf.

The escaping α particle energies for chain numbers (2), (3) and (4) that are shown in Fig 4.10 were observed only in the DSSDs. The remaining energy was deposited in one of the PIN box detectors. These escaping alpha particles occur due to the shallow implantation depth of the recoil in the DSSDs. Figure 4.10 shows that both ^{178}Pb α-decay chains number (2) and (4) terminate at ^{162}W. As stated previously, no α particle of ^{178}Pb correlated beyond the α decay of ^{166}Os and ^{158}Hf were observed in chain number (1) and chain number (3), respectively. The end points of the four observed chains at ^{166}Os, ^{162}W and ^{158}Hf, can be explained due to their α-decay branching ratios having values of 72(13) %, 44(3) % and 45(2) % (taken from Ref. [Page96]), respectively.

The average α-particle energy of ^{178}Pb was deduced as E_α= 7610(30) keV. This value is consistent within errors with the α-particle energy value in Ref. [Batchelder03] (E_α= 7615(30) keV). The error in the average energy was calculated here as the sum of the mean and the systematic error. Furthermore, the Q-value of ^{178}Pb α-decay can be calculated using the equation 2.14 as Q_α= 7785(31) keV.

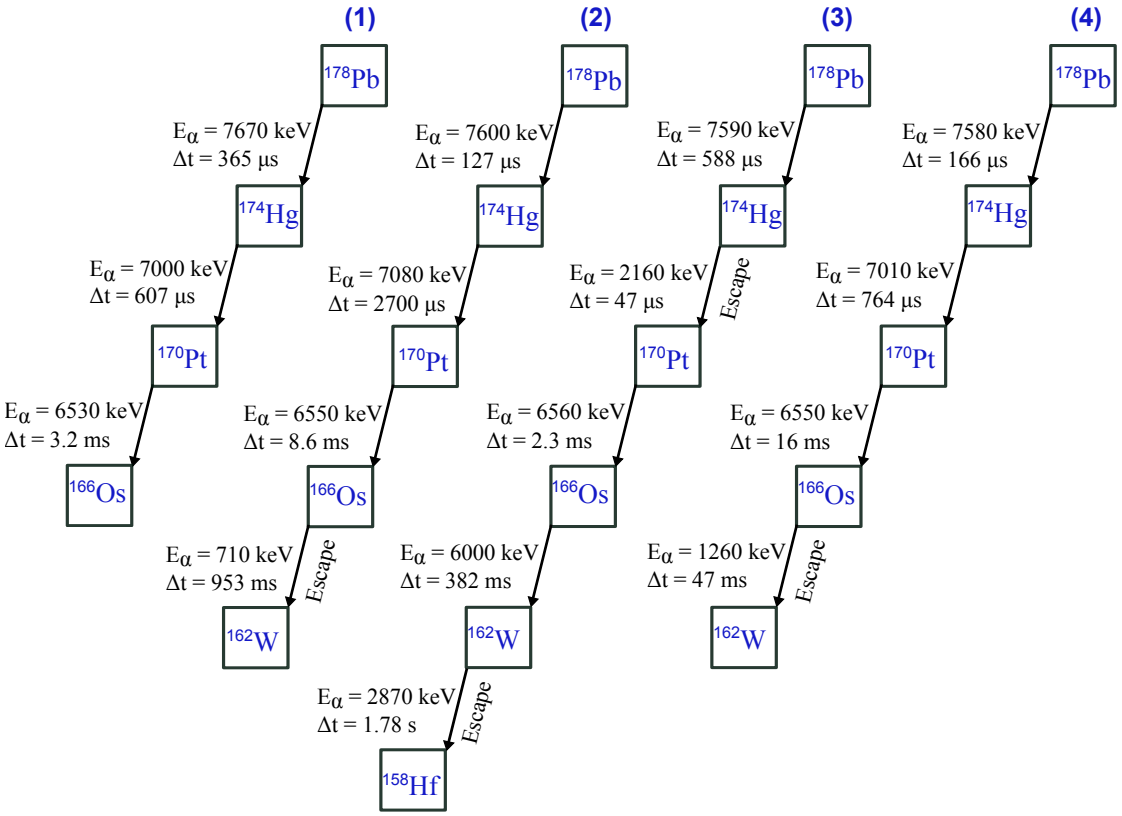

Figure 4.10: α-decay chains of ^{178}Pb observed in the present work. The word escape attached to the arrows means that only part of the α-particle energy was deposited in the DSSDs, while the remaining energy was observed in one of the PIN box detectors. The symbols E_α and Δt corresponds to the α-particle energy detected only in the DSSDs and the time difference between each generation in the chain, respectively.

Thus, the mass excess of ^{178}Pb can be deduced with the help of $Q_\alpha(^{178}\text{Pb})$-value and the known mass excess for the daughter nucleus ^{174}Hg ($\Delta M_d = 6607(34)$ keV) obtained from Ref. [Seweryniak99], as $\Delta M(^{178}\text{Pb}) = 3603(42)$ keV. In addition, Möller *et al.* [Möller95] predicted the mass excess value of ^{178}Pb to be $\Delta M(^{178}\text{Pb}) = 3430$ keV, which is comparable to the value in the present work.

4.3.2 Half-life determination of ^{178}Pb

Due to the low statistics regarding the α-decay of ^{178}Pb (only four counts were observed), the maximum-likelihood method was used to extract the half-life of the ^{178}Pb ground state as $t_{1/2} = 0.21^{+0.21}_{-0.08}$ ms.

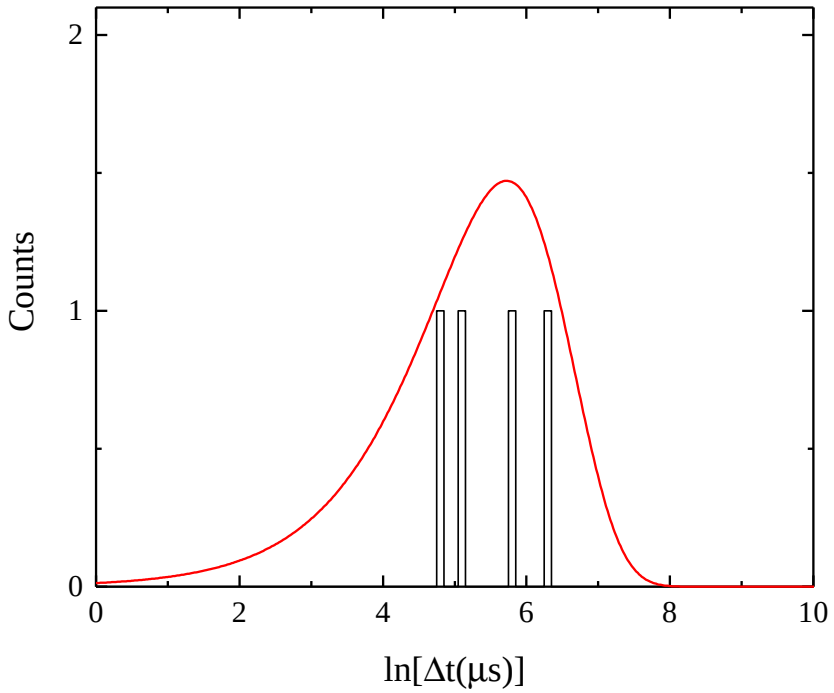

Figure 4.11: Logarithmic-time difference spectrum ln(Δt) between the implanted recoil and α decay of ^{178}Pb. The maximum correlation-search time was 5 ms. The red line is a universal shape distribution defined by Schmidt [Schmidt00] and plotted using the decay constant value taken from the maximum-likelihood method. The figure is adapted from Ref. [Badran16].

The logarithmic time difference ($\Theta_{exp} = \ln(\Delta t)$) spectrum between the implanted recoils in the DSSDs and the α decay of ^{178}Pb is plotted in figure. 4.11. A test procedure proposed by Schmidt [Schmidt00], was performed on the logarithmic time difference data points to determine whether the events originated from the same radioactive decaying nucleus. This procedure was carried out by comparing the experimental standard deviation of the measured logarithmic time distribution with the theoretical prediction. In Figure. 4.11, the red line curve was plotted using the decay constant value obtained from the maximum-likelihood method as stated previously. This universal shape is described in Refs. [Schmidt00, Schmidt84] (see section 3.3.1), where the maximum value of the distribution yields $\ln(1/\lambda)$, where λ is the decay constant. The measured standard deviation value of $\sigma_{\Theta_{exp}} = 0.58$ was extracted from the distribution using the following equation obtained from Ref. [Schmidt00] as

$$\sigma_{\Theta_{exp}} = \sqrt{\frac{\sum_{i=1}^{n}(\Theta_i - \overline{\Theta}_{exp})^2}{n}} \ , \tag{4.1}$$

where $\overline{\Theta}_{exp} = \frac{\sum_{i=1}^{n}\Theta_i}{n}$, and $n = 4$ in this case.
The lower and upper limit of the measured standard deviation are expected to be $0.31 \leq \sigma_{calc} \leq 1.92$ calculated using the Monte Carlo technique, (see table.1 in Ref. [Schmidt00]). $\sigma_{\Theta_{exp}}$ falls well between the lower and upper limits. Thus, confirming the four events that are assigned in the present work to ^{178}Pb originate from the same radioactive decay.

Chapter 5

Discussion

5.1 Decay spectroscopy of ^{179}Pb

5.1.1 Alpha decay of ^{179}Pb

When studying α decay, a comparison between theoretical and measured half-life values can be used to probe the structural differences between the initial and final states in the mother and daughter nuclei, respectively. The Hindrance Factor HF value based on this comparison is a very important feature in α-decay spectroscopy (see section 2.2.1).

The hindrance factor HF for a $\Delta l = 0$ transition for the ^{179}Pb α-decay was calculated using equation 2.24, to be $HF = 1.70(1)$. This value corresponds to an unhindered (favoured) transition. The experimental half-life $t_{1/2}^{exp}$ was taken from the present work along with the assumption that the α-decay branching ratio is $b_\alpha = 100\%$. While the theoretical α-decay half-life $t_{1/2}^{calc}$ was calculated using the Rasmussen method [Rasmussen59]. In addition, the α-decay reduced width of a $\Delta l = 0$ transition, [$9/2^-$ (^{179}Pb ground state) $\longrightarrow$ $9/2^-$ (^{175}Hg excited state)], was calculated using equation 2.22, as $\delta_\alpha^2 = 44(3)$ keV. The α-particle energy and half-life of E$_\alpha$= 7348(5) keV and $t_{1/2}^{exp} = 2.7(2)$ ms, respectively, were used in the previous calculation. The δ_α^2 value for ^{179}Pb α-decay is consistent within errors with $\Delta l = 0$ transitions of the neighbouring odd-A lead nucleus, $\delta_\alpha^2(^{181}\text{Pb}) = 37(4)$ keV [Andreyev09a]. Table 5.1 summarises the α-decay proprieties of ^{179}Pb obtained from the present work and are compared with Ref. [Andreyev10].

The ground state configuration of ^{179}Pb as $I^\pi = 9/2^-$ was based on the following observations. Firstly, the strong coincidences between the 7348(5) keV α-particle energy of ^{179}Pb and the 80 keV γ-ray transition from the $9/2^-$ excited state in

^{175}Hg as discussed in section 4.1. Secondly, the hindrance factor HF and reduced α-width values that supporting a $\Delta l = 0$ unhindered (favoured) α decay of ^{179}Pb.

Table 5.1: Comparison of α-particle energies E_α, half-life values $t_{1/2}$, and α-decay reduced widths δ^2_α for ^{179}Pb from the present work and from Ref. [Andreyev10].

E_α (keV)	$t_{1/2}$ (ms)	δ^2_α (keV)	Reference
7348(5)	2.7(2)	44(3)	Present work
7350(20)	$3.5^{+1.4}_{-0.8}$	33^{+14}_{-10}	[Andreyev10]

The decay scheme of ^{179}Pb constructed using the information obtained from the present work is shown in Fig. 5.1, with the values for ^{175}Hg taken from the present work and from Ref. [O'Donnell09] also included. A direct α-decay transition from the ground state of ^{179}Pb to the ground state of ^{175}Hg should be considered, which would have an energy of 7428 keV [(7348 + 80) keV]. Disentangling these decays from the α-particle and electron energy sum is practically impossible and the lack of any extra events around this energy leads to the conclusion that such a decay is not observed in the present data set. Hence, only an upper intensity limit of $b_\alpha \leq 5\%$ relative to the 7348 keV α decay was calculated from the present data. This transition would be strongly hindered with a lower limit of HF ≥ 37 and an α-decay reduced width upper limit of $\delta^2_\alpha \leq 2$ keV. This is expected as it involves different mother and daughter configurations. The HF value for the non-observed 7428 keV α decay was calculated relative to the unhindered 7348 keV α decay, while the δ^2_α calculated using the Rasmussen method [Rasmussen59].

5.1.2 Limitation of the non-observed $\nu i_{13/2}$ state

In section 2.1.2 the $i_{13/2}$ orbital was discussed and defined as a unique-parity "intruder" state in the shell-model picture. The $\nu i_{13/2}$ intruder state exists near the Fermi surface in odd-mass nuclei around the lead region of the nuclear chart (see for e.g. Refs. [Melerangi03, O'Donnell09]). This state has been observed in the Pb isotopic chain down to ^{183}Pb, where the excitation energy is rather low being at only 79(6) keV [Jenkins02], but to date has not yet been observed in ^{181}Pb. However, Ref. [Carpenter05] mentioned that a gamma-ray transition with a half-life of ~ 10 μs was assigned to decay from the $13/2^+$ and feed the ground state of ^{181}Pb, but no supporting spectra or details were given. The $\nu i_{13/2}$ intruder state also has been studied down the α-decay chain of ^{179}Pb in ^{175}Hg [O'Donnell09], ^{171}Pt, ^{167}Os and ^{163}W in Ref. [Scholey10]. At $Z = 68$ in ^{151}Er [Fukuchi09], which

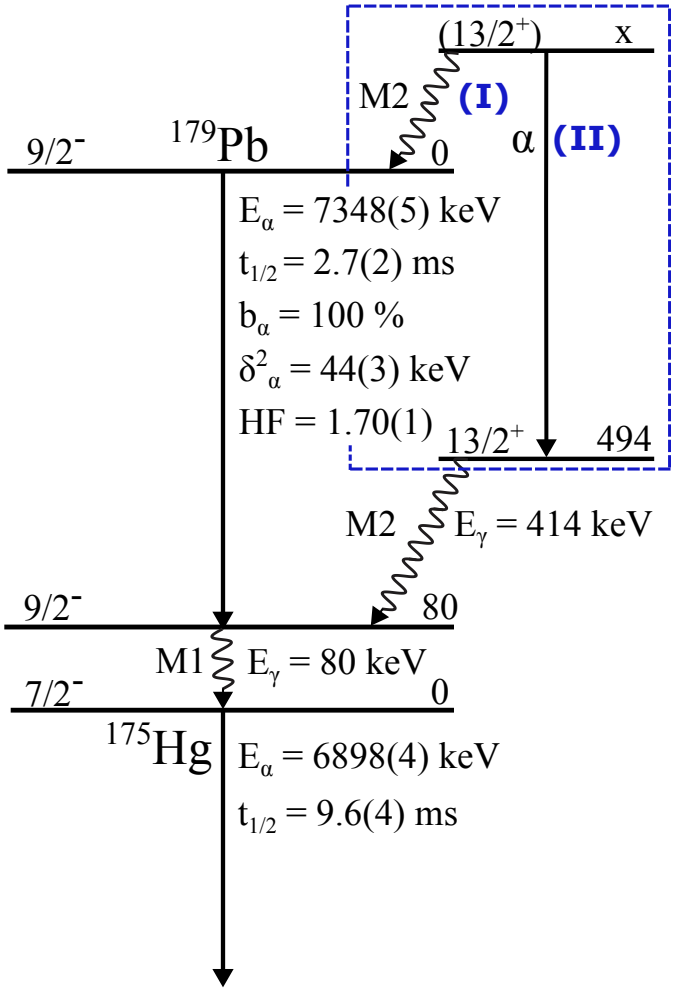

Figure 5.1: Decay scheme of ^{179}Pb and ^{175}Hg deduced in the present work, where E_α, E_γ, b_α, δ^2_α and HF represent the α-particle energy, γ-ray energy, branching ratio, α-decay reduced width and the hindrance factor, respectively. The Rasmussen method [Rasmussen59] was used for α-decay reduced width calculations assuming $\Delta l = 0$ transitions. The $13/2^+$ excited state in ^{175}Hg at 494 keV is taken from Ref. [O'Donnell09]. The dashed blue box shows the two possible decay-modes scenarios (I) and (II) for the $13/2^+$ state in ^{179}Pb, which are discussed in the text. The figure is adapted from Ref. [Badran17].

is part of α-decay chain of ^{179}Pb, the $\nu i_{13/2}$ state is also observed.

In ^{179}Pb, if the $\nu i_{13/2}$ unique-parity intruder state exists it will form an isomeric state having a spin and parity of I^π=$13/2^+$. This isomeric state will decay in one of two ways as shown in Fig. 5.1. The two decay scenarios will now be discussed:

- Scenario (I): The $13/2^+$ isomeric state feeds the $9/2^-$ ground state of ^{179}Pb via an $M2$ transition.
- Scenario (II): The $13/2^+$ isomeric state α decays to a 0.34(3) μs $13/2^+$ isomeric state in ^{175}Hg at an excitation energy of 494 keV, subsequently to the ground state of ^{175}Hg by the cascade of a 414 keV and a 80 keV transitions as reported in Ref. [O'Donnell09].

Figure 5.2(a) shows the competition between two different decay modes regarding the two scenarios (I) and (II) above, where the half-life values as function of $13/2^+$ excitation energy are plotted. The electromagnetic transition will dominate over α decay as can be seen in Fig. 5.2(a), where the half-life in this case will be $\sim$ 1000 - 10000 times shorter than the α decay for any excitation energy of the $13/2^+$ state. The α decay partial half-lives $t^{\alpha}_{1/2}$ for different Q_{α} values were calculated using the Geiger-Nuttall law from equation 2.18, shown as filled red squares in Fig. 5.2(a). The coefficients $A(Z)$ and $B(Z)$, obtained from Ref. [Qi14] were fitted for the $Z \leq 82$ region. For comparison $t^{\alpha}_{1/2}$ calculated from Ref. [Taageper61] are also shown; see open diamonds in Fig. 5.2(a). In Fig. 5.2(a) the filled-blue circles represent the half-life values for an $M2$ transition calculated for a transition from $13/2^+$ state, using Weisskopf estimate [Weisskopf51] from table 2.1 and corrected for internal-conversion obtained from Ref.[Kibedi08]. In the $Z = 82$ region (^{179}Pb α-decay chain; see chapter 1) an $M2$ transition is usually hindered by an factor of $\sim$ 5 - 10, as reported in Ref. [Scholey10]. Hence, the filled-green triangles in Fig. 5.2(a) display the transition rate having this hindrance taken into account.

Now we must consider the $13/2^+$ isomeric state populating the $9/2^-$ ground state of ^{179}Pb via an $M2$ transition. Since no such transition has been observed an upper and lower limit are set. An upper observational transition energy limit of E $\simeq$ 300 keV has been calculated for such a decay based on the flight time through the RITU separator and half-life of the state; see the dashed line in Fig. 5.2(a). Figure 5.2(b) shows the expected experimental number of γ-ray transitions, K-shell X-rays, K and L -shell conversion-electron events as a function of $13/2^+$ state excitation energies. This calculation was based on 105 α-particle events that were assigned to ^{179}Pb α-decay in the present work, assuming 100% population of the ground state goes through the $13/2^+$ state. Conversion-electron coefficients for the K and L -shells for different transition energies were taken from [Kibedi08], while the binding energies of $B_k = 88.0045$ and $B_l = 15.86$ were obtained from [Firestone97]. Furthermore, the detection efficiency of γ rays and conversion electrons for Ge detectors and PINs diodes, respectively, were considered as well. A lower limit of the transition energy can then be set, as E $\simeq$ 180 keV, based on the statistics, the detection efficiency and energy thresholds; see Fig. 5.2(b). From these findings we

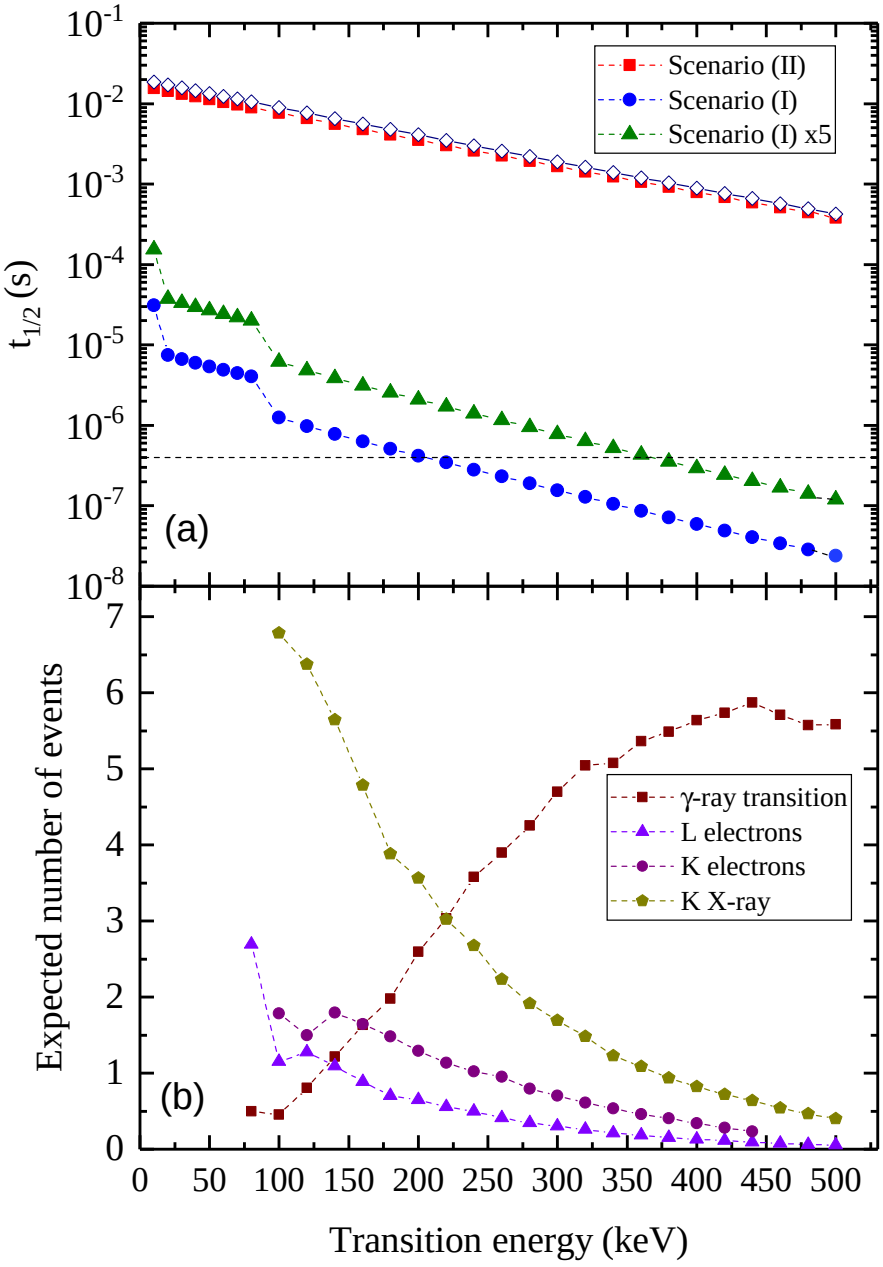

Figure 5.2: (a) Expected half-life values of the transition from $13/2^+$ as a function of its excitation energy, considering two different scenarios (I) and (II) (see text for details); (b) Expected number of γ-ray transitions, K-shell X-rays, K and L conversion-electron events, based on 105 α-particles of ^{179}Pb. An energy threshold of 50 keV was considered in the calculation.

conclude that, the excitation energy of the $13/2^+$ state in ^{179} Pb is not within the range of 180 - 300 keV.

5.2 Decay spectroscopy of ^{179}Tl

5.2.1 Alpha decay of ^{179}Tl

In section 4.2.1, the α-particle energy and half-life of the ^{179}Tl were deduced as E_α = 6557(4) keV and $t_{1/2}$ = 426(10) ms, respectively. The α-decay branching ratio of ^{179}Tl is b_α= 60(2) % taken from Ref. [Andreyev10]. Thus, the α-decay reduced width of a $\Delta l = 0$ transition, [$1/2^+$ (^{179}Tl^g) $\longrightarrow$ $1/2^+$ (^{175}Au^g)], can then be extracted as δ^2_α = 32.0(7) keV using the Rassmussen method [Rasmussen59]. Furthermore, the hindrance factor was calculated to be HF= 1.37(3). This value corresponds to an unhindered (favoured) $\Delta l = 0$ transition.

5.2.2 Excited states in ^{179}Tl

The ground state of odd-A thallium isotopes $^{185-201}$Tl are known to have a spin and parity of $I^\pi = 1/2^+$ [Barzakh13, ens], which can be understood as being due to the $\pi(s_{1/2})^{-1}$ configuration. Recently, the ground state spin of lighter odd-A Tl isotopes, ^{179}Tl ($N = 98$) and ^{181}Tl ($N = 100$), have been assigned as I = 1/2 using laser spectroscopy by Barzakh *et al.* [Barzakh17]. In section 4.2.2, we conclude that the 94.0(5) keV, 584.5(5) keV and 226.0(6) keV transitions depopulate the newly observed $t_{1/2} = 114^{+18}_{-10}$ ns isomeric state in ^{179}Tl. Fig. 5.3 shows the partial level scheme of these γ-ray transitions feeding the ground state of ^{179}Tl. Following the analogy of the heavier odd-A Tl isotopes, the 226 keV level has been assigned as $I^\pi = (3/2^+)$ and de-excites by an $M1$ transition to the $1/2^+$ ground state as shown in Fig. 5.3. The $(3/2^+)$ state can be understood to be associated with a $\pi(d_{3/2})^{-1}$ configuration. This assignment is based on the fact that an excitation energy of 226 keV follows well the smooth systematics of $\pi(d_{3/2})^{-1}$ states along $^{181-201}$Tl isotopes, as can be seen in Fig. 5.4. Moreover, the 584.5 keV transition energy is close to the $2^+ \rightarrow 0^+$ transition energy of 558 keV in the ^{178}Hg [Kondev00] core. Hence, the 584 keV transition is assigned as a $(7/2^+) \rightarrow (3/2^+)$ transition of $E2$ character, where the $(7/2^+)$ state can be understood as a $\pi d_{3/2}$ proton-hole coupled to the 2^+ state of the ^{178}Hg core.

The $9/2^-$ intruder isomeric states are well known along the odd-A thallium isotopic chain $^{181-201}$Tl [ens], originating from one-particle one-hole $\pi(1p-1h)$ excitation to the $\pi h_{9/2}$ orbital above the $Z = 82$ shell gap. Also, the $9/2^-$ intruder states are known to be associated with an oblate shape deformation. In fact, this state

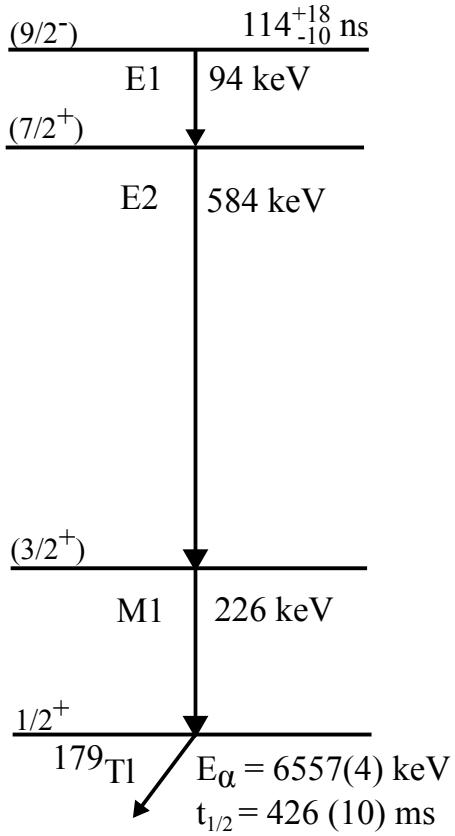

Figure 5.3: A partial level scheme of ^{179}Tl obtained from the present work. The figure is adapted from Ref. [Badran17].

has been observed in the heavier Tl isotopes $^{195-201}$Tl and also in ^{181}Tl to decay via an $E3$ transition to a $3/2^+$ excited state, all having comparable $B(E3)$ values as reported in Ref. [Andreyev09b], where an α-decay branch for this state was observed in ^{181}Tl. On the other hand, in lighter odd-A Tl isotopes the excitation energies of the $9/2^-$ state were deduced mainly from α-decay fine structure of the Bi isotopes as reported in Refs. [Andreyev06, Batchelder99, Coenen85], with the exception of ^{185}Tl [ens]. In the present work, the 94 keV transition in ^{179}Tl has been assigned as $I^\pi = (9/2^-)$ and de-excite via an $E1$ transition to the $(7/2^+)$ state, as is shown in Fig. 5.3. The $E1$ multipolarity assignment for the 94 keV transition from the $(9/2^-)$ intruder state in ^{179}Tl is discussed earlier in section 4.2.2, and also confirmed by the reduced-transition probability deduced value of $B(E1, 94\text{ keV}) = 1.50^{+23}_{-13} \times 10^{-6}$ W.u, (see section 2.2.2). This value in good agreement with typical experimental $B(E1)$ values for known delayed $E1$ transitions in this region, reported in Refs [Rigby08, Lönnroth88, Venhart11, Lane95].

In the present work an excitation energy of 904.5(9) keV was extracted for $(9/2^-)$ intruder state in ^{179}Tl. Figure 5.4 reveals the excitation energy systematics of the $9/2^-$ intruder states as functions of neutron number N along the odd-A Tl isotopic chain, where our newly observed $(9/2^-)$ state in ^{179}Tl at $N = 98$ is placed. These systematics has been discussed previously down to ^{181}Tl in Refs. [Coenen85, Muikku01, Andreyev09b]. In fact, while $(9/2^-)$ state excitation energy in ^{179}Tl at $N = 98$, does not follow the parabolic trend of this state along odd-A $^{179-201}$Tl isotopes (see Fig 5.4), however, it is still increasing as the neutron number decreases toward more neutron deficient nuclei.

In addition, the $11/2^-$ state which is a band member of the $9/2^-$ intruder state band on oblate-shape deformation has been observed to follow a similar parabolic trend along the $^{185-201}$Tl isotopes [Raddon04, Muikku01, ens], as can be seen in Fig. 5.4. Below the mid-shell at $N = 104$, a deviation from this trend is observed at ^{183}Tl, similar to the deviation presently observed for the $9/2^-$ state in ^{179}Tl. Raddon *et al.* [Raddon04] speculated that the $\pi(h_{11/2})^{-1}$ state lies lower in excitation energy than the $11/2^-$ band member below the mid-shell causing this smooth deviation in the parabolic trend. This possibility is indicated by the brackets in Fig 5.4. In Ref. [Barzakh17], a larger deformation of the $9/2^-$ isomeric state was observed in ^{183}Tl compared to its ground state, along with unexpected increase in the isomer shift points to a possible prolate-oblate mixture in this isotope. In addition, the break in the parabolic trend of the $(9/2^-)$ excitation energy at $N = 98$, could be related to the fact that in ^{179}Tl all states are more than 500 keV proton unbound unlike the heavier Tl isotopes, where the proton separation energy for ^{179}Tl is $S_p = -760(40)$ keV [Wang17].

The excitation energy of the α-decaying $\pi(h_{11/2})^{-1}$ isomeric state in ^{179}Tl is still unknown. However, in Refs. [Andreyev09b, Andreyev13b] it was suggested that the excitation energy of the $9/2^-$ intruder state is $\sim$ 300-400 keV above the expected position of the $11/2^-$ state. This prediction was made based on the extrapolation of the $9/2^-$ parabolic trend for Tl isotopes of $A = 181 - 201$ and the excitation energy of the $\pi(h_{11/2})^{-1}$ in ^{179}Tl obtained from linear interpolation of the $11/2^-$ state in the lightest odd-A Tl isotopes. After finding no evidence of transitions between the newly observed $(9/2^-)$ intruder state and the α-decaying $\pi(h_{11/2})^{-1}$ state, as discussed in section 4.2.2 it can be concluded that the excitation energy of these two states is comparable. Also, by comparing the number of events in ^{179}Tl^g ground state with ^{179}Tl^m isomeric state in Fig. 4.4, it can be noticed that the population of both states are comparable. This supports the earlier suggestion that the excitation energies are comparable. Furthermore, the fact that there is a transition from $(9/2^-) \rightarrow (7/2^+)$ state and the lack of transition between the $(9/2^-)$

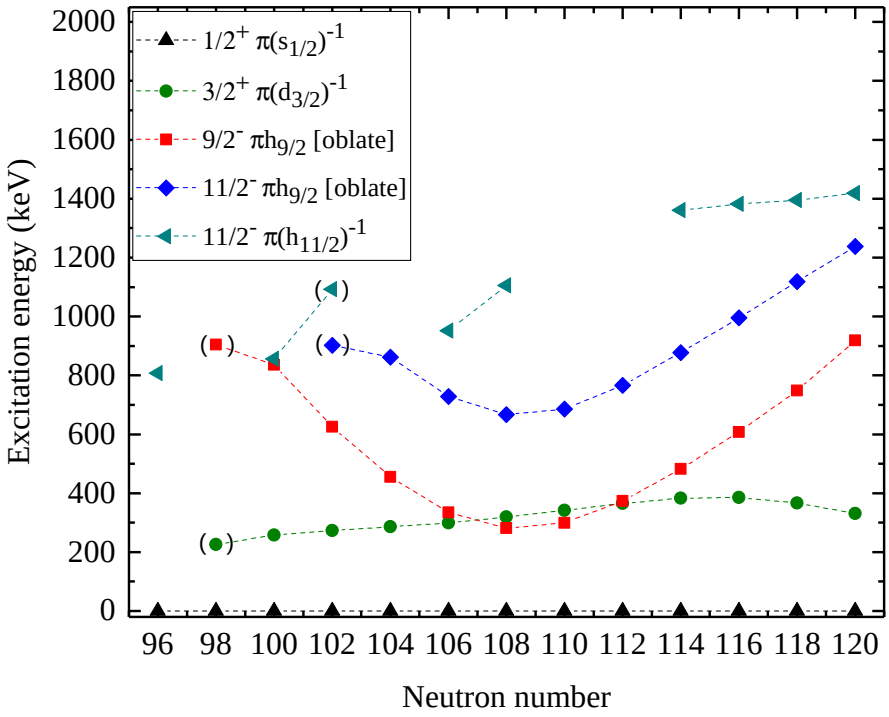

Figure 5.4: A plot of the experimental-excitation energies of $9/2^-$, $3/2^+$ and $11/2^-$ states relative to $1/2^+$ ground state in odd-A Tl isotopes as function of neutron numbers. The experimental values are taken from Refs. [Andreyev09b, ens, Coenen85, Batchelder99, Andreyev06, Raddon04, Carpenter05], and its from the present work for ^{179}Tl. The figure is adapted from Ref. [Badran17].

and $(11/2^-)$ states, also supports the tentative shape assignments of these states, both oblate deformation for the $(7/2^+)$ (2^+ state of ^{178}Hg oblate core [Kondev00] + $\pi d_{3/2}$) and the $(9/2^-)$ states and weakly prolate deformation for the $(11/2^-)$ α-decaying state.

5.3 Alpha decay spectroscopy of ^{178}Pb

Comparison between experimental and theoretical half-lives can be achieved in two ways; via the hindrance factor HF, as mentioned previously in section 5.1.1, and the spectroscopic factor S^{exp}. The experimental α-decay spectroscopic factor S^{exp} can be defined using the ratio between the experimental and theoretical half-lives as follow

$$S^{exp} = \frac{t_{1/2}^{calc}}{t_{1/2}^{exp}} , \tag{5.1}$$

where $t_{1/2}^{exp}$ and $t_{1/2}^{calc}$ are the experimental and the theoretical α-decay partial half-lives, respectively. Table 5.2 shows the S^{exp} values, calculated for ^{178}Pb α-decay using the half-life obtained from the present work and three different models for comparison. Firstly, the Coulomb and Proximity Potential Model (CPPM) [Santhosh15], which is the sum of coulomb barrier, proximity potential and centrifugal potential. The other model is the analytical formulae of Royer *et al.* [Royer00] using the Generalized Liquid Drop Model (GLDM). Finally, the Rasmussen method [Rasmussen59] which is discussed earlier in Sections 2.2.1 and 5.1.1.

Table 5.2 shows a consistency within errors between the experimental half-life value of ^{178}Pb with the theoretical value calculated using the CPPM and Rasmussen method regarding the S^{exp} values. The S^{exp} calculation is extended for even-A lead nuclei between $96 \leq N \leq 112$, using the equation 5.1. Figure 5.5 presents a comparison of the calculated experimental α-decay spectroscopic factor S^{exp} using the three different models, where the $\log_{10}[S^{exp}]$ is plotted as a function of neutron number N. The plot shows an underestimation of the theoretical half-life using the CPPM model up to $N = 106$ where a change to an overestimation is observed

Table 5.2: Experimental spectroscopic factor S^{exp} calculated for ^{178}Pb α decay using three different models, where $t_{1/2}^{calc}$ values are taken from Ref. [Santhosh15].

Model	Spectroscopic factor S^{exp}
Rasmussen	$1.26^{+1.26}_{-0.41}$
CPPM	$0.78^{+0.78}_{-0.26}$
GLDM	$1.90^{+1.90}_{-0.63}$

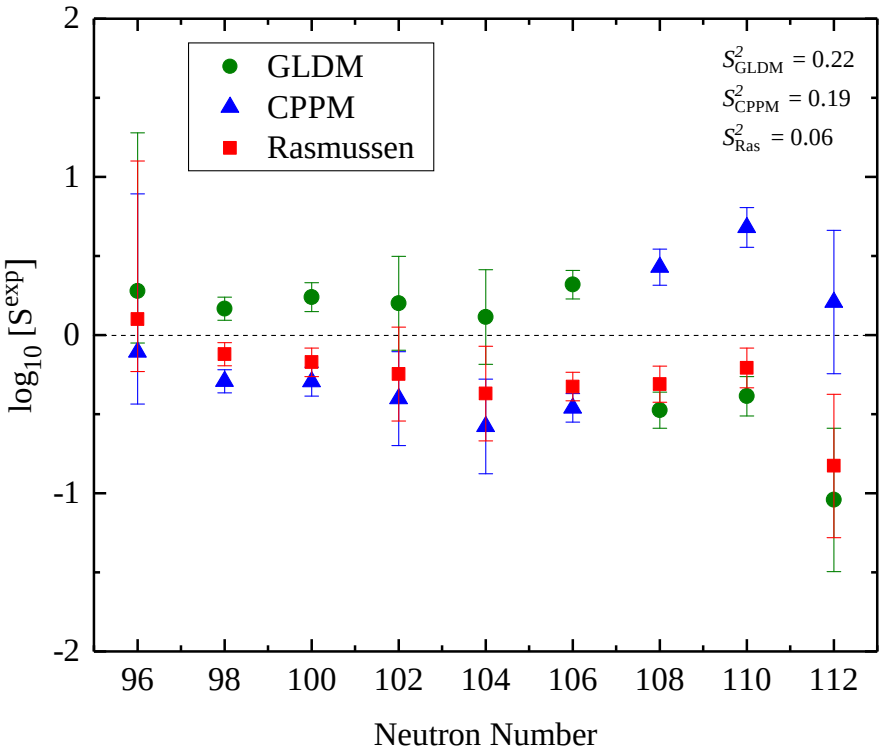

Figure 5.5: Logarithmic experimental spectroscopic-factor $\log_{10}[S^{exp}]$ for even-A lead isotopes as function of the neutron number. The theoretical α-decay half-life values were taken from Refs. [Santhosh15, Rasmussen59] using the CCPM and the GLDM models, and calculated using the Rasmussen method [Rasmussen59]. The dash-line at $\log_{10}[S^{exp}] = 0$, is placed to guide the eye. The variance S^2 of $\log_{10}[S^{exp}]$ was calculated for each of the three models. The figure is adapted form Ref. [Badran16].

up to $N = 112$ as can be noticed in Fig. 5.5. The reverse trend is observed for the GLDM. The Rasmussen method [Rasmussen59] gives the closest agreement along the even-A Pb isotopic chain, where good agreement between the experimental half-life values and the theoretical calculations was observed. The deviation at $N = 112$ is likely due to an inaccurate partial half-life i.e. α-decay branching ratio of ^{194}Pb. In addition, the CPPM shows a good agreement for even-even Pb nuclei apart from the S^{exp} values for $N = 108$ and $N = 110$, where CPPM failed to reproduce an accurate partial half-life for these mass numbers. On the other hand, the agreement with the GLDM for these neutron numbers remains good.

The α-decay hindrance factor for ^{178}Pb was deduced as $HF = 0.80^{+0.80}_{-0.26}$. This

value corresponds to an unhindered (favoured) transition, where the theoretical α-decay half-life was calculated using the Rasmussen method [Rasmussen59]. In this calculation, we assumed that the α-decay branching ratio of ^{178}Pb is b_α = 100 %. This assumption is made based on the fact that the half-life predictions from Möller *et al.* [Möller97] for the α and β decay of ^{178}Pb are $t^{\alpha}_{1/2} = 5.012 \times 10^{-5}$ s and $t^{\beta}_{1/2} = 0.2815$ s, respectively. Thus, the theoretical branching ratio of ^{178}Pb α decay is $b_\alpha \simeq 99.98$ %. The α decay branching ratios for the neighbouring even-A Pb nuclei ^{182,180}Pb [Rahkila10, Toth99, Andreyev09a] were also assumed to be 100 %.

The α-decay reduced width of ^{178}Pb was calculated using Rasmussen method [Rasmussen59], equation 2.22, as $\delta^2_\alpha = 92^{+92}_{-31}$ keV with an assumption of $\Delta l = 0$. The α-particle energy and half-life used in the calculation are E$_\alpha$= 7610(30) keV and t$_{1/2} = 0.21^{+0.21}_{-0.08}$ ms, respectively. The large uncertainty in the α-decay reduced width value is caused by the large error in the ^{178}Pb half-life. While the accuracy of the ^{178}Pb α-particle energy is not a major factor. Table 5.3 shows that the calculated reduced width value of ^{178}Pb$_{96}$ is consistent within errors, with the those of the $N = 96$ isotones ^{176}Hg$_{96}$ and ^{174}Pt$_{96}$ for which the calculations were also performed using the Rasmussen method [Rasmussen59].

Figure 5.6 shows the α-decay reduced width for even-A lead isotopes including the ^{178}Pb value from this work as a function of neutron number between 88 $\leq N \leq$ 112. The α-decay reduced width for even-A Pt and Hg are included in Fig. 5.6 for comparison. Our new δ^2_α value for ^{178}Pb follows the systematic trend along the even-A lead isotopic chain, where the reduced widths of the lightest lead isotopes are greater than those of the mid-shell region. Looking at the systematics of even-A Hg nuclei in Fig. 5.6, it can noticed that as the neutron number decreases δ^2_α values increase. On the other hand the Pt nuclei systematics are markedly

Table 5.3: A comparison between the α-decay reduced widths δ^2_α of ^{178}Pb with $N = 96$ isotones ^{176}Hg and ^{174}Pt. The calculations were performed using the Rasmussen method [Rasmussen59].

Isotope	δ^2_α (keV)	Reference
^{178}Pb$_{96}$	92^{+92}_{-31}	Present work
^{176}Hg$_{96}$	85(13)	[Toth99]
^{174}Pt$_{96}$	95(2)	[Page96]

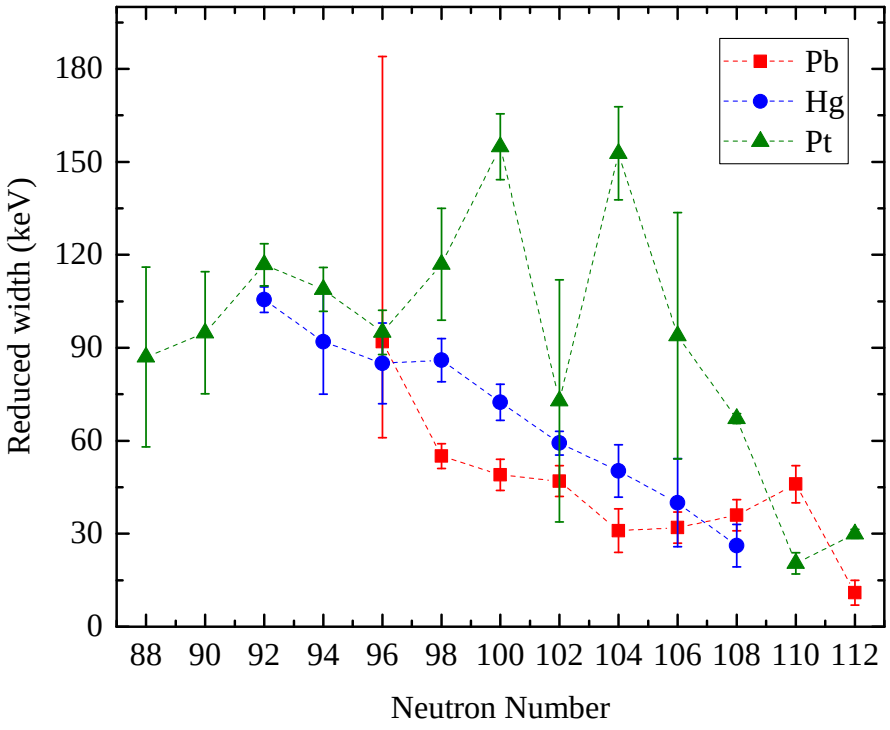

Figure 5.6: α-decay reduced width values as function of neutron number for even-A lead, mercury and platinum nuclei. The experimental values of the Pb isotopes are obtained from Refs [Rahkila10, Venhart12, Andreyev04, Andreyev99a, Bijnens96, Richards96, Toth99, Akovali98], while the experimental values used in Hg and Pt reduced-width calculation were obtained from ENSDF [ens]. The figure is adapted from Ref. [Badran16].

different, where a down turn in the reduced widths below $N = 92$ is observed. Furthermore, in Fig. 5.6 regarding the Pb isotopic chain apart from an overall trend of increasing the magnitude of δ^2_α values as the neutron number decreases, some other features can be noticed. There is an increase below $N = 112$ and then again at $N = 98$, which coincide with the closing and opening of the $i_{13/2}$ neutron orbital. On the other hand, the large deviations around the neutron mid-shell, especially for the Pt nuclei are likely due to inaccurate branching ratios. It can be speculated that the increase of the α-decay reduced width value of ^{178}Pb at $N = 96$, is due to the proximity of the proton dripline, meaning ^{178}Pb becomes proton unbound. Table 5.4 shows that at at $N = 96$, the two-proton separation energy becomes negative, while for ^{180}Pb at $N = 98$ the protons are still bound with a positive two-proton separation energy. However, two neutrons are also required to form an α particle. The two-neutron separation energy for ^{178}Pb is $S_{2n} = 22.13$ MeV and

Table 5.4: The experimental two-proton separation energy S_{2p}^{exp} for ^{178}Pb obtained from the present work and for neighbouring even-A ^{180}Pb. The calculated two-proton separation energy S_{2p}^{calc} values were taken from Ref. [Möller97] and included for the comparison.

Isotope	S_{2p}^{exp} (keV)	S_{2p}^{calc} (keV)
^{178}Pb	- 798(44)	- 470
^{180}Pb	191(18)	590

this value increases as the $N = 82$ shell closure is approached beyond the proton drip line. Still, this weak binding of the protons may further enhance the probability of α-particle preformation and subsequent decay. This relation between both the two-proton and two-neutron separation energy and the preformation probability of α-particle, is still an open question and under theoretical investigation. In addition, the α-decay reduced width values of Pt even-A isotopes start a downward trend as the nuclei become two proton unbound, while the Hg nuclei continuing the upward trend after two-proton separation energy becomes negative. Clearly, more precise data on both half-lives and branching ratios for many isotopes are still needed to have a clear picture of the systematic behaviour of reduced α-widths in vicinity of Z = 82 around the proton drip line.

In Figure 5.7 the experimental α-decay Q-values calculated using equation 2.14, for lead isotopes between $178 \leq A \leq 188$ as function of the the mass number A are plotted. In addition, α-decay Q-values taken from Möller *et al.* [Möller97] and values obtained from Santhosh *et al.* [Santhosh15] were added in Fig. 5.7. The Q-value calculation in Ref. [Santhosh15] was achieved using the following relation,

$$Q = \Delta M_m - \Delta M_d - \Delta M_\alpha + E_{sc} \ , \tag{5.2}$$

where the mass-excess values of the mother, daughter nuclei and the α particle taken from Ref. [Wang12]. The atomic-electron screening effect term in equation 2.17 was taken from Ref. [Huang76]. The graph reveals that there is a good agreement between the experimental values, including the ^{178,179}Pb values from this work, and those obtained from Möller *et al.* [Möller97] when approaches the two proton drip line.

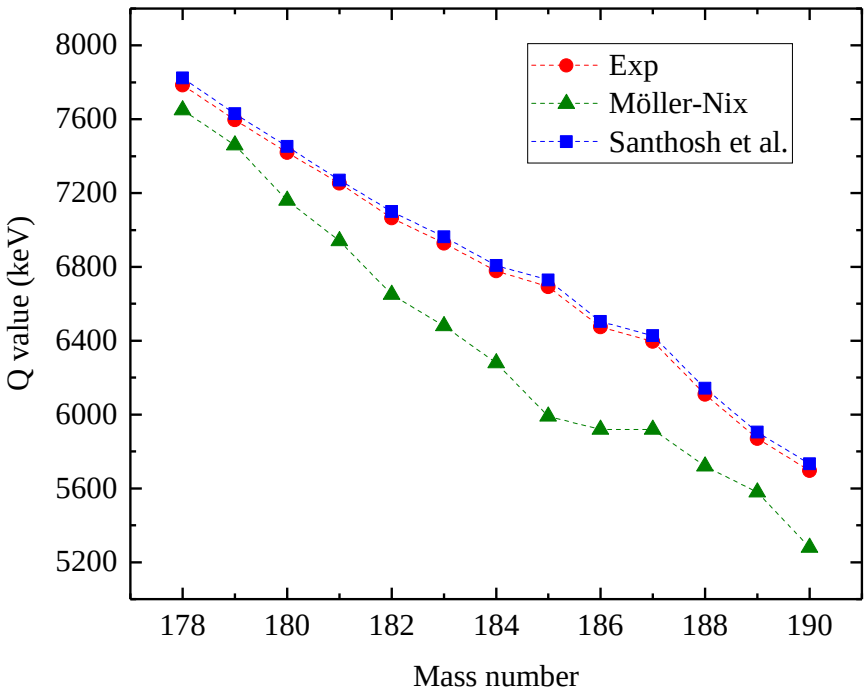

Figure 5.7: The α-decay Q-values as a function of the mass number for different lead isotopes. The filled circles represent the experimental values including the ^{178}Pb Q-value from this work. The filled triangles and squares show the values obtained from Möller *et al.* [Möller97] and Santhosh *et al.* [Santhosh15], respectively.

Chapter 6

Summary

The present thesis, reports on the detailed decay spectroscopy studies of the neutron-deficient nuclei $^{178}_{82}Pb_{96}$, $^{179}_{82}Pb_{97}$ and $^{179}_{81}Tl_{98}$ using the combined system of the gas-filled separator RITU and The GREAT spectrometer. These nuclei have been produced via fusion-evaporation reaction, $^{78}Kr + {}^{104}Pd \rightarrow {}^{182}Pb^{*}$, through $4n$, $3n$ and $2pn$ exit channels, respectively.

Combining RITU and GREAT has allowed detailed decay spectroscopy studies to be performed at the pico-barn production cross-section level of these exotic nuclei. Confirmation of the new isotope ^{178}Pb was reported in this thesis. In total, four events were observed and assigned to ^{178}Pb α-decay. The α-particle energy, Q_α-value and mass excess of E_α= 7610(30) keV, Q_α= 7785(31) keV and 3603(42) keV, respectively, were measured and are in good agreement with the values deduced by Batchelder *et al.* [Batchelder03]. Also, the two-proton separation energy of $S_{2p}^{exp} = -798(44)$ keV was calculated for ^{178}Pb, it is two-proton unbound. Furthermore, a half-life of $t_{1/2} = 0.21^{+0.21}_{-0.08}$ ms was measured for ^{178}Pb and is in agreement with the CPPM calculations by Santhosh *et al.* [Santhosh15]. The α hindrance factor was deduced and corresponds to an unhindered (favoured) $\Delta l = 0$ character for the observed transition. Clearly, further work with higher statistics is required in order to obtain a more precise partial half-life value and provide a clearer picture of the systematic behaviour of the α-decay reduced width in the vicinity of $Z = 82$ for extreme neutron-deficient isotopes approaching $N = 82$.

Furthermore, the proprieties of ^{179}Pb α-decay were deduced with improved accuracy compared with the initial finding by Andreyev *et al.* [Andreyev10]. The α-particle energy and half-life were measured as, $E_\alpha = 7348(5)$ keV and $t_{1/2} = 2.7(2)$ ms, respectively. The ground-state spin and parity of ^{179}Pb was assigned, as $I^\pi = 9/2^-$. This assignment made is based on two facts; (1) the hindrance factor value,

$HF = 1.70(1)$, corresponds to an unhindered (favoured) $\Delta l = 0$ transition and (2) the strong coincidence between the 7348(5) keV α decay and a 80 keV transition from an excited state $9/2^-$ in ^{175}Hg. A detailed discussion regarding the existence of a $\nu i_{13/2}$ state in ^{179}Pb was presented, and a limit of excitation energy and half-life was obtained.

Finally, the relatively large number of decays collected in the present work regarding the ^{179}Tl nucleus compared with the recent study in Ref. [Andreyev13b], allowed us to observe, for the first time, a cascade of γ-ray transitions depopulating a $(9/2^-)$ isomeric state. The proton $(9/2^-)$ intruder state in ^{179}Tl was assumed to be associated with an oblate shape, originating from a one-particle one-hole (1p - 1h) excitation from the $\pi s_{1/2}$ ground state to the $\pi h_{9/2}$ orbital across the shell gap. The excitation energy and half-life of 904.5(9) keV and $t_{1/2} = 114^{+18}_{-10}$ ns were extracted for the proton $(9/2^-)$ intruder state, respectively. A deviation from the parabolic trend of this state around the mid-shell regarding its excitation energy was observed. In addition, α-decay properties of ^{179}Tl were measured in the present work, where a new half-life value of $t_{1/2} = 426(10)$ ms was deduced for the ^{179}Tl ground state. Further work with in-beam data for ^{179}Tl is needed, in order to conduct a γ-γ coincidence analysis and to identify different band structures feeding the isomeric and ground states of ^{179}Tl and eliminate the ambiguities in the spin and parity assignments of the low-lying states.

Bibliography

[Akovali98] Y. Akovali. Nuclear Data Sheets **84**, 1 (1998).

[Andreyev97] A. N. Andreyev *et al.* Zeitschrift für Physik A Hadrons and Nuclei **358**, 63 (1997).

[Andreyev99a] A. N. Andreyev *et al.* Journal of Physics G: Nuclear and Particle Physics **25**, 835 (1999).

[Andreyev99b] A. N. Andreyev *et al.* Phys. Rev. Lett. **82**, 1819 (1999).

[Andreyev00] A. N. Andreyev *et al.* Nature **405**, 430 (2000).

[Andreyev04] A. N. Andreyev *et al.* Phys. Rev. C **69**, 054308 (2004).

[Andreyev06] A. N. Andreyev *et al.* Phys. Rev. C **73**, 044324 (2006).

[Andreyev09a] A. N. Andreyev *et al.* Phys. Rev. C **80**, 054322 (2009).

[Andreyev09b] A. N. Andreyev *et al.* Phys. Rev. C **80**, 024302 (2009).

[Andreyev10] A. N. Andreyev *et al.* Journal of Physics G: Nuclear and Particle Physics **37**, 035102 (2010).

[Andreyev13a] A. N. Andreyev *et al.* Phys. Rev. Lett. **110**, 242502 (2013).

[Andreyev13b] A. N. Andreyev *et al.* Phys. Rev. C **87**, 054311 (2013).

[Appelbe02] D. E. Appelbe *et al.* Phys. Rev. C **66**, 014309 (2002).

[Badran16] H. Badran *et al.* Phys. Rev. C **94**, 054301 (2016).

[Badran17] H. Badran *et al.* Phys. Rev. C **96**, 064314 (2017).

[Baglin09] C. M. Baglin. Nuclear Data Sheets **110**, 265 (2009).

[Barzakh13] A. E. Barzakh *et al.* Phys. Rev. C **88**, 024315 (2013).

[Barzakh17] A. E. Barzakh *et al.* Phys. Rev. C **95**, 014324 (2017).

[Bass80] R. Bass. Deep-Inelastic and Fusion Reactions with Heavy Ions 281--293 (1980).

[Batchelder99] J. C. Batchelder *et al.* Eur. Phys. J **5**, 49 (1999).

[Batchelder03] J. C. Batchelder *et al.* AIP Conference Proceedings **681**, 144 (2003).

[Bijnens96] N. Bijnens *et al.* Z. Phys. **A356**, 3 (1996).

[Bohr75] A. Bohr *et al.* Nuclear structure, volume ii (1975).

[Carpenter05] M. P. Carpenter *et al.* Journal of Physics G: Nuclear and Particle Physics **31**, S1599 (2005).

[Cocolios11] T. E. Cocolios *et al.* Phys. Rev. Lett. **106**, 052503 (2011).

[Coenen85] E. Coenen *et al.* Phys. Rev. Lett. **54**, 1783 (1985).

[Duchêne99] G. Duchêne *et al.* Nuclear Instruments and Methods in Physics Research Section A: Accelerators, Spectrometers, Detectors and Associated Equipment **432**, 90 (1999).

[Enge81] H. Enge *et al.* Phys. Rev. C **24**, 298 (1981).

[ens] Evaluated nuclear structure data file (ensdf). Access via, http://www.nndc.bnl.gov/ensdf/.

[Firestone97] R. Firestone *et al.* The 8th edition of the Table of Isotopes. Hungary, Springer. **29** (1997).

[Fukuchi09] T. Fukuchi *et al.* The Eur. Phys. J **39**, 49 (2009).

[Gamow29] G. Gamow. Zeitschrift für Physik **52**, 510 (1929).

[Geiger11] H. Geiger *et al.* The London, Edinburgh, and Dublin Philosophical Magazine and Journal of Science **22**, 613 (1911).

[Gurney29] R. W. Gurney *et al.* Physical Review **33**, 127 (1929).

[Hauschild13] K. Hauschild. private communication (2013).

[Heyde83] K. Heyde *et al.* Physics Reports **102**, 291 (1983).

[Heyde88] K. Heyde *et al.* Nuclear Physics A **484**, 275 (1988).

[Heyde94] K. Heyde *et al.* Phys. Rev. C **49**, 559 (1994).

[Heyde11] K. Heyde *et al.* Reviews of Modern Physics **83**, 1467 (2011).

[Hilaire07] S. Hilaire *et al.* Eur. Phys. J **33**, 237 (2007).

[Huang76] K. N. Huang *et al.* Atomic Data and Nuclear Data Tables **18**, 243 (1976).

[Igo58] G. Igo. Phys. Rev. Lett. **1**, 72 (1958).

[Jenkins02] D. G. Jenkins *et al.* Phys. Rev. C **66**, 011301 (2002).

[Julin01] R. Julin *et al.* Journal of Physics G: Nuclear and Particle Physics **27**, R109 (2001).

[Kettunen04] H. Kettunen *et al.* Phys. Rev. C **69**, 054323 (2004).

[Kibedi08] T. Kibedi *et al.* Nuclear Instruments and Methods in Physics Research Section A: Accelerators, Spectrometers, Detectors and Associated Equipment **589**, 202 (2008).

[Koivisto01] H. Koivisto *et al.* Nuclear Instruments and Methods in Physics Research Section B: Beam Interactions with Materials and Atoms **174**, 379 (2001).

[Kondev00] F. G. Kondev *et al.* Phys. Rev. C **62**, 044305 (2000).

[Krane88] K. S. Krane *et al.* Introductory nuclear physics, volume 465. Wiley New York (1988).

[Lane95] G. Lane *et al.* Nuclear Physics A **586**, 316 (1995).

[Lazarus01] I. H. Lazarus *et al.* IEEE Transactions on Nuclear Science **48**, 567 (2001).

[Leino95] M. Leino *et al.* Nuclear Instruments and Methods in Physics Research Section B: Beam Interactions with Materials and Atoms **99**, 653 (1995).

[Li15] H. J. Li *et al.* Phys. Rev. C **92**, 014326 (2015).

[Lilley13] J. Lilley. Nuclear physics: principles and applications. John Wiley & Sons (2013).

[Lönnroth88] T. Lönnroth. Zeitschrift für Physik A Atomic Nuclei **331**, 11 (1988).

[Melerangi03] A. Melerangi *et al.* Phys. Rev. C **68** (2003).

[Möller95] P. Möller *et al.* Atomic Data and Nuclear Data Tables **59**, 185 (1995).

[Möller97] P. Möller *et al.* Atomic Data and Nuclear Data Tables **66**, 131 (1997).

[Mottelson55] B. R. Mottelson *et al.* Physical Review **99**, 1615 (1955).

[Muikku01] M. Muikku *et al.* Phys. Rev. C **64**, 044308 (2001).

[Nilsson55] S. G. Nilsson. Dan. Mat. Fys. Medd. **29**, 1 (1955).

[O'Donnell09] D. O'Donnell *et al.* Phys. Rev. C **79**, 051304 (2009).

[Page96] R. D. Page *et al.* Phys. Rev. C **53**, 660 (1996).

[Page03] R. D. Page *et al.* Nuclear Instruments and Methods in Physics Research Section B: Beam Interactions with Materials and Atoms **204**, 634 (2003).

[Perlman57] I. Perlman *et al.* In Kernreaktionen III/Nuclear Reactions III, 109--204. Springer (1957).

[Qi14] C. Qi *et al.* Phys. Lett. B **734**, 203 (2014).

[Raddon04] P. M. Raddon *et al.* Phys. Rev. C **70**, 064308 (2004).

[Rahkila08] P. Rahkila. Nuclear Instruments and Methods in Physics Research Section A: Accelerators, Spectrometers, Detectors and Associated Equipment **595**, 637 (2008).

[Rahkila10] P. Rahkila *et al.* Phys. Rev. C **82**, 011303 (2010).

[Rainwater50] J. Rainwater. Physical Review **79**, 432 (1950).

[Rasmussen59] J. O. Rasmussen. Physical Review **113**, 1593 (1959).

[Reviol92] W. Reviol *et al.* Nuclear Physics A **548**, 331 (1992).

[Richards96] J. D. Richards *et al.* Phys. Rev. C **54**, 2041 (1996).

[Rigby08] S. V. Rigby *et al.* Phys. Rev. C **78**, 034304 (2008).

[Rowe02] M. W. Rowe *et al.* Phys. Rev. C **65**, 054310 (2002).

[Royer00] G. Royer. Journal of Physics G: Nuclear and Particle Physics **26**, 1149 (2000).

[Rutherford99] E. Rutherford. The London, Edinburgh, and Dublin Philosophical Magazine and Journal of Science **47**, 109 (1899).

[Santhosh15] K. P. Santhosh *et al.* Nuclear Physics A **935**, 28 (2015).

[Sarén11] J. Sarén *et al.* Nuclear Instruments and Methods in Physics Research Section A: Accelerators, Spectrometers, Detectors and Associated Equipment **654**, 508 (2011).

[Schmidt84] K. H. Schmidt *et al.* Zeitschrift für Physik A Hadrons and Nuclei **316**, 19 (1984).

[Schmidt00] K. H. Schmidt. Eur. Phys. J **8**, 141 (2000).

[Scholey10] C. Scholey *et al.* Phys. Rev. C **81**, 014306 (2010).

[Seliverstov09] M. D. Seliverstov *et al.* The Eur. Phys. J **41**, 315 (2009).

[Seweryniak99] D. Seweryniak *et al.* Phys. Rev. C **60**, 031304 (1999).

[Singh95] B. Singh. Nuclear Data Sheets **75**, 199 (1995).

[Taageper61] R. Taageper *et al.* Ann. Acad. Sci. Fennicae, Ser. A **6** (1961).

[Taimi15] T. Taimi. private communication (2015).

[Toth84] K. S. Toth *et al.* Phys. Rev. Lett.. **53**, 1623 (1984).

[Toth99] K. S. Toth *et al.* Phys. Rev. C **60**, 011302 (1999).

[Uusitalo97] J. Uusitalo *et al.* Zeitschrift für Physik A Hadrons and Nuclei **358**, 375 (1997).

[Van Duppen00] P. Van Duppen *et al.* Hyperfine Interactions **129**, 149 (2000).

[Venhart11] M. Venhart *et al.* Phys. Lett. B **695**, 82 (2011).

[Venhart12] M. Venhart *et al.* Eur. Phys. J **48** (2012).

[Von Weizsacker35] C. Von Weizsacker. Z. Phys **96**, 431 (1935).

[Wang12] M. Wang *et al.* Chinese Physics C **36**, 1603 (2012).

[Wang17] M. Wang *et al.* Chinese Physics C **41** (2017).

[Wauters94] J. Wauters *et al.* Phys. Rev. Lett. **72**, 1329 (1994).

[Weisskopf51] V. F. Weisskopf. Physical Review **83**, 1073 (1951).